GEOMETRIC NONLINEARITY EFFECTS ON THE BEHAVIOR OF SANDWICH STRUCTURES

A Dissertation
Presented to
The Academic Faculty

By

Zhangxian Yuan

In Partial Fulfillment
of the Requirements for the Degree
Doctor of Philosophy in the
School of Aerospace Engineering

Georgia Institute of Technology

December 2017

GEOMETRIC NONLINEARITY EFFECTS ON THE BEHAVIOR OF SANDWICH STRUCTURES

Approved by:

Professor George A. Kardomateas, Advisor
School of Aerospace Engineering
Georgia Institute of Technology

Professor Dewey H. Hodges
School of Aerospace Engineering
Georgia Institute of Technology

Professor Massimo Ruzzene
School of Aerospace Engineering
Georgia Institute of Technology

Professor Julian J. Rimoli
School of Aerospace Engineering
Georgia Institute of Technology

Professor Yeoshua Frostig
Faculty of Civil and Environmental Engineering
Technion - Israel Institute of Technology

Date Approved: October 31, 2017

To my parents,

Jun Yuan and Huizhu Zhang

ACKNOWLEDGEMENTS

First and foremost, I would like to express my sincere gratitude to my advisor Dr. George A. Kardomateas for his continued support, encouragement, and valuable guidance throughout my Ph.D. study. He gave me the freedom to pursue new ideas and provided insightful discussions. He has been a tremendous mentor for me in both academic life and personal development. I hope I could be as enthusiastic and energetic as him. The working experiences with Dr. Kardomateas will be an invaluable wealth in my life.

Next, I would like to thank Dr. Yeoshua Frostig at Technion - Israel Institute of Technology, Israel. He impressed me with his expertise and knowledge on sandwich composites. His enthusiasm for this area is infectious. His patience and discussions lead me to think the physical meaning behind theory. It is good to know him and work with him.

I would like to thank the rest of my committee members Dr. Dewey H. Hodges, Dr. Massimo Ruzzene, and Dr. Julian J. Rimoli for their serving and helping to improve my dissertation. They also served as my qualifying exam committee members and my course instructors. Their support helped me build a strong foundation to pursue my research.

I am particularly grateful to Dr. Xinwei Wang at Nanjing University of Aeronautics and Astronautics, China, who was my former advisor when I was studied there. He guided me into the area of solid mechanics and computational mechanics. He always leads me to the right direction when I get lost. Special thanks for his helpful discussions during my Ph.D. study at Georgia Tech and proofreading on my dissertation.

The financial support of the Office of Naval Research, the interest and encouragement of the Grant Monitor, Dr. Y.D.S. Rajapakse, and the teaching assistantships provided by the School of Aerospace Engineering are gratefully acknowledged. In addition, I would also thank Dr. Jechiel Jagoda, Dr. Stephen M. Ruffin, and all administrative staff of School of Aerospace Engineering for their continued support during my stay at Georgia Tech.

I would like to thank my friends, my fellow labmates, and all who have directly or indi-

rectly helped me during the completion of my dissertation. It would have been impossible for me to complete this study without their assistance.

Last but not the least, I would like to thank my family for their unconditional love, care, understanding, encouragement, and support. I would not have made it this far without you. Home is where your are.

TABLE OF CONTENTS

LIST OF TABLES

LIST OF FIGURES

SUMMARY

The Extended High-order Sandwich Panel Theory (EHSAPT) accounts for the axial rigidity, the transverse compressibility, and the shear effect of the core. Thus, it is suitable for sandwich composites made of a wide range of core materials, including soft cores and stiff cores. However, its analytical solution is only available to particular cases, i.e., sandwich panels with simply supported edges and subjected to sinusoidally distributed transverse loads. To obtain its solutions under general boundary conditions and loadings, a special finite element is first proposed to implement the EHSAPT with the finite element method. The proposed method extends the application of the EHSAPT and can easily handle arbitrary combinations of boundary conditions and loadings.

Small deformation and infinitesimal strain were considered in the EHSAPT. In this dissertation, the EHSAPT is further developed to include geometric nonlinearities. Both faces and core are considered undergoing large deformation and moderate rotation. The weak form nonlinear governing equations of static behavior are derived from the principle of minimum total potential energy, and the equations of motion for dynamic response are derived from Hamilton's principle. The geometric nonlinearity effects on both static behavior and dynamic response of sandwich structures are investigated.

In the literature, there are various simplifying assumptions adopted in the kinematic relations of the faces and the core when considering the geometric nonlinearities in sandwich structures. It is common that only one nonlinear term that appears in faces is included, and the core nonlinearities are neglected. A critical assessment of these assumptions, as well as the effects of including the other nonlinear terms in the faces and the core is made. It shows that the geometric nonlinearities of the core have significant effects on the behavior of sandwich structures.

The stability behavior is very important to sandwich structures. The compressive strength of the thin faces and the overall behavior of sandwich structure can be realized only if it

is stabilized against buckling. As a compound structure, a sandwich structure has more complicated stability behavior than an ordinary beam. The compressibility of the core significantly affects the stability response and contributes to the local instability phenomenon. Therefore, despite the global buckling (Euler buckling), very common in ordinary beams and plates, wrinkling, characterized as short-wave buckling, may also occur in sandwich structures.

The stability investigation of sandwich structures is carried out based on the derived weak form nonlinear governing equations. The buckling analysis, which determines the buckling mode shape and critical buckling load at a convenient manner, and the nonlinear post-buckling analysis, which evaluates the post-buckling response of sandwich structures, are both presented. Both wrinkling and global buckling are observed. It is shown that although the axial rigidity of the core usually is hundreds times smaller than that of the faces, which is often negligible in the static analysis, it has significant influence on the stability response.

CHAPTER 1
INTRODUCTION AND BACKGROUND

1.1 Literature Review

1.1.1 Generals

Sandwich structures are widely used in aerospace, marine, ground transportation and civil industries due to their extraordinary high specific stiffness, strength, and energy absorption capabilities combined with light weight. A typical sandwich panel consists of two high stiffness thin faces, which are separated by a low density thick core. This configuration enables the sandwich structures to exhibit high bending stiffness with little resultant weight. Both low stiffness soft materials, like non-metallic honeycomb and polymeric foam or relatively higher stiffness metallic honeycomb or balsa wood can be used as the core materials.

Many well-known books about sandwich structures are available, like the book by Plantema [1], Allen [2], Zenkert [3], Carlsson and Kardomateas [4], and Vinson [5]. There are also many excellent review articles well summarized and discussed the up to date researches related to sandwich structures, like review by Noor et al. [6], Altenbach [7], Carrera and Brischetto [8, 9], and Librescu [10].

In the literature, research about the mechanical properties of sandwich structures can be divided into two basic categories. The behavior is predicted using either elasticity theory or equivalent sandwich theory. Back to 1970, Pagano [11, 12] gave the three-dimensional elasticity solution to the linear static behavior of sandwich plates. In 2011, Kardomateas followed Pagano's work and extended the elastic solution to the negative discriminant case [13]. These analytical elasticity solutions serve as benchmarks but are only available for certain loading and boundary conditions and do not include nonlinearities. In addition, sandwich theories have also been developed for a long time. Plantema [1] and Allen [2]

well summarized the work done by the 1960s. The earliest models are called the Classical Lamination Theory (CLT) [14] and the First Order Shear Deformation Theory (FOSDT) [15–19]. In these models, the core is assumed to be incompressible in its transverse direction and the in-plane rigidity is neglected. The CLT also discards the shear resistance and the FOSDT considers a uniform shear strain through the thickness direction. These assumptions may be acceptable for sandwich structures with a high stiffness core, such as a metallic core. But it has been shown to be inaccurate for sandwich structures with a very soft core [13]. Later, models considering the flexible core were developed to overcome this limitation. In 1992, Frostig et al. [20] proposed the High-order Sandwich Panel Theory (HSAPT), in which the transverse compressibility and the shear effects of the core sheet are both included. The HSAPT shows high accuracy for sandwich structures with very "soft" cores. However, the axial rigidity was neglected in this model. The most recently high order sandwich theory is the Extended High-order Sandwich Panel Theory (EHSAPT) [21]. It includes the axial rigidity of the core in addition to the transverse compressibility and shear effect. It has been formulated for sandwich flat beams/wide panels by Phan [22], flat plates by Siddiqui [23], and curved panels by Rodcheuy [24]. By comparison to the elasticity solution, the EHSAPT shows high accuracy in both displacement and stress distributions for a wide range of core materials [21]. Besides, the "zigzag" theories [25–28] and the layerwise theories [29–31], which were originally developed for laminated composites are also introduced to the sandwich constructions. In the zigzag theories, the displacements have a piecewise variation through the thickness. The shear stress is continuous at the layer interfaces. During the years, a number of zigzag models have been developed [32, 33]. Recently, a "Refined Zigzag Theory" (RZT) was proposed by Barut and Madenci [32]. The in-plane and transverse displacement components have a quadratic through-thickness variation and the transverse normal strain is obtained through the assumption of a cubic variation of the transverse normal stress. Iurlaro et al. [33] developed a mixed cubic zigzag model for multilayered composite and sandwich plates. The in-plane

displacements follow a piece-wise cubic distribution and the transverse displacement has a parabolic variation through thickness. The assumed transverse shear stress profile comes from the three-dimensional equilibrium equations. These recent theories were shown to offer improvements especially for thick or highly heterogeneous laminate configurations. In addition, the Variational Asymptotic Method (VAM) is also used to study the laminated composites and sandwich panels. A strain energy function of laminated composite plates was obtained by Atilgan and Hodges [34]. Sutyrin and Hodges [35] developed the asymptotically correct linear laminated plate theory. Yu et al. [36] studied the composite laminated plates with the VAPAS (Variational Asymptotic Plate And Shell analysis). Peereswara et al. [37] analyzed the inter-laminar stresses in honeycomb sandwich panels with VAM.

1.1.2 Geometric Nonlinearity Effects

The major part of the research works related to sandwich structures are performed under the framework of small displacement and small deformation. However, linear assumption is for simplicity and nonlinear behavior is the reality. Sokolinsky and his colleagues [38] compared the linear HSAPT and nonlinear HSAPT with the experimental results from four-point bending tests of a sandwich beam. It was shown that the linear analysis is efficient in estimating the transverse displacements while the geometric nonlinearities should be considered when accurate predictions are required for the longitudinal displacements and peeling stresses.

When it comes to large deformation, in which the geometric nonlinearity need to be considered, the literature is rather limited. In 1948, Reissner [39] presented an analysis of finite deflections of sandwich plates. In 1964, Alwan [40] developed a large-deflection theory in terms of the Airy stress function for sandwich plates with orthotropic cores. In 1992, Dutta and Banerjee [41] derived another set of differential equations in terms of in-plane displacement of the faces and the transverse displacement of the plate for sandwich plates with orthotropic cores. These analytical solutions are limited to simply supported

boundary with sinusoidally distributed loads. In these early studies, although the geometric nonlinearity is considered, the core was assumed to be incompressible in the thickness direction.

In modern sandwich structures, soft cores are widely used due to their advantages of weight saving and efficient manufacturing processes compared to others with metallic cores. Due to the usage of soft materials as the core, the compressibility of the core leads to significant core transverse deformation. Sandwich structures are more likely to show localized effects associated with large deformations and moderate rotations. This has been observed in experiments on sandwich panels subject to impulsive (blast) loading [42]. Thus, geometric nonlinearity effects with a compressible core should be considered.

The large deformation could be considered by imposing the geometric nonlinearities in the kinematic relations. The literature survey reveals that various simplifications are often made when including the geometric nonlinearities. These assumptions and simplifications are made mainly due to the complexity of the governing equations. Usually, in researches involving geometric nonlinearities, only some of the nonlinear terms that appear in the kinematic relations are included.

Most of the researches on this topic only consider large deformation in the faces, while small deformations and infinitesimal linear strain relations are used in the core. Frostig and Baruch's nonlinear HSAPT model [43] assumes the faces undergoing small displacements and large rotations while the core is assumed to deform with small displacements and small rotations. Sokolinsky et al. [44, 45] analyzed the nonlinear static behaviors of sandwich beams by following the nonlinear HSAPT. In 2008, Li and Kardomateas [46] presented a nonlinear higher-order theory for sandwich plates. The nonlinear kinematic relations were adopted in the faces while the core was considered to have large rotations with small displacements.

In some models, although the core considers the large deformation and uses the Green-Lagrange strain during the equation derivation, simplifications are made to simplify the

final equations. In 2003, Hohe and Librescu [47] presented a nonlinear theory for double curved sandwich shells with compressible core. In both faces and core, the large deformation is expressed by the Green-Lagrange strain tensor and then only the nonlinear strain terms with respect to the transverse displacements are kept while the other nonlinear terms are discarded. In 2005, Frostig et al. [48] formulated the nonlinear field equations which use the nonlinear kinematic relations of large displacement and moderate rotation in both faces and core, followed by two simplified models. The simplifications are all made in the core sheet. One model only includes the nonlinear kinematic relations of the shear angle while the other one assumes the linear kinematic relations are still valid. These two models are the models used for the analysis eventually. The later one coincides with the nonlinear HSAPT. In these two models, which can be thought of as a extension of the HSAPT, the axial rigidity of the core sheet is still neglected. In 2014, Dariushi et al. [49] used the Green-Lagrange strain in both faces and core. Since the classical beam theory was adopted in the faces, face sheets have non-zero nonlinear transverse normal strain component and shear strain component while the corresponding linear parts equal to zero.

It is seen that these simplifications are various in the literature and no literature can be found that critically examines the effects and validations of these simplifications. This is actually one of the goals of this dissertation.

1.1.3 Dynamic Response of Sandwich Structures

The investigations on the dynamic response of sandwich structures follows similar approaches as the studies on the static behavior. The elasticity approaches, regarded as the most accurate ones, have been carried out. The closed form elasto-dynamic response of one-dimensional (1D) sandwich panels [50] and two-dimensional (2D) sandwich plates [51] were derived. Thus, elasticity solutions can serve as the benchmark for other approaches but only limited to particular boundary and loading conditions.

Lamination theories and sandwich theories have been successfully applied to investi-

gate the dynamic response of sandwich structures. Ganapathi et al. [52] studied the dynamic response of thick composite/sandwich laminates using the higher-order zig-zag theory. Moreira and Rodrigues [53] used a layer-wise model to analyze the natural modes of soft-core sandwich panels, and comparisons were made with experimental results. Loja et al. [54] proposed several layer-wise models for the study of sandwich beam-type structures, which can combine different shear deformation theories in different layers.

High-order sandwich theories also have been adopted into studies on the wave transmission characteristics [55], free vibration [56], and dynamic response [57] of sandwich structures. In addition, the EHSAPT has successfully solved the impact and dynamic response of sandwich structures for 1D sandwich panels [58] and 2D sandwich plates [59]. The comprehensive comparisons of the blast response of sandwich panels using the First Order Shear Deformation Theory (FOSDT), HSAPT, EHSAPT, and elasticity can be found in [50, 51, 58, 59]. It shows that the FOSDT cannot capture the divergences between faces and core and it significantly overestimates the dynamic displacements. The high-order theory, especially the EHSAPT can well capture the trends of both displacements and stresses. A very good correlation between the EHSAPT and the elasticity solution throughout the duration time was observed.

Besides theoretical and numerical studies, experimental studies on the dynamic response of sandwich structures haven also been carried out [60–65]. The experiments focus on sandwich structures subjected to blast and impact loading along transverse direction.

It is noticed that most of the theoretical investigations on the dynamic and transient response of sandwich structures are based on the small deformation assumptions [50, 51, 53–55, 57–59]. On the other hand, due to the high magnitude of blast loads, and the usage of soft core materials, sandwich structures may experience large deformations, during which the small deformation and infinitesimal strain assumptions are no longer valid. As observed in experiments [61–63], the transverse deflection magnitude can reach or even exceed the magnitude of the total thickness of a sandwich panel. Thus, the geometric nonlinearity

should be included when considering the dynamic response of sandwich structures, especially for blast and impact loads. Similar to the nonlinear static analysis of sandwich structures, simplifications and assumptions are usually applied in the nonlinear dynamic analysis due to the complexity of including all terms in the equations of motion. Indeed, most of the researches on this topic only consider the large deformation in the faces, while the core retains the linear kinematic relations [66]. In some models, simplifications are applied after imposing the nonlinear kinematic relations in both faces and core. Perel and Palazotto [67] performed the dynamic geometrically nonlinear analysis of transversely compressible sandwich plates. The kinematic relation comes from the abbreviated Green-Lagrange strain-displacement relations. The strain components related to the thickness direction only take the linear part, and the other strain components only retain the nonlinear terms related to the transverse displacement.

Therefore, the geometric nonlinearity effect on the dynamic response must be studied. A comprehensive comparisons should be given.

1.1.4 Stability Behavior of Sandwich Structures

The high divergency in both material property and geometry between faces and core raises challenges in the design of sandwich structures. The compressive strength of the thin faces and the overall behavior of sandwich structure can be realized only if it is stabilized against buckling.

As a compound structure, a sandwich structure has more complicated stability behavior than an ordinary beam. The compressibility of the core significantly affects the stability response and contributes to the local instability phenomenon. Therefore, despite the global buckling (Euler buckling), very common in ordinary beams and plates, wrinkling, or known as local buckling, may occur in sandwich structures. The wrinkling is characterized as short-wave buckling of the face layers.

In the earliest study, global buckling and local wrinkling are assumed uncoupled and

are investigated separately. The buckling type and critical buckling load are determined as the one has lower load. In Allen's book [2], different models were proposed to describe the global buckling and wrinkling, respectively. In general, the global buckling mode is determined by an equivalent ordinary beam, and the local wrinkling mode is modelled as the faces rested on an elastic foundation, which is the core. This modelling strategy was widely used [1, 68]. Carlsson and Kardomateas [4] well summarized and compared these formulations for global buckling and wrinkling. The assumption that there is no interaction between global buckling and local buckling simplifies the modelling strategy to the greatest extent and makes it possible to provide simple analytical solutions. With a conservative safety factor, these formulations can provide a good estimate for the engineering design. These formulations all yield similar critical load when global buckling happens, however, the predictions of wrinkling critical load are scattered. Moreover, simply ignoring a buckling mode due to the higher critical load may cause misleading and is dangerous. The buckling mode interaction of sandwich structures may cause the destabilization. Thus, more complex models are required to take these factors into account. In 1986, Hunt [69] examined the interaction buckling via the superposition of one global buckling and two local buckling modes, namely the symmetric wrinkling mode and the asymmetric wrinkling mode. The possibility of the destabilization caused by the mode interaction was shown. In 1988, Hunt and his colleagues [70] extended their early work by adding two extra degrees of freedom to include shear effects. It leads to a formulation of six degrees of freedom. Despite the mode interaction, the localizations behavior also contributes to the destabilization of sandwich structures [71–73]. Then, the study about the stability behavior of sandwich structures is focused on the universal approaches [74, 75] that can describe both global and local buckling simultaneously. By taking different presumed buckling mode shapes, i.e., the global buckling mode has one or several waves, the symmetric wrinkling mode has multiple short waves with opposite sign in top face and bottom face , and the antisymmetric wrinkling mode has multiple short waves with same sign in top face and

bottom face, different types of buckling mode are obtained from same governing equations. The elasticity solutions of global buckling and wrinkling corresponding to the uniform sine wave mode shape are also derived [76, 77]. However, there is no clear evidence showing that the buckling mode of sandwich structures essentially has uniform sine waves, although it is true for ordinary beams and plates.

Sandwich theory, especially the high order theory, has been further developed to study the stability of sandwich structures. Pandit et al. [78] studied the buckling behavior of laminated sandwich plates with soft core based on improved the high order zigzag theory. The buckling analysis based on the HSAPT [20], which accounts for the transverse compressibility and shear effect of the core, was successfully performed [43]. This approach gives a general description of the sandwich panels and is not limited to particular boundary condition. The only simplified assumption is neglecting the axial rigidity of the core, since its magnitude usually about three and two orders smaller than that of the faces. Sokolinsky and Frostig [44, 45, 79, 80] further studies the stability and branching behavior of sandwich structures based on the HSAPT. The sandwich panels with different but similar boundaries and loadings were investigated. By comparisons of the critical buckling load, the buckling mode shape, and the post-buckling behavior, it demonstrated the incapability of the classical approach, which using middle plane to approximate the sandwich panels. As a compound structure, the simply supported boundary may have various definitions to sandwich structures. The actual boundary conditions of each layers should be considered. More recently, the EHSAPT has been applied to study the fundamental stability properties of simply supported sandwich panels [81, 82]. By introducing the presumed buckling shape with uniform magnitude sine waves, the critical load and buckling wave number corresponding to this type of buckling mode were determined.

Perhaps due to the complexity of the stability of sandwich structures, assumptions are usually adopted to simply modelling and solving efforts, e.g., the anti-plane assumption [2, 43–45, 71, 79] in the core, and membrane pre-buckling state [43, 76, 77, 81, 82]. The

anti-plane assumption, which assumes the axial rigidity of the core is negligible since its magnitude usually about two to three orders smaller than that of the faces, is widely used in the investigation related to sandwich structures. Although the validation of this assumption is approved for the static and dynamic behavior, there is no clear evidence showing that the effect caused by the axial rigidity of the core is negligible to the stability response. The membrane pre-buckling state might not be valid since sandwich structures are compound structures containing layers made with different materials. Even only subjected to compressive loads acting along axial direction, sandwich structures may have bending behavior. In Sokolinsky and Forstig's work [44, 45, 79], the pre-buckling state is not limited to membrane state, and it assumes that the critical load can be determined with sufficient accurate when pre-buckling nonlinearity is neglected [79].

The stability analysis of sandwich structures requires to take the geometric nonlinearity into consideration. In literature, it usually only considers the faces undergoing large deformation with moderate rotation, while the core has small deformation kinematic relation [44, 45, 71, 74, 79, 81, 82]. In other words, infinitesimal strains are adopted in the core. In some research, both faces and core take Von Kármán strains as the kinematic relation [72, 73]. The accuracy might be affected especially when considering the post-buckling response.

There are fewer works related to the elastic post-buckling response of sandwich structures available in literature [44, 45, 70, 79, 80], compared to ones focus on the buckling analysis. Studies about the initial post-buckling behavior [83, 84] and elastoplastic post-buckling response [85] were also carried out. It is important to understand the post-buckling response of sandwich panels since the buckling behavior does not essentially mean that sandwich structures lost the load carrying capability.

1.1.5 Solution Techniques of Sandwich Structures

Due to the nature of sandwich structures, the analytical solutions of linear small deformation usually are only available to several particular configurations, e.g., sandwich panels with simply supported edges and subjected to sinusoidal transverse loading, no matter whether the elasticity approach [12, 13] or special sandwich theory [21] is considered. For general and more complicated geometric and loading configurations, a direct analytical solution is not always available; thus, more general numerical approaches are needed. Besides, when geometric nonlinearities are considered, it makes analytical solutions impossible to be obtained even for simply supported sandwich panels under sinusoidal transverse loading. Furthermore, numerical results are not easy to get and various numerical issues may occur regarding sandwich structures. Hence, a stable numerical approach is required.

Two methods have been traditionally used in this regard: the finite difference method [48] and the finite element method [57]. The latter one is more commonly used in the solid mechanics area due to its advantages of easily handling the boundary conditions, presenting clear physical meaning, and standardized formulation. Several special finite elements for sandwich structures have been reported for linear or nonlinear analysis. In general, two kinds of such finite elements have been proposed: One is the layer-by-layer element [52, 86], which is based on the "zigzag" theory. The displacement has a piecewise variation through the thickness. Multiple elements along the thickness direction are needed for laminates and sandwich composite plates. The other kind of element is based on the sandwich theory [57, 87–89]. Only one element is required through the thickness direction and it contains the information of all sheets. Hu et al. [87] used a one-dimensional element with the nonlinear kinematic equation in the skin and linear relation in the core to perform the global and local buckling analysis of sandwich beams. Several elements were formulated based on the high-order theory for the sandwich plate. The linear dynamic and linear static analyses was performed successfully [57, 89].

When geometric nonlinearities are considered and nonlinear kinematic relations are

adopted, the governing equations contain nonlinear terms. Difficulties are raised in solving these equations. It is known that numerous issues may happen when using commercial FEA software, like numerical difficulties and poor convergence [48], since material properties and geometric characteristics are quite different in the faces and the core. Therefore, a stable and accurate numerical approach is required to study sandwich structures with geometric nonlinearity considered.

The solution techniques for nonlinear equations have attracted many researchers for a long time. Many solution methods can be found in the literatures. Iterative methods are often considered to maintain the accuracy, such as, Newton-Raphson and Bisection methods. A great effort has been made to apply these mathematical methods in solving problems in the area of solid mechanics. Riks [90, 91] modified the Newton-Raphson method by adding one auxiliary equation. Therefore, the modified method is able to overcome limit points that appear in the equilibrium path and can successfully obtain nonlinear snap-through behavior. Based on Riks' procedure, Crisfield [92, 93] proposed the arc-length method by considering a constraint equation in terms of the length of the incremental load step. The arc-length method is widely used in the nonlinear analysis [94] and different versions were developed. With appropriate parameters, it can capture smooth nonlinear behaviors, e.g., cylindrical shell subjected to transverse loads [95]. When the nonlinear behavior shows bifurcation phenomenon, special care is required and the branch switching techniques [96, 97] need to be considered. Otherwise, the numerical solution is most likely to stay on one of the branches. Besides switching branches, artificial perturbations can be imposed to yield smooth perturbed branches which are nearby to the original bifurcated branched without perturbations. The imperfections, including both loading imperfections and geometric imperfections, are usually considered in the nonlinear post-buckling analysis of sandwich structures in order to initiate the buckling [88, 98].

1.2 Research Goals

The above discussions of the literature on sandwich structures allow the following conclusions:

- There are very few highly efficient analysis tools available to analyze the mechanical response of sandwich panels under arbitrary boundary conditions and loading conditions.
- The problem of the nonlinear effects has not received proper attention. Various simplifications and assumptions are adopted in the literature, and no literature can be found that critically examines these effects and validate these simplifications.
- Due to the incomplete understanding of geometric nonlinear effects, the issues related to large deformation with moderate rotation are also not well investigated, e.g., stability, nonlinear dynamic response, etc.

Thus, the nonlinear response of sandwich structures deserves to be further investigated. A review of the literature has shown the Extended High-order Sandwich Panel Theory gives high accuracy in both displacement and stress for the linear static case. Hence, it would be appropriate to start with this higher order sandwich theory.

The organization of this dissertation is as follows.

Chapter 2 develops a special finite element, which is able to implement the EHSAPT with the finite element method. It is applied to analyze the linear static behavior of sandwich panels and compared with benchmark elasticity solutions. This EHSAPT-based finite element method serves as an analysis tool for studying the geometric nonlinearity effects on the behavior of the sandwich panels.

Chapter 3 derives the nonlinear version of EHSAPT which considering the large displacements with moderate rotations in both faces and core. The EHSAPT-based element is further developed to include the nonlinear Green-Lagrange strains. The simplifications

about the nonlinear terms widely adopted in other nonlinear sandwich theories are compared and examined.

Chapter 4 performs the nonlinear dynamic analysis of sandwich panels based on the nonlinear EHSAPT. The geometric nonlinearity effect upon dynamic response is studied.

Chapter 5 discusses the buckling behavior of sandwich panels. This chapter focuses on the buckling mode shape and critical buckling load. In the solution approach, the pre-buckling state is determined by a nonlinear static analysis. In other word, the membrane pre-buckling is not enforced. A general approach for arbitrary buckling type without decoupling it into isolated global buckling and wrinkling is presented, and there is no presumed buckling mode shape adopted in the analysis.

Chapter 6 deals with the nonlinear post-buckling response of sandwich panels. Both perfect sandwich panels with branch switching technique and sandwich panels with imperfections are considered. The post-buckling response corresponding to global buckling and wrinkling are studied.

Chapter 7 presents the summary and conclusions.

CHAPTER 2
FINITE ELEMENT FORMULATION BASED ON THE EHSAPT

The modelling of sandwich structures is a challenging task due to the large divergence in the material properties and geometry of the faces and the core. The Extended High-order Sandwich Panel Theory (EHSAPT) was developed recently. It shows high accuracy comparing with the elasticity solution. However, the analytical solution is only available to sandwich panels under small deformation with particular boundary and loading conditions, i.e., a simply supported sandwich panel with sinusoidally distributed transverse loads. The geometric nonlinearity raises the difficulties in seeking the analytical solution, and it usually does not exist in most cases. Therefore, an accurate and robust numerical approach is required to analyze sandwich panels under arbitrary boundary conditions and loads. A special sandwich panel finite element is proposed based on the EHSAPT. It can easily handle arbitrary boundary conditions and loads due to the advantage of the finite element method. In this chapter, sandwich panels with small deformation are considered first. The solution obtained by the proposed EHSAPT-based element is compared with the elasticity solution and ones available in literature. The accuracy and efficiency can be verified.

2.1 Extended High-order Sandwich Panel Theory

2.1.1 Displacement Fields

The finite element formulation follows the new sandwich plate theory EHSAPT [21]. In sandwich composites, the core usually is much thicker than the face sheets and of very low modulus, thus the shear deformation plays an important role. The EHSAPT also includes the transverse compressibility as well as the axial rigidity of the core. Higher order terms are needed to accurately describe the deformation of the core sheet.

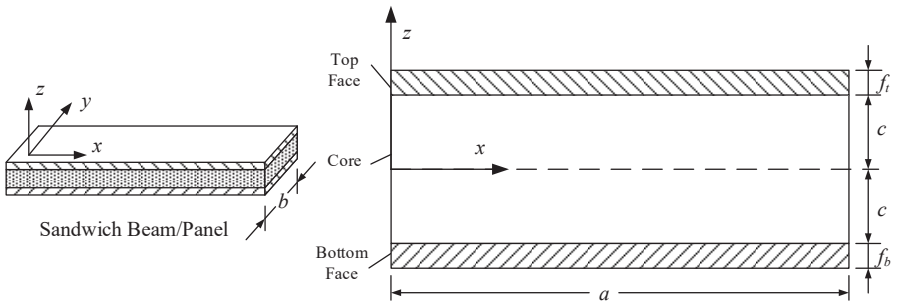

Figure 2.1: Definition of the geometry and coordinate system for the sandwich beam/panel

Consider a sandwich beam or panel consisting of two face sheets bonded to a core, as shown in Fig. 2.1. The thickness of the top face sheet, bottom face sheet and core sheet are f_t, f_b, and $2c$, respectively. The length of the beam/panel is a, and the width is b. The origin of a right-handed Cartesian coordinate is at the left end, with x axis coinciding with the middle line of the core and the z axis in the thickness direction. As a plane problem, we only consider loading in the x-z plane, and this will result in displacements in the x and z directions. The x and z coordinate components of the displacement are denoted with u and w, respectively. Depending on the type of problem and assumptions, either plane stress or plane strain constitutive law can be used for plane problems. In the dissertation, the plane stress condition is adopted in order to be consistent with existing EHSAPT.

In typical sandwich panels, the geometric and material properties are very different between the skins and the core. The thickness ratio of the face sheets and core is very small, and the Young's modulus of the core is much smaller than that of the skins. For the face sheets, the axial strain is the major part, whereas the shear strain can be neglected. For the core, the axial strain, transverse strain, and shear strain need to all be considered. Hence, the displacement field in the face sheets is assumed to follow the Euler-Bernoulli assumptions, whereas a high order displacement pattern is assumed for the core. In the EHSAPT, the core transverse displacement $w(x, z)$ is assumed to be a quadratic function of z and the axial displacement $u(x, z)$ is described by a cubic function of z. The transverse

displacement can be expressed as:

$$w(x,z) = \begin{cases} w^t(x,z) = & w_0^t(x) & (c < z \leq c + f_t) \\ w^c(x,z) = & w_0^c(x) + w_1^c(x)z + w_2^c(x)z^2 & (-c \leq z \leq c) \\ w^b(x,z) = & w_0^b(x) & (-c - f_b \leq z < -c) \end{cases} \tag{2.1}$$

and the axial displacement as

$$u(x,z) = \begin{cases} u^t(x,z) = & u_0^t(x) - \left(z - c - \frac{f_t}{2}\right) w_{0,x}^t(x) & (c < z \leq c + f_t) \\ u^c(x,z) = & u_0^c(x) + \phi_0^c(x)z + u_2^c(x)z^2 + u_3^c(x)z^3 & (-c \leq z \leq c) \\ u^b(x,z) = & u_0^b(x) - \left(z + c + \frac{f_b}{2}\right) w_{0,x}^b(x) & (-c - f_b \leq z < -c) \end{cases} \tag{2.2}$$

where, $w_0^t(x)$, $w_0^c(x)$, and $w_0^b(x)$ are the transverse displacements of center line of the top face, core, and bottom face, respectively. Similarly, $u_0^t(x)$, $u_0^c(x)$, and $u_0^b(x)$ are the axial displacements of the center line of the top face, core, and bottom face, respectively. Also, $\phi_c(x)$ is the slope at the centroid of the core. These unknown quantities are functions of the x coordinate. For convenience, they will be denoted as w_0^k, u_0^k $(k = t, b, c)$, and ϕ^c.

The displacement continuity condition at the interfaces between the face sheets and the core allows solving for the w_1^c, w_2^c, u_2^c, and u_3^c, thus the displacement field is:

$$w^t(x,z) = w_0^t(x) \tag{2.3a}$$

$$w^c(x,z) = \left(\frac{z}{2c} + \frac{z^2}{2c^2}\right) w_0^t(x) + \left(1 - \frac{z^2}{c^2}\right) w_0^c(x) + \left(-\frac{z}{2c} + \frac{z^2}{2c^2}\right) w_0^b(x) \tag{2.3b}$$

$$w^b(x,z) = w_0^b(x) \tag{2.3c}$$

and

$$u^t(x,z) = u_0^t(x) - \left(z - c - \frac{f_t}{2}\right) w_{0,x}^t(x) \tag{2.4a}$$

$$
\begin{aligned}
u^c(x,z) =& \frac{z^2}{2c^2}\left(1+\frac{z}{c}\right)u_0^t(x) + \frac{f_t z^2}{4c^2}\left(1+\frac{z}{c}\right)w_{0,x}^t(x) \\
&+ \left(1-\frac{z^2}{c^2}\right)u_0^c(x) + z\left(1-\frac{z^2}{c^2}\right)\phi_0^c(x) \\
&+ \frac{z^2}{2c^2}\left(1-\frac{z}{c}\right)u_0^b(x) + \frac{f_b z^2}{4c^2}\left(-1+\frac{z}{c}\right)w_{0,x}^b(x)
\end{aligned} \tag{2.4b}
$$

$$
u^b(x,z) = u_0^b(x) - \left(z+c+\frac{f_b}{2}\right)w_{0,x}^b(x) \tag{2.4c}
$$

The displacement field of three layers are represented by these seven functions in terms of x coordinate, namely

$$
\{\widehat{\boldsymbol{U}}(x,z)\} = [\bar{\boldsymbol{N}}(z)]\{\bar{\boldsymbol{U}}(x)\} \tag{2.5}
$$

where $\{\widehat{\boldsymbol{U}}(x,z)\} = [u^t \;\; w^t \;\; u^b \;\; w^b \;\; u^c \;\; w^c]^T$ and $\{\bar{\boldsymbol{U}}(x)\} = [u_0^t \;\; w_0^t \;\; u_0^b \;\; w_0^b \;\; u_0^c \;\; w_0^c \;\; \phi_0^c]^T$.

2.1.2 Kinematic Relations of Small Deformation

When sandwich panels are assumed to undergo small deformation, the infinitesimal kinematic relations hold. Applying the linear strain-displacement relationship:

$$
\epsilon_{xx}(x,z) = \frac{\partial u(x,z)}{\partial x}; \quad \epsilon_{zz}(x,z) = \frac{\partial w(x,z)}{\partial z}; \quad \gamma_{xz}(x,z) = \frac{\partial u(x,z)}{\partial z} + \frac{\partial w(x,z)}{\partial x} \tag{2.6}
$$

the strain components in the entire sandwich panel can be expressed in term of the displacements of the center line. As a consequence of the Euler-Bornoulli assumptions in the faces, the transverse normal strain and shear strain in the top and bottom faces, $\epsilon_{zz}^{t,b}$ and $\gamma_{xz}^{t,b}$, vanish. The axial strain $\epsilon_{xx}^{t,b}$ is the only nonzero strain in the top and bottom face sheets:

$$
\epsilon_{xx}^t = u_{0,x}^t - \left(z-c-\frac{f_t}{2}\right)w_{0,xx}^t \qquad (c < z \le c+f_t) \tag{2.7a}
$$

$$
\epsilon_{xx}^b = u_{0,x}^b - \left(z+c+\frac{f_b}{2}\right)w_{0,xx}^b \qquad (-c-f_b \le z < -c) \tag{2.7b}
$$

In the core, all three strain components for the plane problem exist, and these are:

$$\begin{aligned}\epsilon^c_{xx} =& \frac{z^2}{2c^2}\left(1+\frac{z}{c}\right)u^t_{0,x} + \frac{f_t z^2}{4c^2}\left(1+\frac{z}{c}\right)w^t_{0,xx} + \left(1-\frac{z^2}{c^2}\right)u^c_{0,x} \\ &+ z\left(1-\frac{z^2}{c^2}\right)\phi^c_{0,x} + \frac{z^2}{2c^2}\left(1-\frac{z}{c}\right)u^b_{0,x} + \frac{f_b z^2}{4c^2}\left(-1+\frac{z}{c}\right)w^b_{0,xx}\end{aligned} \tag{2.8a}$$

$$\epsilon^c_{zz} = \left(\frac{z}{c^2}+\frac{1}{2c}\right)w^t_0 - \frac{2z}{c^2}w^c_0 + \left(\frac{z}{c^2}-\frac{1}{2c}\right)w^b_0 \tag{2.8b}$$

$$\begin{aligned}\gamma^c_{xz} =& \left(\frac{z}{c^2}+\frac{3z^2}{2c^3}\right)u^t_0 + \left[\left(\frac{c+f_t}{2c^2}\right)z + \left(\frac{2c+3f_t}{4c^3}\right)z^2\right]w^t_{0,x} \\ &- \frac{2z}{c^2}u^c_0 + \left(1-\frac{3z^2}{c}\right)\phi^c_0 + \left(1-\frac{z^2}{c^2}\right)w^c_{0,x} \\ &+ \left(\frac{z}{c^2}-\frac{3z^2}{2c^3}\right)u^b_0 + \left[-\left(\frac{c+f_b}{2c^2}\right)z + \left(\frac{2c+3f_b}{4c^3}\right)z^2\right]w^b_{0,x}\end{aligned} \tag{2.8c}$$

Eq. (2.7) and Eq. (2.8) can be written in matrix form:

$$\{\boldsymbol{\epsilon}^t\} = [\boldsymbol{L}^t_L]\{\bar{\boldsymbol{U}}\}; \qquad \{\boldsymbol{\epsilon}^b\} = [\boldsymbol{L}^b_L]\{\bar{\boldsymbol{U}}\}; \qquad \{\boldsymbol{\epsilon}^c\} = [\boldsymbol{L}^c_L]\{\bar{\boldsymbol{U}}\} \tag{2.9}$$

where $\{\boldsymbol{\epsilon}^{t,b,c}\} = [\epsilon^{t,b,c}_{xx} \quad \epsilon^{t,b,c}_{zz} \quad \gamma^{t,b,c}_{xz}]^T$ is the strain vector in the top face, bottom face and core, respectively; and $\{\bar{\boldsymbol{U}}\} = [u^t_0 \quad w^t_0 \quad u^b_0 \quad w^b_0 \quad u^c_0 \quad w^c_0 \quad \phi^c_0]^T$ is the displacement vector. Also, $[\boldsymbol{L}^{t,b,c}_L]$ is the differential operator matrix and the subscript L stands for it is the operator matrix for linear strain.

2.1.3 Constitutive Relations

The constitutive laws in the three sandwich layers are:

$$\{\boldsymbol{\sigma}^t\} = [\boldsymbol{C}^t]\{\boldsymbol{\epsilon}^t\}; \qquad \{\boldsymbol{\sigma}^b\} = [\boldsymbol{C}^b]\{\boldsymbol{\epsilon}^b\}; \qquad \{\boldsymbol{\sigma}^c\} = [\boldsymbol{C}^c]\{\boldsymbol{\epsilon}^c\} \tag{2.10}$$

where $\{\boldsymbol{\sigma}^{t,b,c}\} = [\sigma^{t,b,c}_{xx} \quad \sigma^{t,b,c}_{zz} \quad \tau^{t,b,c}_{xz}]^T$ is the stress vector of the top face, bottom face and core, respectively. The $[\boldsymbol{C}^{t,b,c}]$ is the elastic modulus matrix corresponding to the top face, bottom face, and core.

We assume orthotropic material for all three layers, and in this case the elastic modulus

matrix $[\boldsymbol{C}^{t,b,c}]$ is given as:

$$[\boldsymbol{C}^{t,b,c}] = \begin{bmatrix} C_{11}^{t,b,c} & C_{13}^{t,b,c} & 0 \\ C_{13}^{t,b,c} & C_{33}^{t,b,c} & 0 \\ 0 & 0 & C_{55}^{t,b,c} \end{bmatrix} \tag{2.11}$$

where we have denoted $1 \equiv x$, $3 \equiv z$ and $55 \equiv xz$.

Due to zero transverse normal strain and transverse shear strain in the top and bottom face sheets, namely, $\epsilon_{zz}^{t,b}$ and $\gamma_{xz}^{t,b}$ are equal to zero, the $C_{33}^{t,b}$ and $C_{55}^{t,b}$ will not come into the strain energy expressions of the face sheets. The rest of the stiffness parameters are given directly in terms of the elastic moduli and Poisson's ratio by $C_{11}^{t,b} = E_1^{t,b}$ and $C_{13}^{t,b} = \nu_{31}^{t,b} E_1^{t,b}$.

In the orthotropic core, the terms of the $[\boldsymbol{C}^c]$ matrix come from the inverse of the compliance matrix of the orthotropic material [21],

$$\begin{bmatrix} C_{11}^c & C_{13}^c & 0 \\ C_{13}^c & C_{33}^c & 0 \\ 0 & 0 & C_{55}^c \end{bmatrix} = \begin{bmatrix} \frac{1}{E_1^c} & -\frac{\nu_{31}^c}{E_3^c} & 0 \\ -\frac{\nu_{31}^c}{E_3^c} & \frac{1}{E_3^c} & 0 \\ 0 & 0 & \frac{1}{G_{31}^c} \end{bmatrix}^{-1} \tag{2.12}$$

where $C_{11}^c = \frac{E_1^c E_3^c}{E_3^c - E_1^c {\nu_{31}^c}^2}$, $C_{13}^c = \frac{\nu_{31}^c E_1^c E_3^c}{E_3^c - E_1^c {\nu_{31}^c}^2}$, $C_{33}^c = \frac{{E_3^c}^2}{E_3^c - E_1^c {\nu_{31}^c}^2}$, and $C_{55}^c = G_{31}^c$.

It is noticed that the stiffness constants of the core are slightly different from the way these were derived in the elasticity solution [13]. The same stiffness constants should be taken in the elasticity solution and EHSAPT in order to make the solutions comparable. Thus, the constitutive equation used in the elasticity approach [13] is replaced with Eq. (2.12) to yield corresponding elasticity solutions in this dissertation. Because of this, the differences when comparing the EHSAPT results to the elasticity solutions observed in [21] are no longer. The plane strain constitutive law adopted in the elasticity approach [13] can be and should be implemented into the EHSAPT when it is applicable. The comparisons between the EHSAPT and the elasticity, when both use the stiffness constants derived in

the elasticity approach, [13], can be found in Ref. [99]. A good agreement is also observed.

Thus, all the strain and stress components of the sandwich beam/panel can be expressed in terms of the unknown displacement vector $\{\bar{\boldsymbol{U}}\}$ according to the ESHAPT.

2.2 EHSAPT-based Element Formulation

EHSAPT contains high-order terms to describe the deformation of the sandwich cross section. As a result, the analytical solution is not easy to obtain, and sometimes it doesn't even exist. On the other hand, the finite element method (FEM) is a commonly used numerical method in mechanics and can easily handle various combinations of loading and boundary conditions. Hence, the EHSAPT will be used to formulate a finite element and, in this way, develop a new simple, convenient, and accurate approach, which can have the advantages of both the EHSAPT and FEM, to simulate and predict the behavior of sandwich structures. To achieve this goal, an original sandwich element is formulated with 10 degrees of freedom (DOF) per "node". The "node" is actually a nodal line, since the DOFs are placed at different locations along the thickness direction, as shown in Fig. 2.2. Three of them are the transverse displacements of the midline of the top face, bottom face and core, denoted as $w^{t,b,c}$. Another three DOFs are the first order derivatives of $w^{t,b,c}$ with respect to the x coordinate, which are the $dw^{t,b,c}/dx$. Another three are the axial displacements of the midline of the top face, bottom face and core, $u^{t,b,c}$. The last one is the rotation angle of the core's center line, ϕ^c. The proposed element contains both ϕ^c and dw^c/dx as degrees of freedom. Although there is no direct physical meaning when considering the boundary condition corresponding to the term dw^c/dx, this term can be set free, meaning we can set its counterpart force equal to zero, at the boundaries. Numerical results will show that this formulation yields very accurate results, as compared to elasticity. It should be noted that the DOF of dw^c/dx plays an important role to ensure the same shape function can be applied to the mid-line transverse displacement of the core and the face sheets. Otherwise, the core would exhibit a lower order of continuity between adjacent elements than the face

sheets, and the midline deflection pattern of the core and face sheets would be inconsistent. If dw^c/dx is not included, the deflection distribution of the core midline would be linear in a 2-node element and would only have C^0 continuity, whereas that of face sheets would be a cubic curve in a 2-node element and would have C^1 continuity. The accuracy would be decreased dramatically, as observed in numerical experiments.

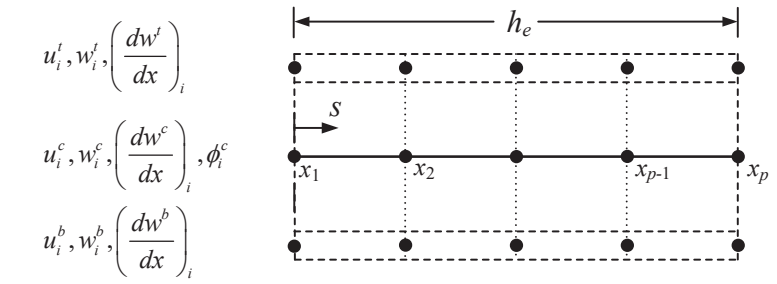

Figure 2.2: Sketch of a p-node EHSAPT-based element

So, the displacement vector of i-th node is:

$$\{\boldsymbol{U}_i\} = \left[u_i^t \quad w_i^t \quad \left(\frac{dw}{dx}^t\right)_i \quad u_i^b \quad w_i^b \quad \left(\frac{dw}{dx}^b\right)_i \quad u_i^c \quad w_i^c \quad \left(\frac{dw}{dx}^c\right)_i \quad \phi_i^c\right]^T \tag{2.13}$$

2.2.1 Displacement Interpolation Function

The element may have several nodes, e.g., a 2-node element, a 3-node element or even an element with more than 3 nodes can be formulated. For a p-node element, Lagrange interpolation polynomials of degree $p-1$ are used to interpolate the axial displacement field $\tilde{u}^{t,b,c}$ and the rotation angle of the core sheet $\tilde{\phi}^c$, within one element. For the transverse displacement field $\tilde{w}^{t,b,c}$, Hermite interpolation polynomials of degree $2p-1$ are used to ensure the C^1 continuity between adjacent elements.

The sketch of a p-node EHSAPT-based element is shown in Fig. 2.2. A p-node EHSAPT-based element has p nodes in x direction. In the element, nodes are denoted as $1, 2, ..., p$

locally, where the node 1 is the first node and node p is the last node. The x coordinates of these nodes are $x_1, x_2, ..., x_p$, respectively. Therefore the length of the element is $h_e = x_p - x_1$. By introducing the element local coordinate $s = x - x_1$ and thus $s_i = x_i - x_1,\ (i = 1, 2, ..., p)$, the axial displacement functions of three layers, $\tilde{u}^{t,b,c}$, and the rotation of the core, $\tilde{\phi}^c$, are assumed to be

$$\tilde{u}^t(s) = \sum_{i=1}^{p} L_i(s) u_i^t \tag{2.14a}$$

$$\tilde{u}^b(s) = \sum_{i=1}^{p} L_i(s) u_i^b \tag{2.14b}$$

$$\tilde{u}^c(s) = \sum_{i=1}^{p} L_i(s) u_i^c \tag{2.14c}$$

$$\tilde{\phi}^c(s) = \sum_{i=1}^{p} L_i(s) \phi_i^c \tag{2.14d}$$

where $L_i(s)$ is Lagrange interpolation function defined by

$$L_i(s) = \prod_{k=1,\ k\neq i}^{p} \frac{s - s_k}{s_i - s_k} \tag{2.15}$$

The transverse displacement of three layers, $\tilde{w}^{t,b,c}$, are assumed as,

$$\tilde{w}^t(s) = \sum_{i=1}^{p} H_i^{(0)}(s) w_i^t + \sum_{i=1}^{p} H_i^{(1)}(s) \left(\frac{dw^t}{dx}\right)_i \tag{2.16a}$$

$$\tilde{w}^b(s) = \sum_{i=1}^{p} H_i^{(0)}(s) w_i^b + \sum_{i=1}^{p} H_i^{(1)}(s) \left(\frac{dw^b}{dx}\right)_i \tag{2.16b}$$

$$\tilde{w}^c(s) = \sum_{i=1}^{p} H_i^{(0)}(s) w_i^c + \sum_{i=1}^{p} H_i^{(1)}(s) \left(\frac{dw^c}{dx}\right)_i \tag{2.16c}$$

where $H_i^{(0)}(s)$ and $H_i^{(1)}(s)$ are Hermite interpolation functions defined by

$$H_i^{(0)}(s) = \left[1 - 2(s - s_i) L_i'(s_i)\right] L_i^2(s) \tag{2.17a}$$

$$H_i^{(1)}(s) = (s - s_i) L_i^2(s) \tag{2.17b}$$

$L_i(s)$ is Lagrange interpolation function given by Eq. (2.15), and its first order derivative evaluated at s_i is

$$L_i'(s_i) = \left.\frac{dL_i(s)}{ds}\right|_{s=s_i} = \sum_{k=1,\ k\neq i}^{p} \frac{1}{s_i - s_k} \tag{2.18}$$

Writing this in matrix form, one has

$$\{\tilde{\boldsymbol{U}}(s)\} = [\boldsymbol{N}(s)] \begin{Bmatrix} \{\boldsymbol{U}_1\} \\ \{\boldsymbol{U}_2\} \\ \cdots \\ \{\boldsymbol{U}_p\} \end{Bmatrix} = [\boldsymbol{N}(s)]\{\boldsymbol{U}_e\} \tag{2.19}$$

where $[\boldsymbol{N}(s)]$ is the interpolation matrix with dimension $7 \times (10p)$, and $\{\boldsymbol{U}_e\}$ is the element nodal displacement vector.

Substituting Eq. (2.19) into Eq. (2.5), the displacement of the sandwich panel is given as,

$$\{\widehat{\boldsymbol{U}}(x,z)\} = [\tilde{\boldsymbol{N}}(s,z)]\{\boldsymbol{U}_e\} \tag{2.20}$$

where $[\tilde{\boldsymbol{N}}(s,z)] = [\bar{\boldsymbol{N}}(z)][\boldsymbol{N}(s)]$. Each row is denoted as a row vector, then it has $[\tilde{\boldsymbol{N}}(s,z)] = \left[[\tilde{\boldsymbol{N}}_u^t]^T \ [\tilde{\boldsymbol{N}}_w^t]^T \ [\tilde{\boldsymbol{N}}_u^b]^T \ [\tilde{\boldsymbol{N}}_w^b]^T \ [\tilde{\boldsymbol{N}}_u^c]^T \ [\tilde{\boldsymbol{N}}_w^c]^T\right]^T$.

The 2-node element is the simplest and easiest EHSAPT-based element to use and (as proved later) is of high accuracy, its detailed expression of interpolation matrix $[\boldsymbol{N}(s)]$ is given in Appendix A. When a sandwich panel is modelled with m 2-node elements, there are a total of $n = m + 1$ nodes. The finite element model is shown in Fig. 2.3.

2.2.2 Element Formulation of Small Deformation

Considering Eqs. (2.9) and (2.19), a strain interpolation matrix can be defined for the faces and the core as

$$[\boldsymbol{B}_L^k] = [\boldsymbol{L}_L^k][\boldsymbol{N}] \qquad k = t, b, c \tag{2.21a}$$

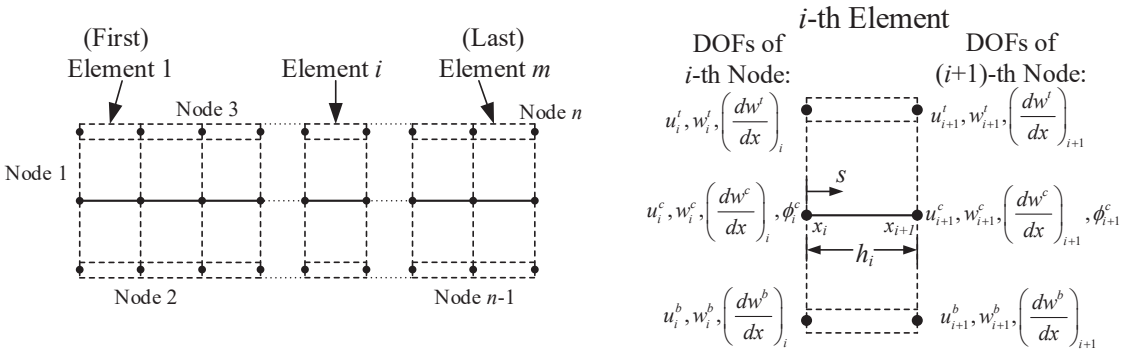

Figure 2.3: Finite Element model using 2-node EHSAPT-based element, $n = m + 1$

Thus, one has

$$\{\boldsymbol{\epsilon}^k\} = [\boldsymbol{B}_L^k]\{\boldsymbol{U}_e\} \qquad k = t, b, c \tag{2.21b}$$

with

$$[\boldsymbol{B}_L^t] = \begin{Bmatrix} \frac{\partial[\tilde{\boldsymbol{N}}_u^t]}{\partial x} \\ [\boldsymbol{0}] \\ [\boldsymbol{0}] \end{Bmatrix}; \quad [\boldsymbol{B}_L^b] = \begin{Bmatrix} \frac{\partial[\tilde{\boldsymbol{N}}_u^b]}{\partial x} \\ [\boldsymbol{0}] \\ [\boldsymbol{0}] \end{Bmatrix}; \quad [\boldsymbol{B}_L^c] = \begin{Bmatrix} \frac{\partial[\tilde{\boldsymbol{N}}_u^c]}{\partial x} \\ \frac{\partial[\tilde{\boldsymbol{N}}_w^c]}{\partial z} \\ \frac{\partial[\tilde{\boldsymbol{N}}_u^c]}{\partial z} + \frac{\partial[\tilde{\boldsymbol{N}}_w^c]}{\partial x} \end{Bmatrix} \tag{2.21c}$$

The second row and third row of $[\boldsymbol{B}_L^t]$ and $[\boldsymbol{B}_L^b]$ vanish automatically due to the Euler-Bernoulli assumptions adopted in faces.

Applying the constitutive law, Eq. (2.10), the stress in the top face $\{\boldsymbol{\sigma}^t\}$, bottom face $\{\boldsymbol{\sigma}^b\}$, and core $\{\boldsymbol{\sigma}^c\}$, can be expressed in terms of the nodal displacement vector, $\{\boldsymbol{U}_e\}$:

$$\{\boldsymbol{\sigma}^k\} = [\boldsymbol{C}^k]\{\boldsymbol{\epsilon}^k\} = [\boldsymbol{C}^k][\boldsymbol{B}_L^k]\{\boldsymbol{U}_e\} \qquad k = t, b, c \tag{2.22}$$

A unit width is considered to simplify the presentation. The total potential energy per unit width of the element is

$$\Pi^e = \int_0^{h_e} \left[\int_c^{c+f_t} \{\boldsymbol{\epsilon}^t\}^T \{\boldsymbol{\sigma}^t\} dz + \int_{-c}^{c} \{\boldsymbol{\epsilon}^c\}^T \{\boldsymbol{\sigma}^c\} dz + \int_{-c-f_b}^{-c} \{\boldsymbol{\epsilon}^b\}^T \{\boldsymbol{\sigma}^b\} dz \right] ds - W^e \tag{2.23}$$

where W^e is the work done by the external force. The element unit width stiffness matrix of

small deformation, $[\boldsymbol{K}_{e_L}]$, can be derived by applying the principle of minimum potential energy, i.e., by taking the first variation of Eq. (2.23) with respect to $\{\boldsymbol{U}_e\}$. The top face, the bottom face, and the core, all contribute to the stiffness of the sandwich panel:

$$[\boldsymbol{K}_{e_L}] = [\boldsymbol{K}^t_{e_L}] + [\boldsymbol{K}^c_{e_L}] + [\boldsymbol{K}^b_{e_L}] \tag{2.24}$$

where $[\boldsymbol{K}^t_{e_L}]$, $[\boldsymbol{K}^c_{e_L}]$ and $[\boldsymbol{K}^b_{e_L}]$ are the element stiffness matrices per unit width resulting from the top face, the core, and the bottom face, respectively. These can be computed explicitly as:

$$[\boldsymbol{K}^t_{e_L}] = \int_0^{h_e} \int_c^{c+f_t} [\boldsymbol{B}^t_L]^T [\boldsymbol{C}^t] [\boldsymbol{B}^t_L] dz ds \tag{2.25a}$$

$$[\boldsymbol{K}^c_{e_L}] = \int_0^{h_e} \int_{-c}^{c} [\boldsymbol{B}^c_L]^T [\boldsymbol{C}^c] [\boldsymbol{B}^c_L] dz ds \tag{2.25b}$$

$$[\boldsymbol{K}^b_{e_L}] = \int_0^{h_e} \int_{-c-f_b}^{-c} [\boldsymbol{B}^b_L]^T [\boldsymbol{C}^b] [\boldsymbol{B}^b_L] dz ds \tag{2.25c}$$

Various loads, such as concentrated forces, distributed forces, and moments, can be applied to the sandwich panel. All of these loads can be and need to be turned into generalized nodal forces (same as in the general finite element method). The element load vector can be obtained by taking the variation of the work done by the external forces W^e in Eq. (2.23). Consider the most general distributed loading case and denote by $p^{t,c,b}$ the distributed axial force per unit width applied to the mid-surface of the top face, core, and bottom face, as well as by $q^{t,c,b}$ the distributed transverse force per unit width applied to the mid-surface of of the top face, core, and bottom face. Also, by $m^{t,c,b}$ the distributed moment per unit width applied to the mid-surface of of the top face, core, and bottom face, respectively.

For consistency and convenience, introduce three differential operator matrices:

$$[\boldsymbol{A}^t] = \begin{bmatrix} 1 & 0 & 0 & 0 & 0 & 0 & 0 \\ 0 & 1 & 0 & 0 & 0 & 0 & 0 \\ 0 & \dfrac{\partial}{\partial s} & 0 & 0 & 0 & 0 & 0 \end{bmatrix} \; ; \quad [\boldsymbol{A}^b] = \begin{bmatrix} 0 & 0 & 1 & 0 & 0 & 0 & 0 \\ 0 & 0 & 0 & 1 & 0 & 0 & 0 \\ 0 & 0 & 0 & \dfrac{\partial}{\partial s} & 0 & 0 & 0 \end{bmatrix} \; ;$$
$$[\boldsymbol{A}^c] = \begin{bmatrix} 0 & 0 & 0 & 0 & 1 & 0 & 0 \\ 0 & 0 & 0 & 0 & 0 & 1 & 0 \\ 0 & 0 & 0 & 0 & 0 & 0 & 1 \end{bmatrix} \tag{2.26}$$

The corresponding equivalent nodal loads at the top face, bottom face, and core can be explicitly computed as:

$$\{\boldsymbol{R}_e^t\} = \int_0^{h_e} [\boldsymbol{N}]^T [\boldsymbol{A}^t]^T \begin{Bmatrix} p^t \\ q^t \\ m^t \end{Bmatrix} ds \; ; \quad \{\boldsymbol{R}_e^c\} = \int_0^{h_e} [\boldsymbol{N}]^T [\boldsymbol{A}^c]^T \begin{Bmatrix} p^c \\ q^c \\ m^c \end{Bmatrix} ds \; ;$$
$$\{\boldsymbol{R}_e^b\} = \int_0^{h_e} [\boldsymbol{N}]^T [\boldsymbol{A}^b]^T \begin{Bmatrix} p^b \\ q^b \\ m^b \end{Bmatrix} ds \tag{2.27}$$

where $\{\boldsymbol{R}_e^t\}$, $\{\boldsymbol{R}_e^c\}$ and $\{\boldsymbol{R}_e^b\}$ are the equivalent nodal concentrated loads per unit width resulting from the distributed loads of the top face, the core, and the bottom face sheet. Moreover, when concentrated forces or moments are applied at the center surface of the top face, core, and bottom faces (such as the axial forces denoted as $P^{t,c,b}$ per unit width, shear forces denoted as $V^{t,c,b}$ per unit width, or bending moments denoted as $M^{t,c,b}$ per unit width), these concentrated loads can be added directly to the load vector corresponding to the nodal displacement.

The element equivalent nodal concentrated load is the summation of the loads from the

top face, bottom face, and core; thus one has

$$\{\boldsymbol{R}_e\} = \{\boldsymbol{R}_e^t\} + \{\boldsymbol{R}_e^c\} + \{\boldsymbol{R}_e^b\} \tag{2.28}$$

Once the element stiffness matrix and element nodal loads are derived, the structural stiffness matrix $[\boldsymbol{K}]$ and load vector of the entire sandwich beam/panel $[\boldsymbol{R}]$ can be easily obtained by assembling all the elements. The structural equilibrium equation of sandwich panels with small deformation is

$$[\boldsymbol{K}_L]\{\boldsymbol{U}\} = \{\boldsymbol{R}\} \tag{2.29}$$

2.3 Numerical Examples and Verifications

FORTRAN programs are written, and static analyses of the sandwich beams subjected to various loadings and boundary conditions are presented. To verify the derivation of formulas and the solution procedures, some results are compared to results available in the literature and other theoretical results.

2.3.1 Example 1: Simple Supported Sandwich Beam

Consider a simplify supported sandwich beam subjected to a sinusoidally distributed load. For this particular case, the theoretical elasticity results are also available [13] for the geometrical parameters of $f_t = f_b = 2$ mm, $2c = 16$ mm and $a = 400$ mm. The stiffness constants as given by Eq. (2.12) are used in the elasticity approach. The sandwich material configuration consists of graphite epoxy faces and glass phenolic honeycomb core, and the material properties are listed in Table 2.1. A distributed load $q^t = q_0 \sin(\pi x/a)$ is applied to the top face sheet. This configuration is analyzed with the 2-node element described in the previous section. For further insight into this element and method, besides the elasticity, the results are also compared with results from a direct application and closed form

solution of the EHSAPT theory, as well as the earlier HSAPT theory [20].

Table 2.1: Material properties (Moduli data are in GPa)

	E_1	E_2	E_3	G_{23}	G_{31}	G_{12}	ν_{32}	ν_{31}	ν_{12}
Graphite-epoxy face	181.0	10.3	10.3	5.96	7.17	7.17	0.40	0.016	0.277
Glass-Phenolic honeycomb core	0.032	0.032	0.300	0.048	0.048	0.013	0.25	0.25	0.25

The boundary conditions for this simply supported beam are $\tilde{w}^t = \tilde{w}^b = \tilde{w}^c = 0$ at $x = 0$ and $x = a$. Considering that both the geometry and loading are symmetric, the axial displacement should equal to zero at the middle. For convenience, we assume an even number of elements, m, which would yield an odd number of nodes, n=$m + 1$; in this case the boundary conditions are applied as:

$$w_1^t = w_1^b = w_1^c = 0 \qquad \text{[first node]} \tag{2.30a}$$

$$w_n^t = w_n^b = w_n^c = 0 \qquad \text{[last node]} \tag{2.30b}$$

$$u_{(n+1)/2}^t = u_{(n+1)/2}^b = u_{(n+1)/2}^c = 0 \qquad \text{[middle node]} \tag{2.30c}$$

Normalized results are given in the following, where the stresses are normalized with q_0 and the displacements are normalized with

$$w_{\text{norm}} = \frac{3q_0a^4}{2\pi^4 E_1^t f_t^3} \tag{2.31}$$

Fig. 2.4 gives the normalized transverse displacement of the middle point at the top sheet when different number of elements are used. That point is also the maximum transverse displacement point over the sandwich beam. The number of elements ranges from 2 to 100. Fig. 2.4 shows that the results converge very fast. Parts of the results are listed in Table 2.2. In addition, the elasticity value and the one from a closed form analytical solution of the EHSAPT are also listed in Table 2.2. The relative error is defined with respect

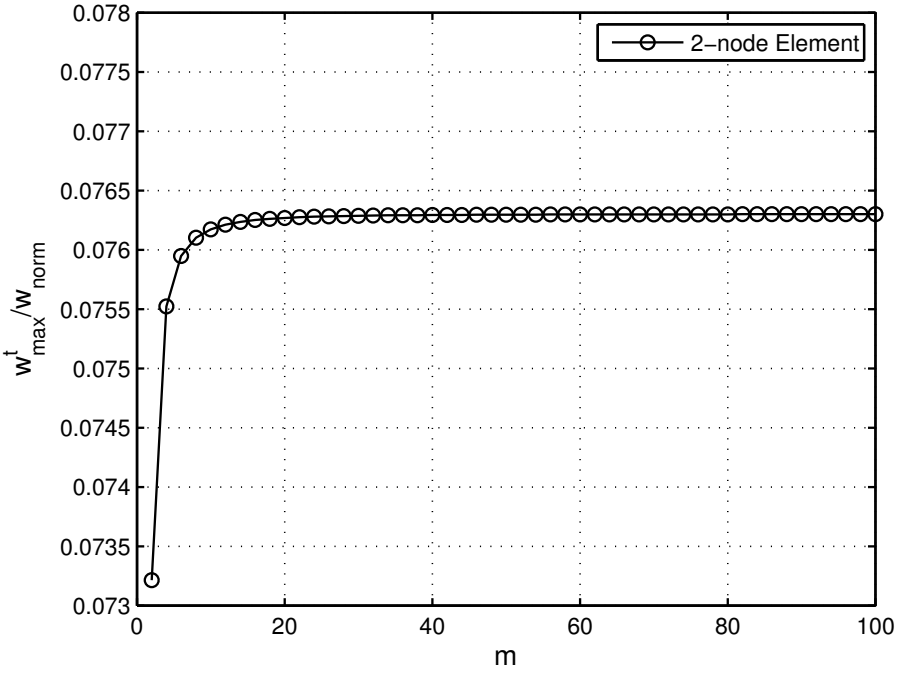

Figure 2.4: Transverse displacement of the middle point vs number of elements, m

to the elasticity value by

$$\text{Relative Error } (\%) = \frac{w^t_{\text{max}} - w_{\text{elasticity}}}{w_{\text{elasticity}}} \times 100\% \tag{2.32}$$

When only 6 elements are used, the relative error is around than 0.5%. To evaluate the convergence rate of the proposed element, the natural logarithms of the error between the EHSAPT analytical solution and the EHSAPT-based finite element solution versus the natural logarithms of the reciprocal of the element number m is plotted in Fig. 2.5. It is seen that the data points lie on the linear fitting line with a slope of 1.9908. Therefore, it proves the proposed EHSAPT-based element has quadratic convergence.

Fig. 2.6 shows the normalized transverse displacement over the length of the sandwich beam. Results using different methods are plotted in the same figure. "FEM" marks the results obtained by 50 uniform length 2-node-20dof EHSAPT-based elements developed in this chapter. So, $m = 50$ and $n = 51$. From Fig. 2.6, it can be seen that the EHSAPT-based

Table 2.2: Effect of number of elements on the accuracy

Number of elements	$w^t_{\max}/w_{\text{norm}}$	Relative Error (%)
2	0.073213334	-4.0923
4	0.075521306	-1.0689
6	0.075947838	-0.5102
8	0.076100493	-0.3102
10	0.076172055	-0.2165
16	0.076250361	-0.1139
30	0.076286583	-0.0664
50	0.076295831	-0.0543
100	0.076299737	-0.0492
EHSAPT	0.076301039	-0.0475
Elasticity	0.0763373	

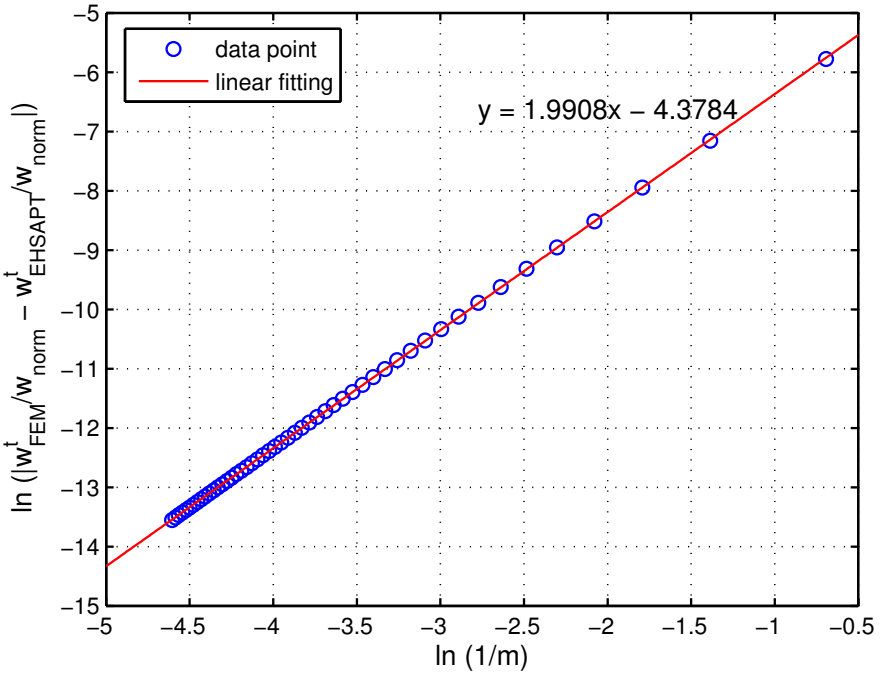

Figure 2.5: Convergence rate of the EHSAPT-based element

finite element solution agrees well with both the elasticity solution and the EHSAPT theory; in this case, the HSAPT is also in agreement. The classical sandwich beam theory assumes that both faces and core obey the Euler-Bernoulli assumption, which implies that the shear modulus is considered to be infinite in both faces and core. This results in over-stiffening the structure and the curve in Fig. 2.6 is much lower than the elasticity and in significant error. Meanwhile, the first order shear theory [4], which considers the shear effect of the core, is also inadequate and results in over-softening the beam, hence the displacement predicted is also in considerable error and much higher than the elasticity theory (the latter is regarded as the exact value).

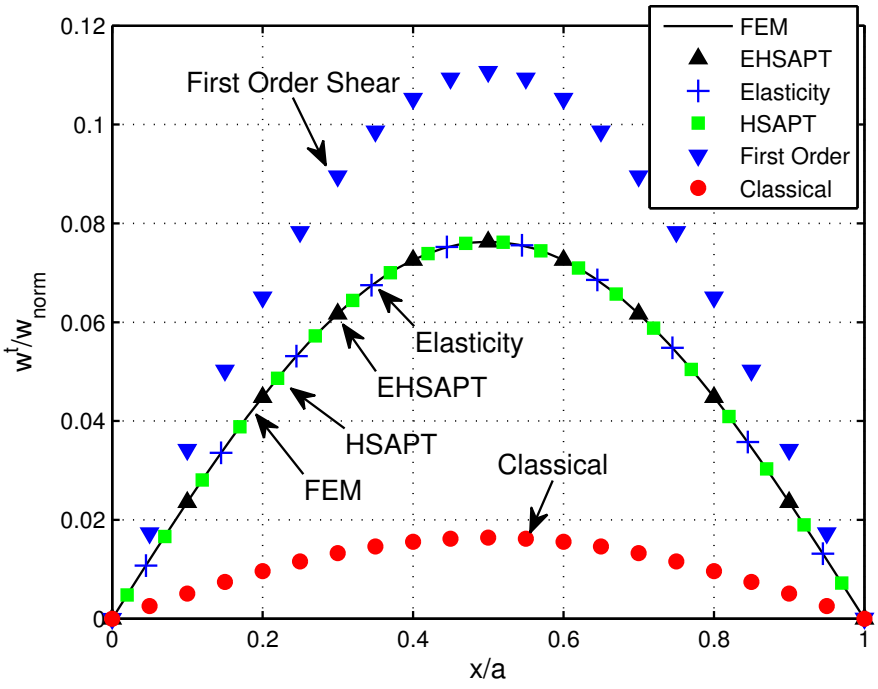

Figure 2.6: Transverse displacement at the mid-point of the top face

The distribution of the normalized axial stress σ^c_{xx} and normalized transverse stress σ^c_{zz} of the middle point ($x = a/2$) in the core sheet are plotted in Figs. 2.7 and 2.8 (50 EHSAPT-based 2-node elements are used). Again, the EHSAPT-based element obtained the same results as the EHSAPT theory. These two are exactly the same as the elasticity solution in both the axial and the transverse stresses. It should be noted that the small differences

in the axial stress results between the EHSAPT and the elasticity, which were observed in Ref. [21], are not observed now because same core stiffness constants are adopted in both EHSAPT and elasticity approaches. The HSAPT neglects the in-plane rigid resulting in a zero axial stress (Fig. 2.7). Both classical and first order theories yield a symmetrically distributed axial stress; thus, they cannot capture the offset predicted by elasticity (Fig. 2.7). From Fig. 2.8, we can see that the results using the EHSAPT-based element, the EHSAPT theory, the elasticity and the HSAPT coincide with each other. Because both classical and first order theories assume the core to be incompressible, a zero transverse stress is observed with these theories (Fig. 2.8).

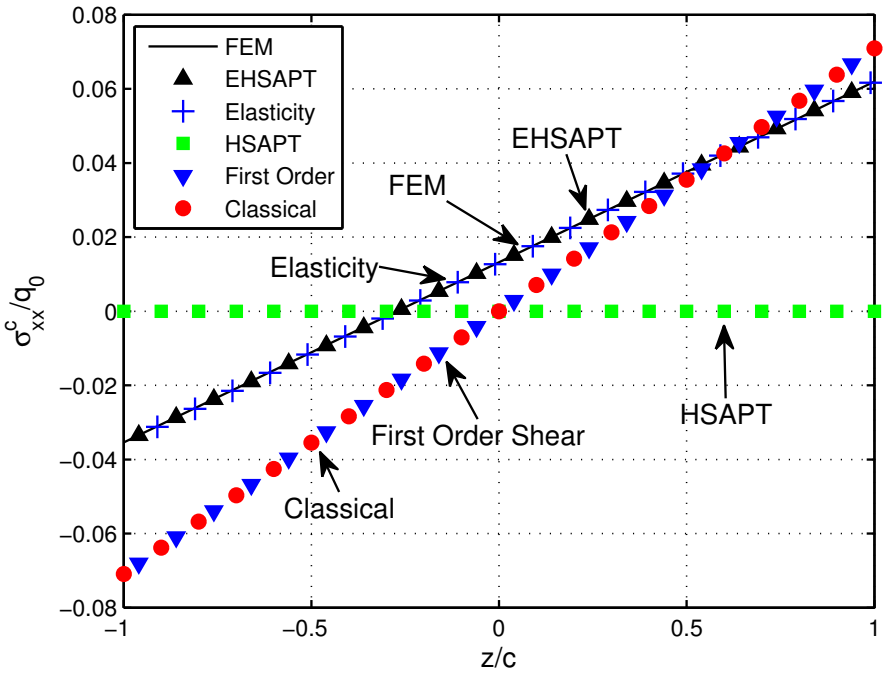

Figure 2.7: Through-thickness distribution of the axial stress in the core, σ^c_{xx}

Fig. 2.9 shows the shear stress distribution along the thickness of the core at $x = a/10$. Only the results obtained by the EHSAPT-based element, the closed form EHSAPT, the elasticity, and the HSAPT are given. 50 and 100 uniform 2-node 20-dof elements are used in the finite element analysis. The results are marketed by "FEM 50 Elem" and "FEM 100 Elem", respectively. In Fig. 2.9, the error between the "FEM 50 Elem" and "EHSAPT"

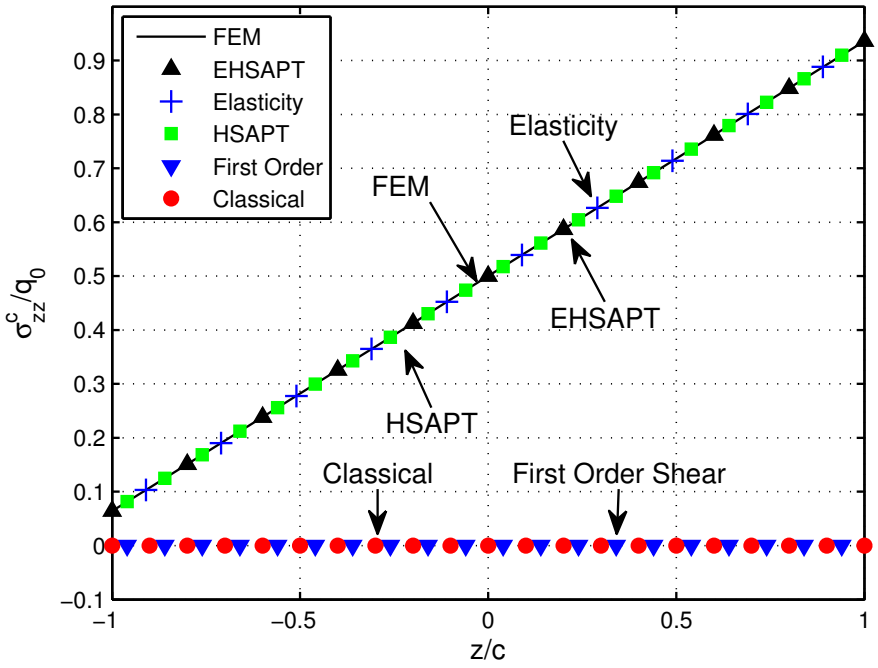

Figure 2.8: Through-thickness distribution of the transverse normal stress in the core, σ^c_{zz}

or "Elasticity" might seems to be larger then the differences in Figs. 2.6-2.8. When considering the scale of the y axis, the maximum relative error between the elasticity solution and the "FEM 50 Elem" is -0.02%. When 100 elements are used, the difference is only -0.01%. The HSAPT gives a constant shear stress within the core (Fig. 2.9). Thus, only with the EHSAPT or this newly formulated element, one can predict the same parabolic distribution shear stress distribution along the thickness as elasticity theory.

2.3.2 Example 2: Cantilever Sandwich Beam

Next, one example considering concentrated load and constrained only face sheets will be analyzed. The novel sandwich beam element will be shown to be very efficient and capable of solving various combinations of loadings and boundaries.

Consider a cantilever sandwich beam with tip concentrated load, as shown in Fig. 2.10. The geometric parameters are $a = 254$ mm, $f_t = f_b = 5$ mm and $c = 19$ mm. The E-glass vinylester composite is used in the face sheets, which has Young's modulus $E_1^{t,b} = 13,600$

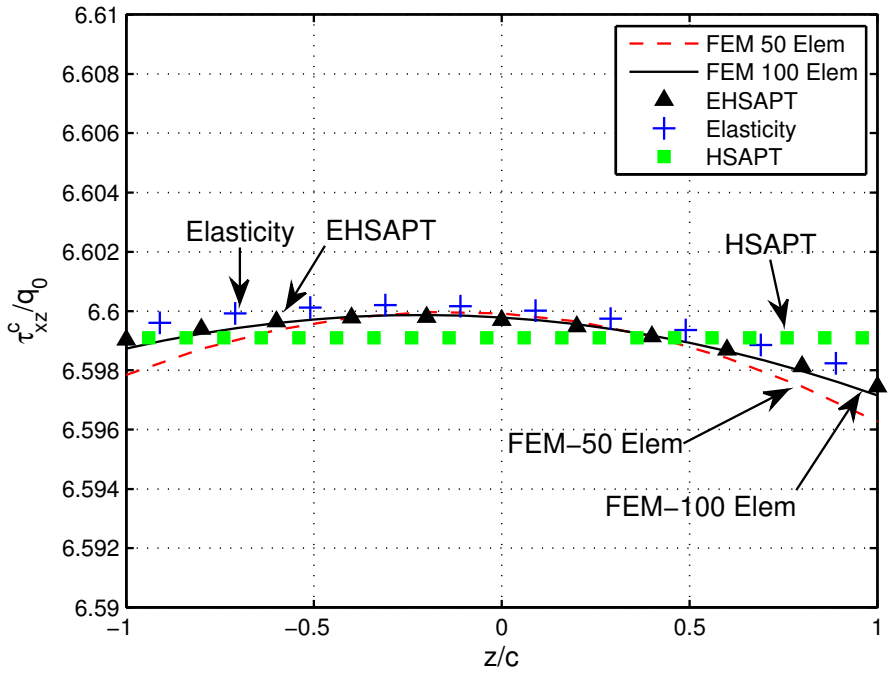

Figure 2.9: Through-thickness distribution of the transverse shear stress in the core, τ^c_{xz}

MPa. The core is isotropic and is made out of Corecell foam with Young's Modules $E^c = 32$ MPa and Poisson's ratio $\nu^c = 0.3$. The tip load $P = 10$ N per unit width and is applied at the right edge of the top face sheet. In practice, constraints on rotation are only applied to the face sheets for the cantilever sandwich beam. So, the boundary conditions at the first node are expressed as:

$$w_1^t = w_1^b = 0 \tag{2.33a}$$

$$\left(\frac{dw^t}{dx}\right)_1 = \left(\frac{dw^b}{dx}\right)_1 = 0 \tag{2.33b}$$

$$u_1^t = u_1^b = 0 \tag{2.33c}$$

In the FEM analysis, 50 uniform length 2-node 20-dof elements will be used. So, $m = 50$ and $n = 51$. When using the EHSAPT, the analytical solution is not available for such loading and boundary conditions. To get the results, the seven equilibrium equations need to be further developed to be 18 first order equations with 18 unknowns. In particular,

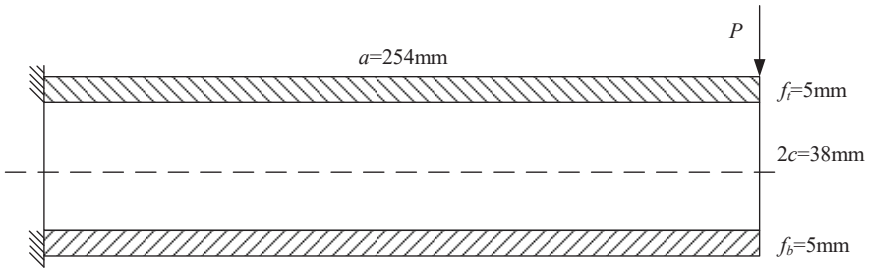

Figure 2.10: Sketch of the sandwich cantilever beam

9 of the 18 unknowns are the displacements or their first order derivatives, which are the $u_0^{t,b,c}$, $w_0^{t,b,c}$, $w_{0,x}^{t,b}$, and ϕ_0^c. Another 9 terms are the corresponding equivalent resultant axial forces, shear forces, and bending moments of the top, core, and bottom sheets. With the variation form of the total potential energy, the equivalent resultant forces and moments are defined by collecting the corresponding coefficients. Also, 9 equations that essentially are the first order derivatives of the equivalent resultant forces in terms of the 18 unknowns can be obtained. Another 9 equations are the derivatives of the 9 displacement unknowns. With this further derivation, one can establish a first-order ODE system with boundary conditions either about displacements or equivalent resultant forces. Then, a numerical boundary value problem solver in MATLAB is used to solve this 1st-order ODE system. The solver is a finite difference code and uses a collocation formula and the collocation polynomial provides a C^1-continuous solution that is fourth-order accurate uniformly in the interval of interest (known as Lobatto formula). Mesh selection and error control are based on the residual of the continuous solution.

The axial and transverse displacements of the two faces and the core are plotted in Figs. 2.11 and 2.12. The results obtained by the FE approach, marked as "FEM", and the analytical EHSAPT, marked as "EHSAPT", are both given. The novel element yields the same results as the EHSAPT. From Fig. 2.11, it can be seen that the top face is elongated and the bottom is compressed. It is interesting to notice that the core only shrinks near the loading edge. At the constrained edge, the middle line of the core shows almost no motion

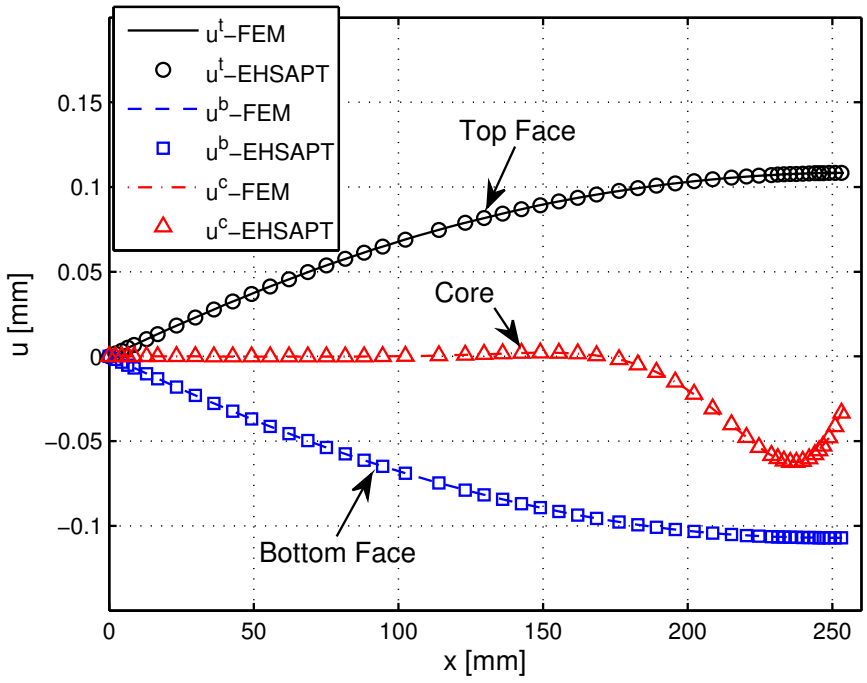

Figure 2.11: Axial displacement along the length (cantilever sandwich beam case)

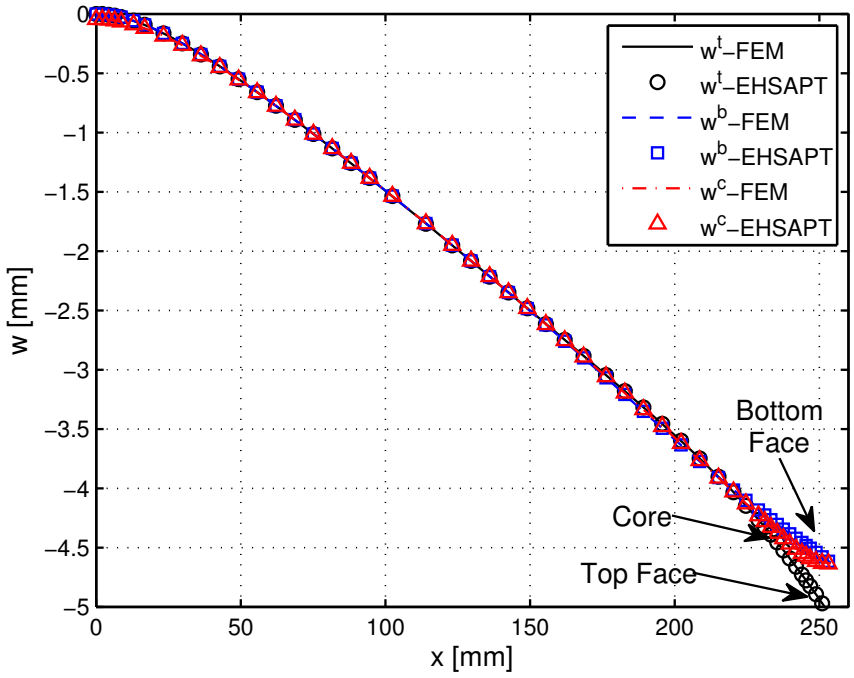

Figure 2.12: Transverse displacement along the length (cantilever sandwich beam case)

in the axial direction. Fig. 2.12 shows that the transverse displacement of the faces and the core are almost the same when it is far away from the loading edge. Near the right edge, the transverse displacement of the top face is larger than the bottom face, which reflects the compression in the thickness direction caused by the concentrated load applied at the load, and which is accommodated by the compressible core.

Using Eq. (2.20), the deformed configuration of the whole sandwich beam can be reconstructed with the node displacements obtained from the FEM analysis. Fig. 2.13 shows the deformed shape of the sandwich cantilever beam from the FEM results. To make it clear, only the left edge and the right edge are plotted. The red dash line is the initial configuration, and the blue solid line is the deformed configuration. Fig. 2.13a (left end) shows that the cross section of the core through the thickness is twisted (it was a straight line before the deformation). The upper part and the lower part move forward and backward, respectively in Fig. 2.13b (right end). The displacement assumptions used in EHSAPT (i.e., Euler-Bernoulli assumptions in the face sheets and higher displacement functions assumed in the core) can be clearly seen in Fig. 2.13b.

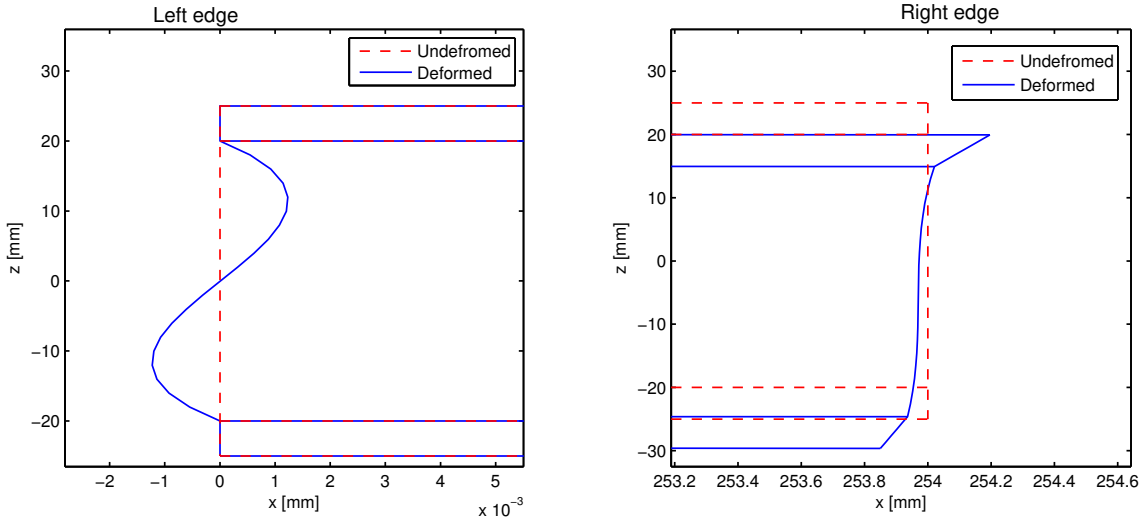

(a) (b)

Figure 2.13: Deformed configuration of the sandwich cantilever beam

The shear stress distribution at several cross sections is shown in Fig. 2.14. Both FEM

results and EHSAPT results are given. The curves represent the results obtained from the FEM and the symbols are the results obtained from the EHSAPT. Again, these two results also perfectly agree with each other. The parabolic distributions are well captured by both EHSPAT and the novel finite element approach. The shear stress shows a more significant variation along the thickness at the region close to the edge.

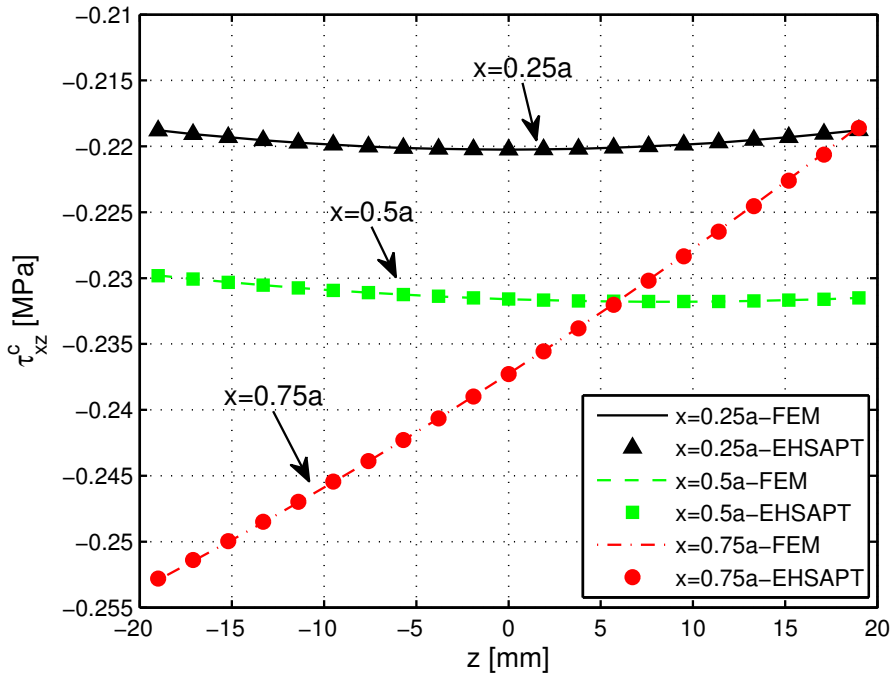

Figure 2.14: Through-thickness distribution of the transverse shear stress at various cross sections (cantilever sandwich beam case)

2.4 Conclusions

A novel sandwich beam/panel finite element is formulated based on the Extended High-order Sandwich Panel Theory (EHSAPT) which was recently introduced. The theory makes different assumptions for the displacement profiles of the face sheets and the core. The cross section deformation is described by 10 DOFs at each node. The deformed configuration and stress distribution of the whole structures can be reconstructed from the nodal displacements, which involve displacements and rotations of the central surface of the two

face sheets and the core. The cross section of the core can deform freely and is not required to remain plane after deformation. The theory employs higher order terms and the nonlinear (nearly parabolic) shear stress distribution in the core is well captured. It should be noted that using same core stiffness constants in both EHSAPT and elasticity approach [13] can eliminate the small differences in the axial stress results between the EHSAPT and the elasticity, which were observed in Ref. [21].

Sandwich panels with small deformation are considered in this chapter. Two static examples are analyzed to verify the convergence, accuracy, efficiency, and the capability of the novel sandwich beam element. The results are compared with analytical solutions from the EHSAPT, the elasticity, the classical sandwich beam theory, the first order shear theory, and the earlier sandwich panel theory, HSAPT. It shows that the presented finite element can yield great accuracy at very low computational cost. The results always agree with the EHSAPT, whose results are the closest ones to those of elasticity theory. Unlike the EHSAPT, the novel finite element approach can easily deal with all kinds of loading and boundary conditions.

CHAPTER 3
GEOMETRIC NONLINEARITY EFFECTS ON STATIC BEHAVIOR OF SANDWICH STRUCTURES

The EHSAPT-based finite element is successfully implemented in the linear static analysis of sandwich panels. The linear EHSAPT formulation is validated for the small deformation and can be regarded as a simplified version of the nonlinear formulation. When considering the large displacements with moderate rotations, the geometric nonlinearity effect can be introduced via the kinematic relations. Despite the nonlinear kinematic relations are used in the formulation, same displacement assumptions of different sheets are still adopted, namely, the faces are considered as Euler-Bernoulli beams with bending and axial rigidities while the core has a high order displacement pattern, given by Eq. (2.3) and Eq. (2.4).

3.1 EHSAPT for Large Displacements with Moderate Rotations

3.1.1 Kinematic Relations

During the deformation, the materials are assumed within the linear elastic region and only geometric nonlinearities are considered. All sheets are considered undergoing large displacements with moderate rotations. If the Green-Lagrange strain is used directly, and recalling the displacement assumptions of the face sheet, listed by Eq. (2.3) and Eq. (2.4), the strain components of the face sheets are

$$\epsilon_{xx}^{t,b}(x,z) = \frac{\partial u^{t,b}(x,z)}{\partial x} + \frac{1}{2}\left[\frac{\partial u^{t,b}(x,z)}{\partial x}\right]^2 + \frac{1}{2}\left[\frac{\partial w^{t,b}(x,z)}{\partial x}\right]^2 \tag{3.1a}$$

$$\epsilon_{zz}^{t,b}(x,z) = \frac{1}{2}\left[\frac{\partial u^{t,b}(x,z)}{\partial z}\right]^2 \tag{3.1b}$$

$$\gamma_{xz}^{t,b}(x,z) = \frac{\partial u^{t,b}(x,z)}{\partial x}\frac{\partial u^{t,b}(x,z)}{\partial z} \tag{3.1c}$$

Compared to the general Green-Lagrange strain, some terms are neglected due to the zero value as a result of Eqs. (2.3)-(2.4). Notice that the Green-Lagrange strain results into non-zero transverse normal strain and shear strain in the face sheets. However, when an Euler-Bernoulli beam is considered, we usually consider only the axial normal strain ϵ_{xx} regardless of the analysis being linear or nonlinear. In the literature, some researchers include these two strain components ϵ_{zz} and γ_{xz} with zero linear part and non-zero nonlinear part in the face sheets, e.g., in Ref. [49]. The effects of these two additional strain components would be discussed later. For convenience, the strain components of the face sheets are written as,

$$\epsilon_{xx}^{t,b}(x,z) = \frac{\partial u^{t,b}(x,z)}{\partial x} + \frac{\alpha_1}{2}\left[\frac{\partial u^{t,b}(x,z)}{\partial x}\right]^2 + \frac{\alpha_2}{2}\left[\frac{\partial w^{t,b}(x,z)}{\partial x}\right]^2 \tag{3.2a}$$

$$\epsilon_{zz}^{t,b}(x,z) = \frac{\alpha_3}{2}\left[\frac{\partial u^{t,b}(x,z)}{\partial z}\right]^2 \tag{3.2b}$$

$$\gamma_{xz}^{t,b}(x,z) = \alpha_4 \frac{\partial u^{t,b}(x,z)}{\partial x}\frac{\partial u^{t,b}(x,z)}{\partial z} \tag{3.2c}$$

where the values of α_i can be 0 or 1. These coefficients are in the nonlinear terms to control whether the corresponding term is included or neglected.

Similarly, the strain components in the core sheet are written as follows:

$$\epsilon_{xx}^{c}(x,z) = \frac{\partial u^{c}(x,z)}{\partial x} + \frac{\beta_1}{2}\left[\frac{\partial u^{c}(x,z)}{\partial x}\right]^2 + \frac{\beta_2}{2}\left[\frac{\partial w^{c}(x,z)}{\partial x}\right]^2 \tag{3.3a}$$

$$\epsilon_{zz}^{c}(x,z) = \frac{\partial w^{c}(x,z)}{\partial z} + \frac{\beta_3}{2}\left[\frac{\partial u^{c}(x,z)}{\partial z}\right]^2 + \frac{\beta_4}{2}\left[\frac{\partial w^{c}(x,z)}{\partial z}\right]^2 \tag{3.3b}$$

$$\begin{aligned}\gamma_{xz}^{c}(x,z) = {} & \frac{\partial u^{c}(x,z)}{\partial z} + \frac{\partial w^{c}(x,z)}{\partial x} + \\ & + \beta_5 \frac{\partial u^{c}(x,z)}{\partial x}\frac{\partial u^{c}(x,z)}{\partial z} + \beta_6 \frac{\partial w^{c}(x,z)}{\partial x}\frac{\partial w^{c}(x,z)}{\partial z}\end{aligned} \tag{3.3c}$$

Again, coefficients β_j $(j = 1...6)$ are used, and their values equal to either 0 or 1. When $\beta_j = 1$, the corresponding term is included in the kinematic relation and vice versa.

Hence, by controlling the different combinations of α_i and β_j, the kinematic relations

can be reduced to the various simplified models. Some particular cases are listed:

1. $\alpha_i = \beta_j = 0$: Linear EHSAPT [21, 99];

2. $\alpha_2 = 1$, $\alpha_i = \beta_j = 0$, $(i \neq 2,\ j = 1...6)$: Only faces nonlinear;

3. $\alpha_2 = 1$, $\alpha_i = \beta_j = 0$, $(i \neq 2,\ j = 1...6)$, and $E_1^c = 0$: Nonlinear HSAPT [38, 44, 45, 48];

4. $\beta_2 = \beta_3 = 1$, $\beta_j = 0$, $(j = 1, 4, 5, 6)$: Neglecting the higher order nonlinear terms of the core, e.g., the $[u^c_{,x}(x,z)]^2$ in comparison to the $u^c_{,x}(x,z)$ in the ϵ^c_{xx}, etc.

The kinematic relations are given by Eqs. (3.2) and (3.3). Similar to Eq. (2.9), the strain vector can be further divided into a linear part and a nonlinear part. Considering the EHSAPT displacement assumptions Eqs.(2.3) and (2.4), the general strain expressions of the faces and the core are represented by the displacement vector, $\{\bar{\boldsymbol{U}}\} = [u_0^t \ \ w_0^t \ \ u_0^b \ \ w_0^b \ \ u_0^c \ \ w_0^c \ \ \phi_0^c]^T$. By collecting terms, it takes following form:

$$\{\boldsymbol{\epsilon}^k\} = \left[\boldsymbol{L}_L^k\right]\{\bar{\boldsymbol{U}}\} + \frac{1}{2}\left[\boldsymbol{L}_{NL}^k\left(\{\bar{\boldsymbol{U}}\}\right)\right]\{\bar{\boldsymbol{U}}\} \qquad k = t, b, c \tag{3.4}$$

where the first term of the right hand side stands for the linear part of the strain vector, and $[\boldsymbol{L}_L^{t,b,c}]$ is the same as the one used in the linear EHSAPT. The second term gives the nonlinear strain part, and $\left[\boldsymbol{L}_{NL}^k\left(\{\bar{\boldsymbol{U}}\}\right)\right]$ is a function of the displacement vector $\{\bar{\boldsymbol{U}}\}$ and depends on the nonlinear coefficients α_i and β_j. It will be denoted as $\left[\boldsymbol{L}_{NL}^k\right]$ for short.

Due to the square terms of the Green-Lagrange strain, the variation form of strain vector is given as,

$$\delta\{\boldsymbol{\epsilon}^k\} = \left(\left[\boldsymbol{L}_L^k\right] + \left[\boldsymbol{L}_{NL}^k\right]\right)\delta\{\bar{\boldsymbol{U}}\} \qquad k = t, b, c \tag{3.5}$$

3.1.2 Constitutive Relations

The stress vector in the three sheets is $\{\boldsymbol{\sigma}^{t,b,c}\} = [\sigma_{xx}^{t,b,c} \ \ \sigma_{zz}^{t,b,c} \ \ \tau_{xz}^{t,b,c}]^T$, and can be obtained by the same constitutive law given by Eq. (2.10) and Eq. (2.12).

In the face sheets, when $\alpha_3 = \alpha_4 = 0$, the stiffness constants of the face sheets are simply $C_{11}^{t,b} = E_1^{t,b}$, and the stresses are $\sigma_{xx}^{t,b} = C_{11}^{t,b}\epsilon_{xx}^{t,b}$. When $\alpha_3 = 1$, or $\alpha_4 = 1$, $C_{ij}^{t,b}$ are obtained in the same way as the core.

3.2 Element Formulation with Geometric Nonlinearity

As described in Section 2.2.1, the EHSAPT-based element can have 2 nodes or more than 2 nodes. Here, the 2-node element will be used due to its simplicity and high accuracy shown in linear static cases. Hence, when the sandwich beam is discretized by m elements, there are $n = m + 1$ nodes totally.

Using the element displacement vector $\{\tilde{\boldsymbol{U}}(s)\}$ of Eq. (2.19) instead of the midline displacement $\{\bar{\boldsymbol{U}}\}$, which appears in Eqs. (2.3) and (2.4), and plugging into Eq. (3.4), the strain is expressed in terms of the element nodal displacements, as follows:

$$\{\boldsymbol{\epsilon}^k\} = [\boldsymbol{B}_L^k]\{\boldsymbol{U}_e\} + \frac{1}{2}[\boldsymbol{B}_{NL}^k]\{\boldsymbol{U}_e\} \qquad k = t, b, c \tag{3.6}$$

where $[\boldsymbol{B}_L^k] = [\boldsymbol{L}_L^k][\boldsymbol{N}(s)]$ and $[\boldsymbol{B}_{NL}^k] = [\boldsymbol{L}_{NL}^k][\boldsymbol{N}(s)]$. Notice that $[\boldsymbol{B}_L^k]$ is the same as the one used in the linear analysis given by Eq. (2.21c) and is independent of $\{\boldsymbol{U}_e\}$. The second part stands for the nonlinear part $\{\boldsymbol{\epsilon}_{NL}\}$, and $[\boldsymbol{B}_{NL}^k]$ depends on $\{\boldsymbol{U}_e\}$.

In the top and bottom faces, $[\boldsymbol{B}_{NL}^t]$ and $[\boldsymbol{B}_{NL}^b]$ are given as,

$$[\boldsymbol{B}_{NL}^k] = \begin{Bmatrix} \alpha_1 \frac{\partial[\tilde{\boldsymbol{N}}_u^k]}{\partial x}\{\boldsymbol{U}_e\}\frac{\partial[\tilde{\boldsymbol{N}}_u^k]}{\partial x} + \alpha_2 \frac{\partial[\tilde{\boldsymbol{N}}_w^k]}{\partial x}\{\boldsymbol{U}_e\}\frac{\partial[\tilde{\boldsymbol{N}}_w^k]}{\partial x} \\ \alpha_3 \frac{\partial[\tilde{\boldsymbol{N}}_u^k]}{\partial z}\{\boldsymbol{U}_e\}\frac{\partial[\tilde{\boldsymbol{N}}_u^k]}{\partial z} \\ \alpha_4 \left(\frac{\partial[\tilde{\boldsymbol{N}}_u^k]}{\partial x}\{\boldsymbol{U}_e\}\frac{\partial[\tilde{\boldsymbol{N}}_u^k]}{\partial z} + \frac{\partial[\tilde{\boldsymbol{N}}_u^k]}{\partial z}\{\boldsymbol{U}_e\}\frac{\partial[\tilde{\boldsymbol{N}}_u^k]}{\partial x} \right) \end{Bmatrix} \qquad k = t, b \tag{3.7a}$$

In the core, $[\boldsymbol{B}^c_{NL}]$ is given as,

$$[\boldsymbol{B}^c_{NL}] = \begin{Bmatrix} \beta_1 \frac{\partial[\tilde{\boldsymbol{N}}^c_u]}{\partial x}\{\boldsymbol{U}_e\}\frac{\partial[\tilde{\boldsymbol{N}}^c_u]}{\partial x} + \beta_2 \frac{\partial[\tilde{\boldsymbol{N}}^c_w]}{\partial x}\{\boldsymbol{U}_e\}\frac{\partial[\tilde{\boldsymbol{N}}^c_w]}{\partial x} \\ \beta_3 \frac{\partial[\tilde{\boldsymbol{N}}^c_u]}{\partial z}\{\boldsymbol{U}_e\}\frac{\partial[\tilde{\boldsymbol{N}}^c_u]}{\partial z} + \beta_4 \frac{\partial[\tilde{\boldsymbol{N}}^c_w]}{\partial z}\{\boldsymbol{U}_e\}\frac{\partial[\tilde{\boldsymbol{N}}^c_w]}{\partial z} \\ \beta_5 \left(\frac{\partial[\tilde{\boldsymbol{N}}^c_u]}{\partial x}\{\boldsymbol{U}_e\}\frac{\partial[\tilde{\boldsymbol{N}}^c_u]}{\partial z} + \frac{\partial[\tilde{\boldsymbol{N}}^c_u]}{\partial z}\{\boldsymbol{U}_e\}\frac{\partial[\tilde{\boldsymbol{N}}^c_u]}{\partial x}\right) + \beta_6 \left(\frac{\partial[\tilde{\boldsymbol{N}}^c_w]}{\partial x}\{\boldsymbol{U}_e\}\frac{\partial[\tilde{\boldsymbol{N}}^c_w]}{\partial z} + \frac{\partial[\tilde{\boldsymbol{N}}^c_w]}{\partial z}\{\boldsymbol{U}_e\}\frac{\partial[\boldsymbol{N}^c_w]}{\partial x}\right) \end{Bmatrix} \tag{3.7b}$$

The variation of the strain is

$$\delta\{\boldsymbol{\epsilon}^k\} = \left([\boldsymbol{B}^k_L] + [\boldsymbol{B}^k_{NL}]\right)\delta\{\boldsymbol{U}_e\} \qquad k = t, b, c \tag{3.8}$$

3.2.1 Nonlinear Element Matrix

Same as the linear EHSAPT-based element formulation, the nonlinear element stiffness matrix comes from the minimization of the total element potential energy that consists of the strain energy of top face, core, and bottom face and the work of external load, as shown in Eq. (2.23). By plugging the nonlinear strain expressions Eq. (3.6) into Eq. (2.23) and taking the variation principal, the element stiffness matrix is computed by

$$\begin{aligned} [\boldsymbol{K}_e] =& [\boldsymbol{K}_{e_L}] + [\boldsymbol{K}_{e_{NL}}] \\ =& \sum_{k=t,b,c} [\boldsymbol{K}^k_{e_L}] + \sum_{k=t,b,c} [\boldsymbol{K}^k_{e_{NL}}] \end{aligned} \tag{3.9a}$$

with

$$[\boldsymbol{K}^k_{e_L}] = \iint_{v^k} [\boldsymbol{B}^k_L]^T [\boldsymbol{C}^k][\boldsymbol{B}^k_L] dzds \qquad k = t, b, c \tag{3.9b}$$

$$\begin{aligned} [\boldsymbol{K}^k_{e_{NL}}] = & \iint_{v^k} \left(\tfrac{1}{2}[\boldsymbol{B}^k_L]^T[\boldsymbol{C}^k][\boldsymbol{B}^k_{NL}] + \tfrac{1}{2}[\boldsymbol{B}^k_{NL}]^T[\boldsymbol{C}^k][\boldsymbol{B}^k_{NL}]\right. \\ & \left. + [\boldsymbol{B}^k_{NL}]^T[\boldsymbol{C}^k][\boldsymbol{B}^k_L]\right) dzds \qquad k = t, b, c \end{aligned} \tag{3.9c}$$

where v^k stands for the space domain of the top face, the bottom face, or the core within the element. $[\boldsymbol{K}_{e_L}]$ is the linear part, which is the same as the one used in the linear

small deformation analysis given by Eq. (2.25), and $[\boldsymbol{K}_{e_{NL}}]$ is the nonlinear part and is the function of the displacement vector. When the nonlinear coefficients α_i and β_j all equal to zero, $[\boldsymbol{K}_{e_{NL}}]$ is eliminated. In this case, only the linear part is left and it is exactly the same as the one used in the linear analysis in Chapter 2.

Assembling the element matrices yields the structural stiffness matrix $[\boldsymbol{K}]$. $[\boldsymbol{K}]$ is also called the secant stiffness matrix. It contains a linear part and a nonlinear part. Both face sheets and the core contribute to these two parts. The structural force vector $\{\boldsymbol{R}\}$ and displacement vector $\{\boldsymbol{U}\}$ are the same as those that appear in the linear static analysis. Therefore, the weak form equilibrium equations are given as,

$$\{\boldsymbol{G}(\{\boldsymbol{U}\},\lambda)\} = [\boldsymbol{K}]\{\boldsymbol{U}\} - \{\boldsymbol{R}\} = \{\boldsymbol{0}\} \tag{3.10}$$

Eq. (3.10) gives the nonlinear governing equations of sandwich panels in equilibrium state. The arc-length method [92, 93] is used to solve this nonlinear problem and to track the equilibrium path.

3.2.2 Tangent Stiffness Matrix of the EHSAPT-based Element

The Jacobian matrix of Eq. (3.10) is usually required in the iterative solving procedure for nonlinear equations. The Jacobian matrix of Eq. (3.10) is also called the tangent stiffness matrix and is given by

$$[\boldsymbol{K}_T] = \frac{\partial\{\boldsymbol{G}(\{\boldsymbol{U}\},\lambda)\}}{\partial\{\boldsymbol{U}\}} \tag{3.11}$$

$[\boldsymbol{K}_T]$ can be approximated by numerical differential for simplicity. The tangent stiffness is also needed in the stability analysis of sandwich panels, and an accurate tangent stiffness matrix is required to obtained a good estimation of critical buckling loads and switching equilibrium branches of the post-buckling response. Thus, the explicit formula of tangent stiffness is given and used herein. Taking the variation of Eq. (3.10) yields the tangent stiffness matrix. Similar to the element stiffness matrix, the element tangent stiffness of the

EHSAPT-based element has a linear part and the rest is nonlinear,

$$\begin{aligned}[\boldsymbol{K}_{T_e}] =& [\boldsymbol{K}_{e_L}] + [\boldsymbol{K}_{T1_e}] + [\boldsymbol{K}_{T2_e}] \\ =& \sum_{k=t,b,c} [\boldsymbol{K}^k_{e_L}] + \sum_{k=t,b,c} [\boldsymbol{K}^k_{T1_e}] + \sum_{k=t,b,c} [\boldsymbol{K}^k_{T2_e}]\end{aligned} \tag{3.12a}$$

where the linear part $[\boldsymbol{K}^k_{e_L}]$ is the same as the linear element stiffness matrix and is given by Eq. (3.9b), and other nonlinear parts related to the nodal displacement are

$$\begin{aligned}[\boldsymbol{K}^k_{T1_e}] = \quad & \iint_{v^k} \left([\boldsymbol{B}^k_L]^T [\boldsymbol{C}^k] [\boldsymbol{B}^k_{NL}] + [\boldsymbol{B}^k_{NL}]^T [\boldsymbol{C}^k] [\boldsymbol{B}^k_{NL}] \right. \\ & \left. + [\boldsymbol{B}^k_{NL}]^T [\boldsymbol{C}^k] [\boldsymbol{B}^k_L] \right) dzds \qquad\qquad k = t, b, c\end{aligned} \tag{3.12b}$$

$$\begin{aligned}[\boldsymbol{K}^k_{T2_e}] = \quad & \iint_{v^k} \sigma^k_{xx} \left(\alpha_1 \frac{\partial[\tilde{\boldsymbol{N}}^k_u]^T}{\partial x} \frac{\partial[\tilde{\boldsymbol{N}}^k_u]}{\partial x} + \alpha_2 \frac{\partial[\tilde{\boldsymbol{N}}^k_w]^T}{\partial x} \frac{\partial[\tilde{\boldsymbol{N}}^k_w]}{\partial x} \right) dzds \\ & + \iint_{v^k} \sigma^k_{zz} \left(\alpha_3 \frac{\partial[\tilde{\boldsymbol{N}}^k_u]^T}{\partial z} \frac{\partial[\tilde{\boldsymbol{N}}^k_u]}{\partial z} \right) dzds \\ & + \iint_{v^k} \tau^k_{xz} \left(\alpha_4 \frac{\partial[\tilde{\boldsymbol{N}}^k_u]^T}{\partial x} \frac{\partial[\tilde{\boldsymbol{N}}^k_u]}{\partial z} + \alpha_4 \frac{\partial[\tilde{\boldsymbol{N}}^k_u]^T}{\partial z} \frac{\partial[\tilde{\boldsymbol{N}}^k_u]}{\partial x} \right) dzds \qquad k = t, b\end{aligned} \tag{3.12c}$$

$$\begin{aligned}[\boldsymbol{K}^c_{T2_e}] = \quad & \iint_{v^c} \sigma^c_{xx} \left(\beta_1 \frac{\partial[\tilde{\boldsymbol{N}}^c_u]^T}{\partial x} \frac{\partial[\tilde{\boldsymbol{N}}^c_u]}{\partial x} + \beta_2 \frac{\partial[\tilde{\boldsymbol{N}}^c_w]^T}{\partial x} \frac{\partial[\tilde{\boldsymbol{N}}^c_w]}{\partial x} \right) dzds \\ & + \iint_{v^c} \sigma^c_{zz} \left(\beta_3 \frac{\partial[\tilde{\boldsymbol{N}}^c_u]^T}{\partial z} \frac{\partial[\tilde{\boldsymbol{N}}^c_u]}{\partial z} + \beta_4 \frac{\partial[\tilde{\boldsymbol{N}}^c_w]^T}{\partial z} \frac{\partial[\tilde{\boldsymbol{N}}^c_w]}{\partial z} \right) dzds \\ & + \iint_{v^c} \tau^c_{xz} \left(\beta_5 \frac{\partial[\tilde{\boldsymbol{N}}^c_u]^T}{\partial x} \frac{\partial[\tilde{\boldsymbol{N}}^c_u]}{\partial z} + \beta_5 \frac{\partial[\tilde{\boldsymbol{N}}^c_u]^T}{\partial z} \frac{\partial[\tilde{\boldsymbol{N}}^c_u]}{\partial x} \right. \\ & \qquad \left. + \beta_6 \frac{\partial[\tilde{\boldsymbol{N}}^c_w]^T}{\partial x} \frac{\partial[\tilde{\boldsymbol{N}}^c_w]}{\partial z} + \beta_6 \frac{\partial[\tilde{\boldsymbol{N}}^c_w]^T}{\partial z} \frac{\partial[\tilde{\boldsymbol{N}}^c_w]}{\partial x} \right) dzds\end{aligned} \tag{3.12d}$$

3.3 Numerical Examples of Static Behavior

In this part, two sandwich panels loaded in three point bending will be analyzed with the 2-node EHSAPT-based element including the geometric nonlinearities. Two different core materials will be used, in order to investigate the relative merits of various simplifications on the nonlinear kinematic relations. The results will also be compared to numerical results obtained by the commercial finite element code ADINA.

The geometry follows the sandwich panel used by Frostig et al. [48]. The length of the panel is $a = 300$ mm. It contains two face sheets with same thickness, $f_t = f_b = 0.50$

mm, and a core of thickness $2c = 19.05$ mm. The top and bottom face sheets are made out of Kevlar with equivalent modulus of elasticity of 27.4 GPa. The core is made out of lightweight foam, Rohacell 50, with extensional modulus equal to 52.5 MPa and shear modulus, $G_{31}^c = 21.0$ MPa or Rohacell 200 WF with extensional modulus 350.0 MPa and shear modulus 150.0 MPa. A concentrated load is applied at the middle, and the beam/panel is loaded in three point bending. The displacement constraint is applied at the lower surface, i.e., the edges of the bottom sheet. Since the geometric and loading exhibits symmetry about the mid-span, only the left half beam is analyzed. Together with the symmetry conditions, the boundary conditions applied to the EHSAPT-based finite element model are

$$w_1^b = 0 \qquad \text{[first node]} \tag{3.13a}$$

$$u_n^t = u_n^b = u_n^c = 0 \qquad \text{[last node]} \tag{3.13b}$$

$$\left(\frac{dw^t}{dx}\right)_n = \left(\frac{dw^b}{dx}\right)_n = \left(\frac{dw^c}{dx}\right)_n = \phi_n^c = 0 \qquad \text{[last node]} \tag{3.13c}$$

To ensure accuracy, 340 EHSAPT-based 2-node elements are used to build this half beam model. That's $m = 340$ and $n = m + 1 = 341$. Furthermore, the elements are non-uniformly distributed and placed with a bias towards the edges and the center of the beam, where load concentrations occur.

The commercial FEA software ADINA is used to compare the results. It is well known that numerous issues may happen when using commercial software like numerical difficulties and poor convergence. Thus, extra attention is needed to build the nonlinear finite element model. A two-dimensional model with very fine mesh is built, as shown in Fig. 3.1. The nine-node plane stress element is used to model the face sheets and core. Through the thickness direction, 4 elements are used in the face sheets and 15 elements are placed in the core. There is a total of 19,787 nodes in the model. The large displacement and small strain analysis control option is chosen to consider the geometric nonlinearities.

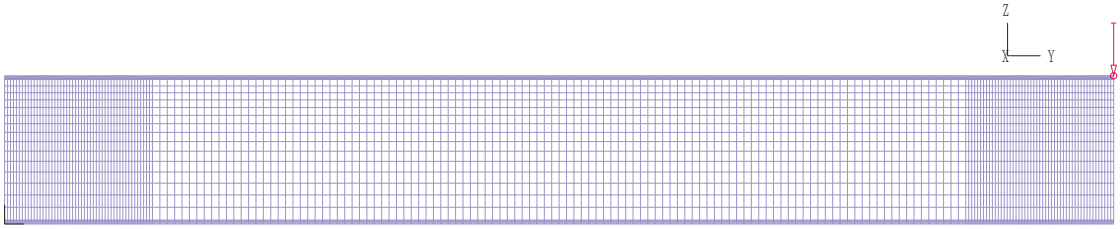

Figure 3.1: Two-dimensional finite element model in ADINA

3.3.1 Example 1: Soft Core Sandwich Panel

The first example to consider is a sandwich panel with a low density very soft core, Rohacell 50 foam. Various simplified models, which are reflected by the different combinations of coefficients α_i and β_j are used. The corresponding applied load versus transverse displacement curves at the middle point of top face are given in Fig. 3.2. The middle point is where the load is applied and where the maximum transverse displacement is reached. These curves are denoted as curves 0 to 12 for convenience. Curve 0 is the result based on the linear version of EHSAPT, neglecting all nonlinear terms. The linear kinematic relation, infinitesimal strain, is used and displacement is proportional to the applied load. The result obtained by the commercial FE code ADINA is included in the figure as curve 12. Due to numerical issues, ADINA cannot yield further results for displacements larger than 14 mm. The curve goes back because elements are distorted. The element edges would penetrate each other under higher load. When changing the mesh size and the load step size, this issue cannot be overcome. This numerical issue always happens around that point and it is interesting to notice that models with coarse elements can indeed go a little bit further. The other curves are results using EHSAPT with different coefficients α_i and β_j. Only the coefficients with values equal to 1, are noted, and all others are assumed to be equal to zero. With the exception of the linear result, curve 0, all other curves exhibit nonlinear response when the load is higher than 500 N. When the load is under 500 N, and the maximum transverse displacement smaller than 3.5 mm, all curves agree well and are almost identical to the linear result, this is the region where the infinitesimal strain relation is

valid. Under higher applied load, notable discrepancies among the different simplifications are observed.

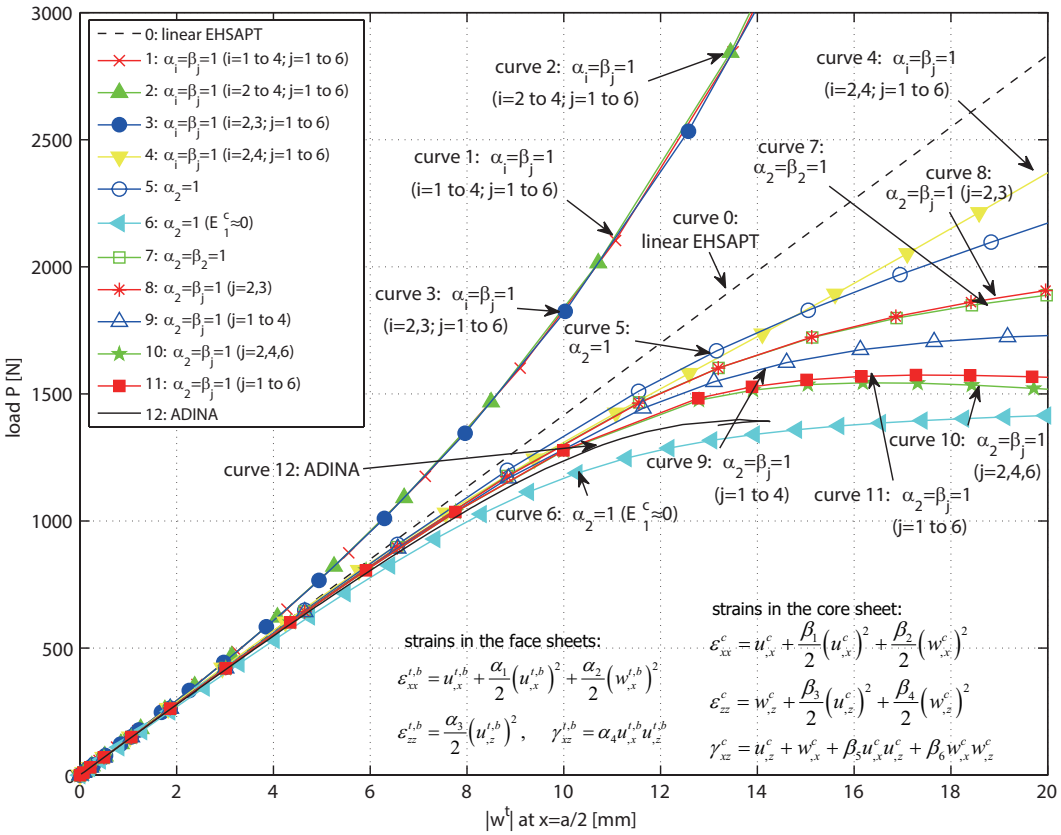

Figure 3.2: Load versus mid-span displacement of sandwich panel with soft core

Curves 1 to 4 consider the transverse normal strain $\epsilon_{zz}^{t,b}$ or/and transverse shear strain $\gamma_{xz}^{t,b}$ in the faces. These two strain components are the consequence of using the Green-Lagrange strain directly under the assumed displacement field of the faces. These three curves show a distinctly different nonlinear behavior when compared to the other results, including ADINA. According to these curves, the sandwich panel becomes stiffer when the load is increased, which is unreasonable. This unusual result is because the nonzero nonlinear terms of transverse normal stain and transverse shear strain cause the sandwich panel to be "locked". Recall that the Euler-Bernoulli assumptions used in the face sheets imply that the transverse rigidity and shear modulus are large enough that there is no transverse

normal strain and shear strain in the face sheets (these assumptions are expressed in the displacement field). Any nonzero transverse normal strain and shear would cause a large stress component that would make the beam to be locked. Hence, only the axial normal strain should be considered in the face sheets. There is no problem in the linear analysis since $\epsilon_{zz}^{t,b}$ and $\gamma_{xz}^{t,b}$ vanish automatically. However, when considering large displacements and using the Green-Lagrange strain in the faces, α_3 and α_4 should be zero in order to be in agreement with the Euler-Bernoulli assumptions. In addition, α_1 can also be zero since $(u_{,x}^{t,b})^2$ usually can be neglected compared to $(w_{,x}^{t,b})^2$, which can be seen from curves 1 and 2. So, the strain that needs to be considered in the faces should the same as the ordinary Euler-Bernoulli beam, i.e. only $\alpha_2 = 1$.

Curve 5 and 6 are the results when the nonlinear kinematic relation is only used in the faces while the core is assumed to retain the linear kinematic relation. This is the most commonly used assumption in sandwich panel nonlinear theories that considering the geometric nonlinearities, e.g., Ref. [44–46, 48]. These two curves exhibit the same softening tendency as ADINA and the other models. Curve 6 neglects the axial rigidity of the core by setting $E_1^c = 52.5 \times 10^{-5}$ MPa, as an approximation to zero. This degenerates the nonlinear EHSAPT to the nonlinear HSAPT. As expected, it yields similar results as using nonlinear HSAPT directly [48]. A limit point is observed in curve 6 around 1438 N while it is reported as 1423 N in Ref. [48]. Since the axial rigidity is neglected, curve 6 is the lowest curve among these results, even in the linear region.

Curves 7 to 11 list several representative simplified models that include full or part of the nonlinear kinematic relation in the core. Curve 7 only includes the same nonlinear term as the faces, $(w_{,x}^{t,b})^2$, and the other terms are neglected. Curve 8 neglects the higher order nonlinear terms (i.e. it neglects $(u_{,x}^c)^2$ in comparison to $u_{,x}^c$ in the ϵ_{xx}^c, $(w_{,z}^c)^2$ in comparison to $w_{,z}^c$ in the ϵ_{zz}^c, $u_{,x}^c u_{,z}^c$ in comparison to $u_{,z}^c$ in γ_{xz}^c, and $w_{,x}^c w_{,z}^c$ in comparison to $w_{,x}^c$ in γ_{xz}^c). These two yield almost same results. Curve 9 takes the full nonlinear expressions of ϵ_{xx}^c and ϵ_{zz}^c and only the linear part in the shear strain γ_{xz}^c. Curve 11 includes all the

nonlinear terms in the core while curve 10 only includes the nonlinear terms related to the transverse displacement. These two are very close to each other. Among these results, curves 10 and 11 are the two results that are the closest to ADINA. To this point, one may draw the conclusion that the nonlinear strain terms of the core have a great effect and cannot be neglected. Also, it can be concluded that the nonlinear effects caused by the transverse deflection have a more pronounced effect. It can also be seen that the EHSAPT-based element can get the whole response curves without any numerical difficulties while the ADINA fails to converge at some point in the nonlinear region.

A comparison between the nonlinear EHSAPT and the linear EHSAPT appears in Fig. 3.3. It plots the axial and transverse displacements along the axial direction at load $P = 1300$ N. The nonlinear EHSAPT refers to the case of $\alpha_2 = \beta_j = 1, (j = 1...6)$ and is plotted with line. The linear EHSAPT is plotted with markers. The linear EHSAPT and nonlinear analysis give similar transverse displacement distribution while the axial displacements are completely different. The linear analysis predicts the axial displacement of the three sheets as a symmetric pattern, the top face and bottom face rotate with respect to the core. But when the geometric nonlinearities are included, the edges would move towards to the center. Although the transverse deflections along the x direction are similar in these analysis, it can be seen that the localized effect (local dimpling at the load application) can only be captured when considering the large displacement and nonlinear kinematic relation. Thus, it is necessary to include the geometric nonlinearities in order to obtain accurate displacement results that includes the local dimpling.

Fig. 3.4 and Fig. 3.5 give the through-thickness strain and stress distributions of the core at $P = 1300$ N. Both EHSAPT ($\alpha_2 = \beta_j = 1,\ j = 1...6$) and ADINA results are given. Green-Lagrange strains are used by both EHSAPT and ADINA. The conjugate stress is the second Piola-Kirchhoff stress. Since the direct stress output of ADINA is the Cauchy stress, the stress results denoted as ADINA are the corresponding second Piola-Kirchhoff stress results obtained based on the constitutive law and the ADINA strain result. The

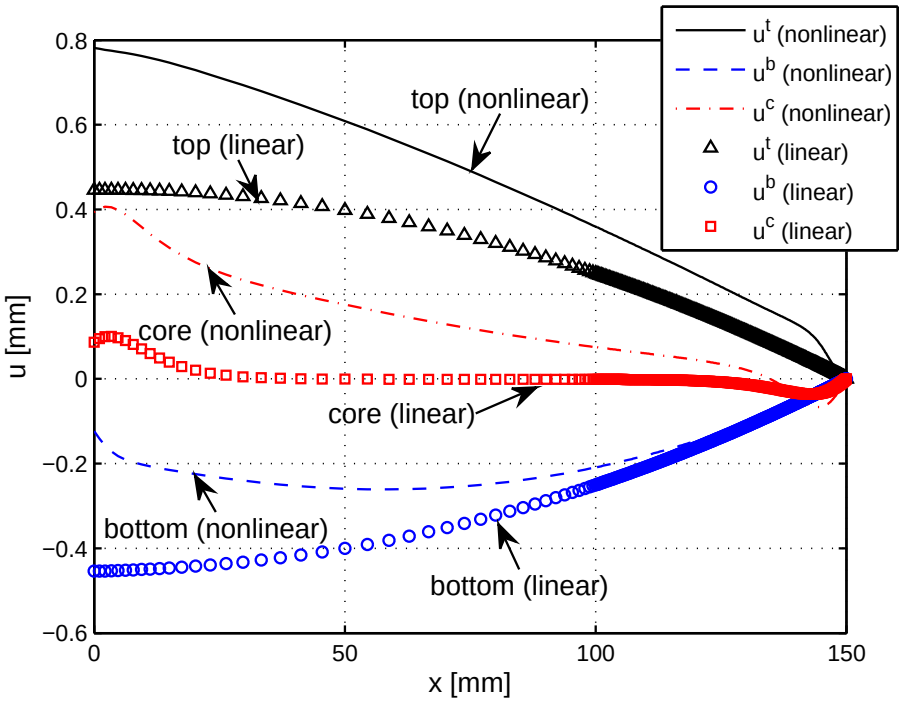

(a)

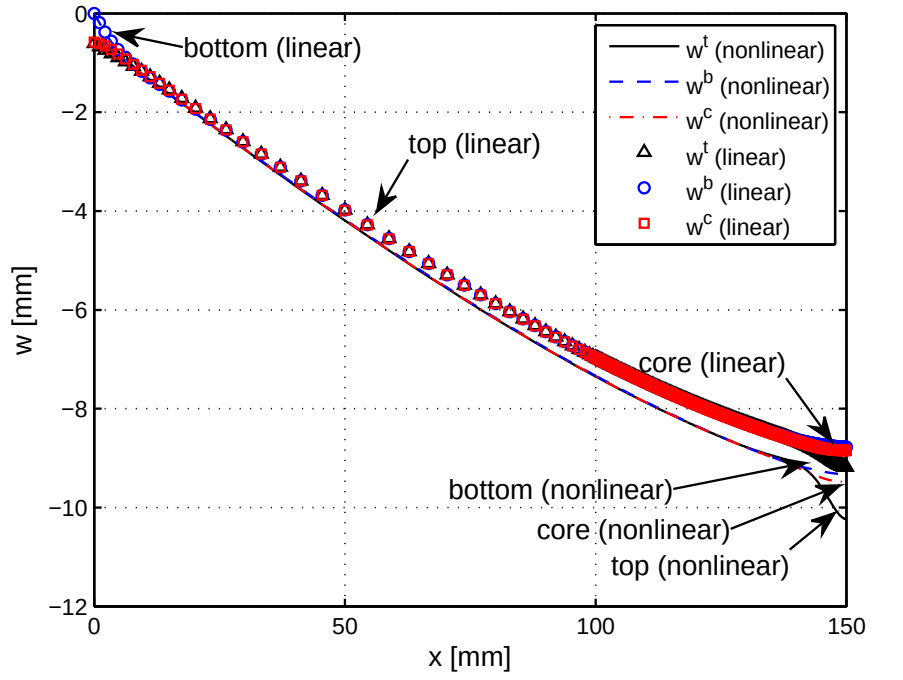

(b)

Figure 3.3: Displacement profile in faces and core at $P = 1300$ N: (a) axial displacement; (b) transverse displacement

linear EHSAPT results are also plotted. Fig. 3.4 is the cross section located at $x = 0.5a$ (load application) and Fig. 3.5 is at $x = 0.4a$. Recall the displacement assumptions used in EHSAPT, namely the axial displacement field of the core, u^c, is assumed to be a cubic function of z, while the transverse displacement, w^c, is a quadric polynomial, as shown in Eqs. (2.3) and (2.4). Hence, the linear part (major part) of the ϵ^c_{zz} can only be a linear function of z. The axial strain ϵ^c_{xx} and shear strain γ^c_{xz} along the z direction are cubic functions. So, the EHSAPT is not expected to yield the exactly same strain and stress distributions as ADINA in cases that the distribution exhibits a high nonlinearity but rather, an approximated result. For example, at $x = 0.5a$, where the concentrated load is applied, the strains and stresses have extreme high values near load concentration. Hence, EHSAPT gives a reasonable approximation to the ADINA results, shown in Fig. 3.4. It should be pointed out that, only one element is used by EHSAPT through the thickness, while 15 elements are used in the ADINA model through the thickness. Fig. 3.5 gives the strain and stress results at $x = 0.4a$ ($x = 120$ mm). At this location, the axial normal strain and stress is exactly the same as ADINA. Also, a good approximated result is obtained for the shear strain and stress. The transverse normal stresses are not the same, due to the linear transverse strain implied by the EHSAPT displacement field assumption, plotted in Fig. 3.5b. But EHSAPT gives the same stress magnitude level. This is an unavoidable limitation of EHSAPT. Both Figs. 3.4 and 3.5 show that the linear EHSAPT is not adequate to predict the strains and stresses when $P = 1300$ N and that the geometric nonlinearities have a very noticeable effect on the strain and stress distributions.

In addition to the stress, the resultant force is another way to measure the load distribution among the different sheets for sandwich structures. Sometimes it is more meaningful and can illustrate how the load is transmitted between the different sheets. Fig. 3.6 plots the resultant force of the three sheets. Both EHSAPT results and ADINA results are given. To compare the resultant force magnitude in each sheet, the resultant force of the top face is given with a negative value. Fig. 3.6 shows that EHSAPT yields almost the same resultant

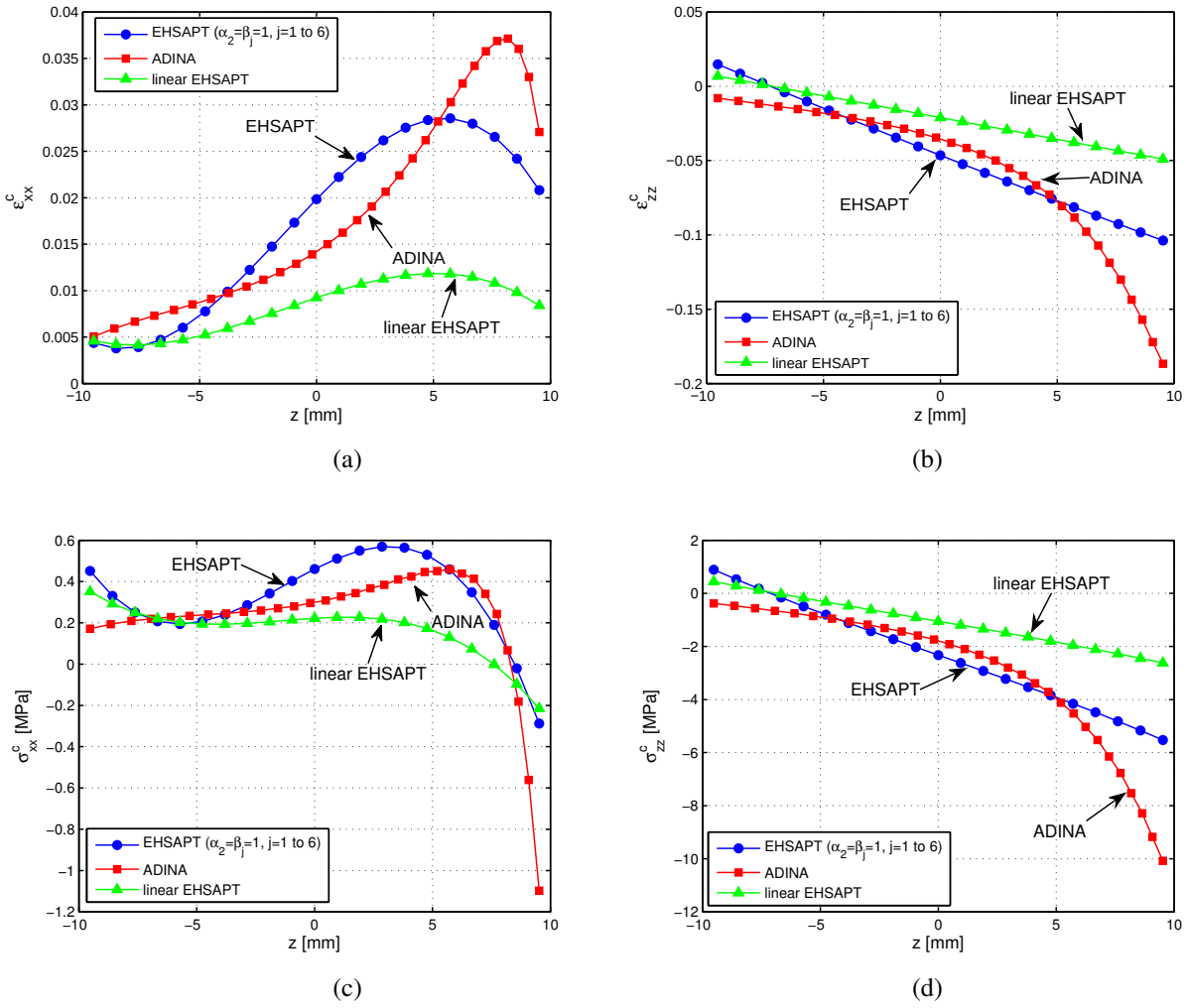

Figure 3.4: Strain and stress distribution in the core at $x = 0.5a$: (a) axial strain; (b) transverse normal strain; (c) axial stress; (d) transverse normal stress

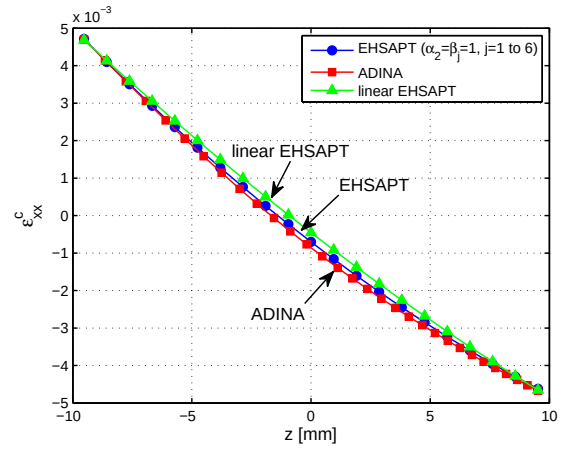

(a)

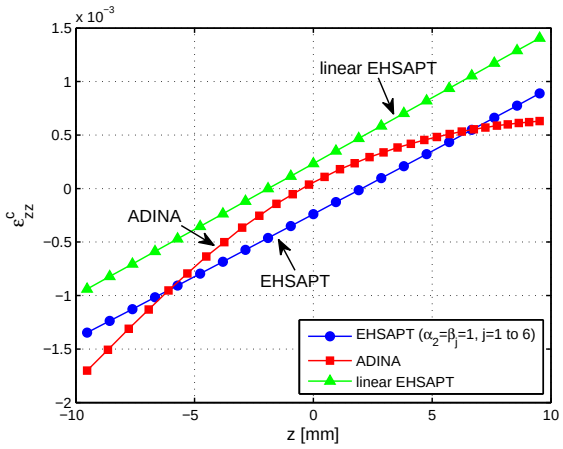

(b)

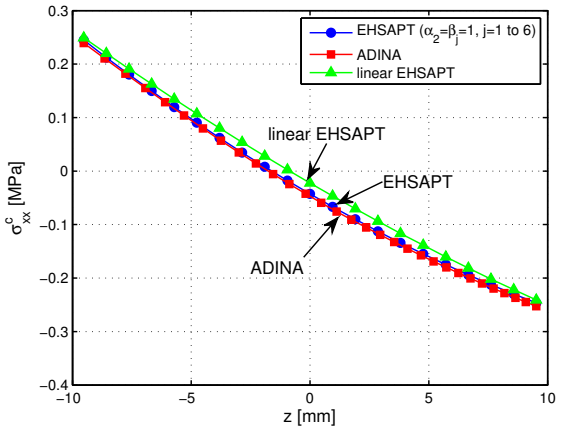

(c)

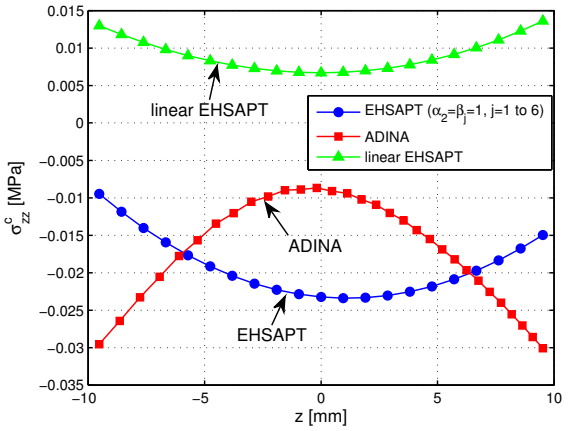

(d)

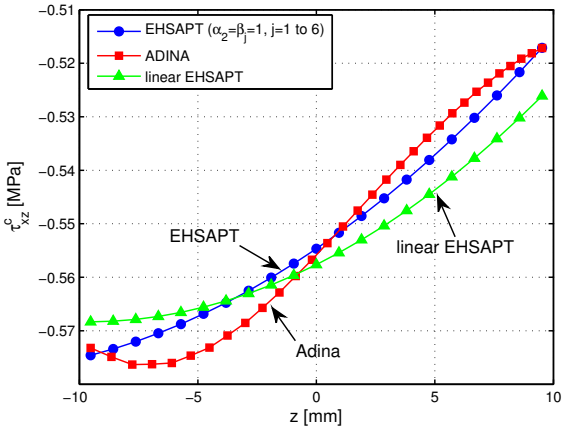

(e)

Figure 3.5: Strain and stress distribution in the core at $x = 0.4a$: (a) axial strain; (b) transverse normal strain; (c) axial stress; (d) transverse normal stress, and (e) transverse shear stress

axial force as ADINA, before ADINA fails. It is seen that the resultant force in the bottom face keeps increasing as the panel deforms but the resultant force in the top face increases initially and eventually drops down. The resultant force in the core is much smaller than that of the faces. This resultant axial force response reveals clearly the details of the non-linear behavior of a sandwich beam under three point bending. In a sandwich structure, the bending moment is mainly balanced by the faces. With the moment caused by an axial internal force in the top and bottom faces, the external load is balanced. In the example considered, the top face is in compression while the bottom face is in tension. With the increasing of the applied load, the top face buckles since it is under compression. Once it reaches its limit point, it cannot take more axial load, the bottom face and the core become the only components to bear the load. That is why initially the axial load of the top face is similar to that in the bottom, but at some point, the resultant force in the top face starts to drop while the force in the bottom face still increases and has a larger magnitude then the top face.

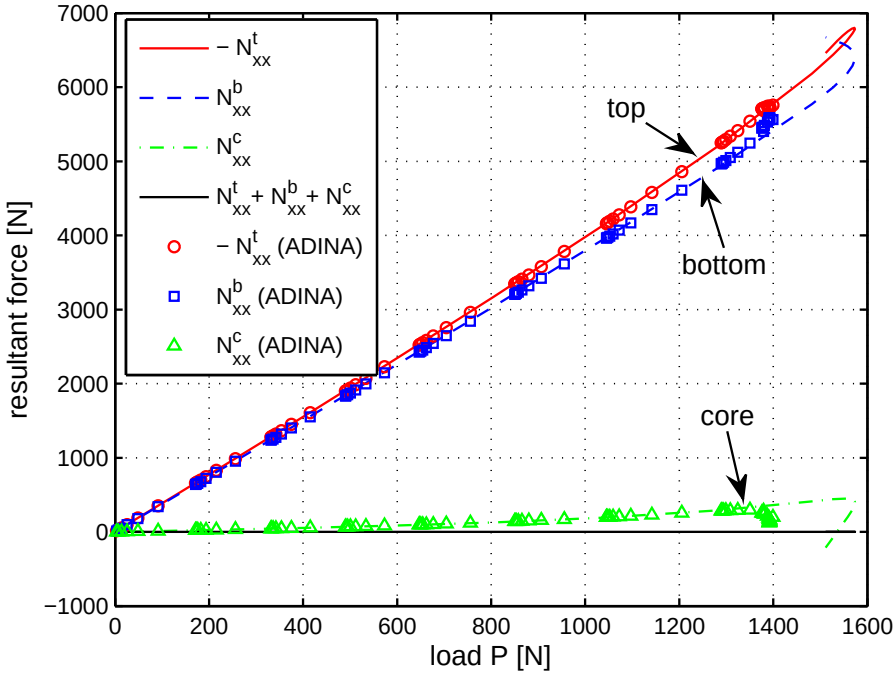

Figure 3.6: Resultant axial force versus applied load

3.3.2 Example 2: Moderate Core Sandwich Panel

In this example, the geometry, loading conditions and boundary conditions are the same as in the previous example. Kevlar is used to construct the faces and similar foam, but with higher stiffness, Rohacell 200 WF is used as the core material. Rohacell 200 WF has a higher density with higher elastic modulus, and its elastic modulus is 350.0 MPa and its shear modulus is 150.0 MPa. Thus, it is about 7 times stiffer than Rohacell 50, which was used in the first example.

The transverse deflection at mid-span of the top face versus the applied load curves are given in Fig. 3.7. Several selected simplified cases are included. Curve 0 is the linear EHSAPT result. Curve 5 is the result from ADINA. Curves 1 to 4 are the nonlinear EHSAPT results. In these curves, the face sheet only considers one nonlinear term, the $(w^{t,b}_{,x})^2$. Due to the stiffer material used in the core, the response predicted by ADINA is closer to the linear result (curves up to a deflection value of 20mm). It should be noticed that the commonly used assumption, that the face sheet undergoes large displacement only and the core employs the linear kinematic relation, leads to a stiffer nonlinear response, which is unrealistic. Indeed, when the nonlinear kinematic relation is only included in the faces (curve 1), the slope becomes larger and the curve 1 is above the linear result. Curve 2 represents the case that only uses the nonlinear kinematic relation in the faces, but the axial rigidity of the core is neglected. It degenerates the EHSAPT to the nonlinear HSAPT. Curve 2 lies on the lower side of the linear results, but it is much lower than the ADINA results, even in the small deflection part. Curves 3 and 4 are the results when using the nonlinear kinematic relation in both faces and core. Again, they yield the closest result to the commercial software ADINA. Even when only one nonlinear term $(w^{c}_{,x})^2$ is considered in the core (in addition to the faces), the result is much improved, as shown as curve 3. This example shows that it is not sufficient to only consider the large displacement and geometric nonlinearities in the faces, especially when the core has high rigidity. In that case, the results may even be worse than the linear analysis result.

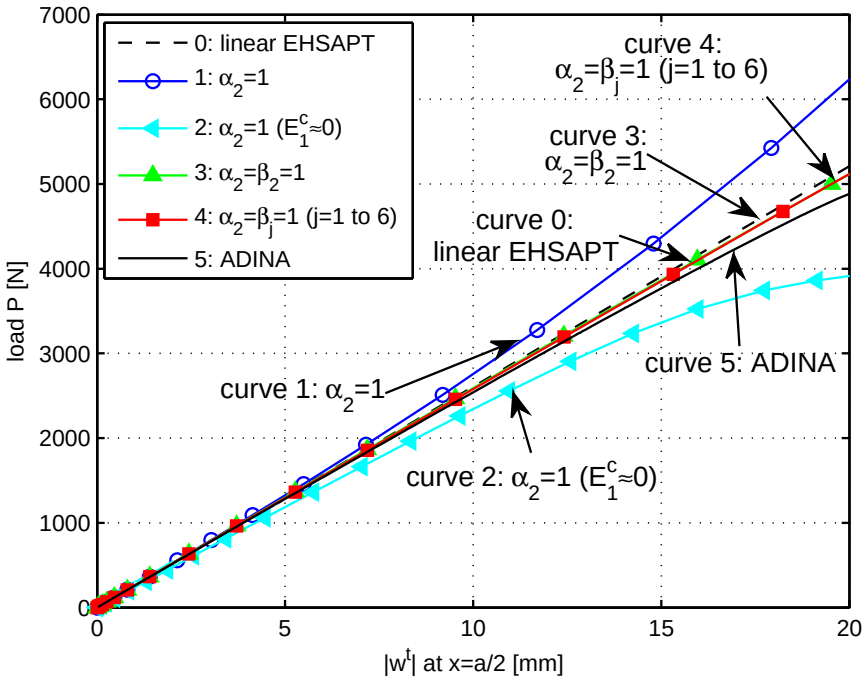

Figure 3.7: Load versus mid-span displacement of sandwich panel with moderate core

3.4 Conclusions

The geometric nonlinear effects in sandwich panels are analyzed based on the EHSAPT. Large displacements with moderate rotations are considered in both faces and the core, and the Green-Lagrange strain is used in all layers. In addition, the previously developed EHSAPT-based element (which was used to solve the linear static problem) is further developed to include the geometric nonlinearity effects. The nonlinear response is successfully obtained with the arc-length method. In the literature, various simplifications have been made when considering the large deformation of sandwich structures. These simplifications are critically assessed. Thus, a series of simplified models are derived, analyzed, and compared to verify the validity of these assumptions.

By comparison with results obtained by the commercial FEA software ADINA, the proposed method and solving procedure are verified. The numerical examples reveal that these simplified kinematic relations yield similar results under small deformations, where

the response is almost linear. When the sandwich panel exhibits nonlinear behavior, divergences are observed. It is concluded that in the faces, only the axial normal strain nonlinear term should be included. The transverse normal strain and shear strain nonlinear terms of the faces should not be included because they come from the nonlinear terms of the Green-Lagrange strain and violate the Euler-Bernoulli assumption adopted in the faces by the EHSAPT. When the axial rigidity of the core is considered, as in the EHSAPT, the geometric nonlinearities of the core are important and cannot be ignored, especially when the core is of higher stiffness. In this case, considering that only the faces undergo large deformation can lead to a stiffer response, which is unrealistic. For other theories that neglect the axial rigidity of the core, such as the HSAPT, considering the large displacement only in the faces can still get the correct response tendency. But the response curve is lower, and the deformation is larger than it is expected, even at the small deformation region. In sum, the nonlinear EHSAPT, including the full Green-Lagrange strain in the core sheet and nonlinear axial normal strain in the faces yields the closest results to ADINA, for both soft core material and harder core material. In the example with soft core, it successfully captures the limit point, whereas the top face buckles and cannot take more axial load.

The EHSAPT-based element is successful in performing the static analysis considering the geometric nonlinearities. The one-dimensional model used by this element shows high efficiency when compared to ADINA or similar commercial FEA software. A two-dimensional model needs to be built when using ADINA and special care is needed to avoid the numerical difficulties. When using ADINA, the numerical difficulties are observed and are also observed in other literatures [48]. The proposed EHSAPT-based element can yield the entire nonlinear static response curve.

CHAPTER 4

NONLINEAR DYNAMIC RESPONSE OF SANDWICH STRUCTURES

In practical applications, sandwich structures have a high chance to be subjected to dynamic loads, e.g., blast, gust or impact. These sudden loads usually have very high initial magnitudes and decay fast. Meanwhile, since soft materials are used in the core, large deformations may be occurring during the transient dynamic response. As observed in the the experiments [61–63], the sandwich panel undergoes severe through-thickness deformations during blast loading, and the deflection magnitude can reach or even exceed the magnitude of the total thickness of the sandwich panel. In this chapter, the geometric nonlinearity effect on the dynamic response of sandwich panels are studied.

4.1 Solution Approach

The nonlinear dynamic formulation follows the same displacement assumptions of the nonlinear static formation of EHSAPT. In particular, the Euler-Bernoulli assumptions are adopted in the faces while the high order displacement pattern is considered in the core. The EHSAPT-based element is used in the spatial domain to derive the equations of motion, and the direct time integration is used in the time domain to yield the numerical solutions.

4.1.1 Spatial Domain: Nonlinear EHSAPT-based Element

Implementing the EHSAPT-based element, the displacement fields of sandwich panels are given by Eq. (2.20). Since the dynamic response is considered, displacements are functions of time t and are rewritten as,

$$\{\widehat{\boldsymbol{U}}(x,z,t)\} = [\tilde{\boldsymbol{N}}(s,z)]\{\boldsymbol{U}_e(t)\} \tag{4.1}$$

As a result, the velocity is given as,

$$\{\dot{\widehat{\boldsymbol{U}}}\} = [\tilde{\boldsymbol{N}}]\{\dot{\boldsymbol{U}}_e\} \tag{4.2}$$

where the over dot represents the first order derivative with respect to time t.

The equations of motion are derived from Hamilton's principle:

$$\delta L = \sum_{e=1}^{m} \int_{t_1}^{t_2} \left(\delta T^e - \delta \Pi^e\right) dt = 0 \tag{4.3}$$

where T^e is the element kinetic energy and Π^e is the element potential energy.

The element potential energy Π^e is the same as the one discussed in the nonlinear static analysis. It includes the strain energy and the external potential energy associated with the applied loads. Thus, applying the variational principle yields the element stiffness matrix $[\boldsymbol{K}_e]$ and element nodal equivalent force vector $\{\boldsymbol{R}_e\}$, which are given by Eq. (3.9) and Eq. (2.28), respectively. The structural stiffness matrix $[\boldsymbol{K}(t)]$, and structural force vector $\{\boldsymbol{R}(t)\}$ are obtained after assembling the element matrices. Compared to ones appeared in static analysis, the only difference is that these matrices are functions of time t.

The top face, the bottom face and the core all contribute to the kinetic energy. Therefore, the variation of the element kinetic energy is:

$$\delta T^e = \sum_{k=t,b,c} \delta T^k = \sum_{k=t,b,c} \iint_{v^k} \delta\{\dot{\widehat{\boldsymbol{U}}}\}^T [\boldsymbol{I}^k]\{\dot{\widehat{\boldsymbol{U}}}\}\rho^k dz dx \quad k = t, b, c \tag{4.4a}$$

where v^k is the space domain of each layer, $\rho^{t,b,c}$ are the mass densities of the top face, the bottom face and the core, respectively; $[\boldsymbol{I}^t]$,$[\boldsymbol{I}^b]$ and $[\boldsymbol{I}^c]$ are 6×6 matrices and defined as

$$\begin{cases} I^t_{11} = I^t_{22} = 1 \\ I^t_{ij} = 0 \quad \text{others} \end{cases} ; \quad \begin{cases} I^b_{33} = I^b_{44} = 1 \\ I^b_{ij} = 0 \quad \text{others} \end{cases} ; \quad \begin{cases} I^c_{55} = I^c_{66} = 1 \\ I^c_{ij} = 0 \quad \text{others} \end{cases} \tag{4.4b}$$

Substituting Eq. (4.2) into Eq. (4.4a) yields the consistent element mass matrix:

$$[\boldsymbol{M}_e] = \sum_{k=t,b,c} [\boldsymbol{M}_e^k] = \sum_{k=t,b,c} \iint_{v^k} [\tilde{\boldsymbol{N}}]^T [\boldsymbol{I}^k][\tilde{\boldsymbol{N}}]\rho^k dzds \tag{4.5}$$

Assembling the element mass matrix yields the structural mass matrix $[\boldsymbol{M}]$. Therefore, the equations of motion are:

$$[\boldsymbol{M}]\{\ddot{\boldsymbol{U}}(t)\} + [\boldsymbol{K}(t)]\{\boldsymbol{U}(t)\} = \{\boldsymbol{R}(t)\} \tag{4.6}$$

with initial conditions:

$$\{\boldsymbol{U}(t=0)\} = \{\boldsymbol{U}\}_{t_0} \tag{4.7a}$$

$$\{\dot{\boldsymbol{U}}(t=0)\} = \{\dot{\boldsymbol{U}}\}_{t_0} \tag{4.7b}$$

where $\{\boldsymbol{U}(t)\}$ and $\{\ddot{\boldsymbol{U}}(t)\}$ are the displacement and acceleration at time t; $\{\boldsymbol{U}\}_{t_0}$ and $\{\dot{\boldsymbol{U}}\}_{t_0}$ are the prescribed initial displacement and initial velocity.

When damping is considered, then Eq. (4.6) becomes

$$[\boldsymbol{M}]\{\ddot{\boldsymbol{U}}(t)\} + [\boldsymbol{D}(t)]\{\dot{\boldsymbol{U}}(t)\} + [\boldsymbol{K}(t)]\{\boldsymbol{U}(t)\} = \{\boldsymbol{R}(t)\} \tag{4.8}$$

where $\{\dot{\boldsymbol{U}}(t)\}$ is the velocity and $[\boldsymbol{D}(t)]$ is the damping matrix. If proportional damping is introduced, the damping matrix can be given as $[\boldsymbol{D}] = d_1[\boldsymbol{M}] + d_2[\boldsymbol{K}]$, and d_1, d_2 are the damping coefficients.

4.1.2 Time Domain: Direct Time Integration

Eqs. (4.7)-(4.8) can be solved by various algorithms and numerical methods. Here, the time domain response is obtained by an explicit direct time integration method, the central difference method. Applying the finite difference method in the time domain, the velocity

and acceleration at time t_n are evaluated as:

$$\{\dot{\boldsymbol{U}}\}_{t_n} = \frac{1}{2\Delta t}\left(\{\boldsymbol{U}\}_{t_{n+1}} - \{\boldsymbol{U}\}_{t_{n-1}}\right) \tag{4.9a}$$

$$\{\ddot{\boldsymbol{U}}\}_{t_n} = \frac{1}{\Delta t^2}\left(\{\boldsymbol{U}\}_{t_{n+1}} - 2\{\boldsymbol{U}\}_{t_n} + \{\boldsymbol{U}\}_{t_{n-1}}\right) \tag{4.9b}$$

where Δt is the time step size. The subscript t_n stands for the current time step $t = t_n$, t_{n-1} is the previous time step, and t_{n+1} is the next time step.

Substituting Eq. (4.9) into equation of motion, Eq. (4.8), yields the displacement vector at $t = t_{n+1}$,

$$\begin{aligned}\left(\frac{1}{\Delta t^2}[\boldsymbol{M}] + \frac{1}{2\Delta t}[\boldsymbol{D}]_{t_n}\right)\{\boldsymbol{U}\}_{t_{n+1}} =& \{\boldsymbol{R}\}_{t_n} - \left([\boldsymbol{K}]_{t_n} - \frac{2}{\Delta t^2}[\boldsymbol{M}]\right)\{\boldsymbol{U}\}_{t_n} \\ &- \left(\frac{1}{\Delta t^2}[\boldsymbol{M}] - \frac{1}{2\Delta t}[\boldsymbol{D}]_{t_n}\right)\{\boldsymbol{U}\}_{t_{n-1}}\end{aligned} \tag{4.10}$$

Since the geometric nonlinearity is considered, the stiffness matrix $[\boldsymbol{K}]_{t_n}$ depends on the displacement $\{\boldsymbol{U}\}_{t_n}$ and requires to be updated at each time step. The linear part of the stiffness matrix is stored in the program, and only the nonlinear part of the stiffness matrix needs to be formulated at each time step. No equilibrium iteration is involved since the explicit method is used. Moreover, if damping is not considered, i.e., $[\boldsymbol{D}] = [\boldsymbol{0}]$, the coefficient matrix in front of $\{\boldsymbol{U}\}_{t_{n+1}}$ is constant. Thus, the inverse calculation is performed only once.

The calculation of $\{\boldsymbol{U}\}_{t_{n+1}}$ involves $\{\boldsymbol{U}\}_{t_{n-1}}$ and $\{\boldsymbol{U}\}_{t_n}$. Thus, a start up procedure is needed for the first step $t = t_0$. It is given from Eq. (4.9),

$$\{\boldsymbol{U}\}_{t_{-1}} = \{\boldsymbol{U}\}_{t_0} - \Delta t\{\dot{\boldsymbol{U}}\}_{t_0} + \frac{\Delta t^2}{2}\{\ddot{\boldsymbol{U}}\}_{t_0} \tag{4.11}$$

and $\{\ddot{\boldsymbol{U}}\}_{t_0}$ is calculated from Eq. (4.8) at $t = t_0$.

The central difference method is a conditionally stable method, which means that the time step size Δt must be smaller than a critical value Δt_{cr} to ensure numerical stability.

In the spatial domain, the EHSAPT element is used. Thus, Δt_{cr} is evaluated as,

$$\Delta t_{cr} = \frac{2}{\omega_{\max}} \tag{4.12}$$

where $\omega_{\max}$ is the maximum natural frequency for the smallest element. This is obtained by solving the eigenvalue problem $|[\boldsymbol{K}_e] - \omega^2[\boldsymbol{M}_e]| = 0$ in the element with the smallest element length. Note that this is a rough approximation. During the nonlinear dynamic response, the $[\boldsymbol{K}_e]$ keeps changing; Δt_{cr} might be decreased when the sandwich panel stiffens, and be increased if the sandwich panel softens [100]. Therefore, a small time step size is required to ensure numerical stability, especially when the geometric nonlinear effect is considered.

4.2 Numerical Results and Discussion

A sandwich panel subjected to a blast load is considered. For comparisons, the dimensions and materials of the sandwich panel and loading are the same as ones in the literature [50, 58, 63]. The sandwich panel has face thickness $f_t = f_b = 5$ mm, core thickness $2c = 38$ mm, length $a = 152.4$ mm, and width $b = 102$ mm. For the faces, E-glass vinyl-ester composite is used and the material properties are $E_1^f = E_2^f = E_3^f = 13600$ MPa, $\nu_{12}^f = \nu_{13}^f = 0.25$ and $\nu_{32}^f = 0.35$, and the density ρ^f =1800 kg/m^3. The core is made out of Corecell$^{\mathrm{TM}}$ A300 styrene acrylonitrile foam, with $E_1^c = E_2^c = E_3^c = 32.0$ MPa, $\nu_{12}^c = \nu_{13}^c = 0.25$ and $\nu_{32}^c = 0.35$, and of density $\rho^c = 58.5$ kg/m^3. The blast load is sinusoidally distributed at the top face sheet and exponentially decays with the time,

$$q^t(t) = -510e^{-1.25t} \sin \frac{\pi x}{a} \quad \text{N/mm} \tag{4.13}$$

where the unit of t is milliseconds (ms), 1 ms$= 10^{-3}$ s. The magnitude of the load decays to less than 1% in 4 ms, as shown in Fig. 4.1.

The sandwich panel is initially at rest with zero displacement and velocity. The dam-

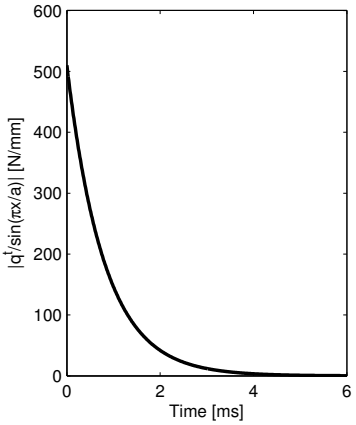

Figure 4.1: Blast load profile

ping is not considered. Both edges are simply supported, namely the transverse displacement is constrained and the edges can move freely in the axial direction. So, the boundary conditions are:

$$w_1^t(t) = w_1^b(t) = w_1^c(t) = 0 \qquad \text{[first node]} \tag{4.14a}$$

$$w_n^t(t) = w_n^b(t) = w_n^c(t) = 0 \qquad \text{[last node]} \tag{4.14b}$$

$$u_{(n+1)/2}^t(t) = u_{(n+1)/2}^b(t) = u_{(n+1)/2}^c(t) = 0 \qquad \text{[middle node]} \tag{4.14c}$$

where the last Eq. (4.14c) is used to eliminate the rigid body motion.

High accuracy was observed when using the 2-node EHSAPT-based element performing the linear static and nonlinear static analysis. Thus, the 2-node element is used herein. A convergence study was carried out and ensured the result accuracy. In the results presented, 50 elements were used and $n = 51$ nodes were uniformly distributed. Therefore, as a flat sandwich panel is considered, the corresponding EHSAPT-based element model is a 1D straight line with 51 uniformly distributed nodes. In contrast, the conventional FEM usually requires a 2D or 3D FE model and thus it takes extra modeling work and more computation cost for one more or two more dimensions. Time step size is chosen as $\Delta t = 0.5 \times 10^{-4}$ ms, while the critical value is $\Delta t_{cr} = 3.05 \times 10^{-4}$ ms for this mesh.

4.2.1 Verification of Linear Dynamic Based on the EHSAPT

To verify the derivations and programs, the linear dynamic response based on the EHSAPT [$\alpha_i = 0, i = 1...4$ in Eq. (3.2), and $\beta_j = 0, j = 1...6$ in Eq. (3.3)] is first compared with the closed form dynamic elasticity solution [50]. In the early results, it was shown that the linear EHSAPT can yield a very close solution to the linear elasticity. However, some noticeable minor differences were observed in both static [21] and dynamic [58] response. In Chapter 2, it was shown that these small deviations were due to inconsistent constitutive definitions for the core in the elasticity and EHSAPT solutions. By adopting the same constitutive definitions, identical displacements and stresses to the elasticity for the static case were obtained. Thus, the same modification is applied herein in the linear dynamic analysis. The constitutive equation used in the elasticity approach [50] is replaced with the one adopted in the EHSAPT, given by Eq. (2.12). In the elasticity approach, a numerical inverse Laplace transform method (the Euler method) was used to acquire the time space response. This method can provide accurate results for the first few milliseconds, but may suffer numerical issues for a longer duration. Thus, the comparisons and verifications between the elasticity and linear EHSAPT are made in the first 2 ms.

The displacement responses obtained by the elasticity and linear EHSAPT are given in Figs. 4.2-4.3. Fig. 4.2 plots the transverse displacement of the centroid of each layer, w_0^t, w_0^b and w_0^c, at the middle span of the sandwich panel ($x = a/2$). The linear EHSAPT results are plotted with solid lines and the linear elasticity solutions are in dash lines. In the figure, the results are identical. The small deviations between the linear EHSAPT dynamic approach and linear elasticity, which could be seen in Refs. [50, 58], are no longer.

The axial displacements, u, of the middle of the faces and the core at the left edge ($x = 0$) are plotted in Fig. 4.3. In Ref. [58], the EHSAPT yielded similar general trends but was lagging to the elasticity. In Fig. 4.3, the linear EHSAPT and the linear elasticity match well in both magnitude and phase. Very slight differences can only be observed at several regions near the peaks. The core sheet shows relatively higher frequency response

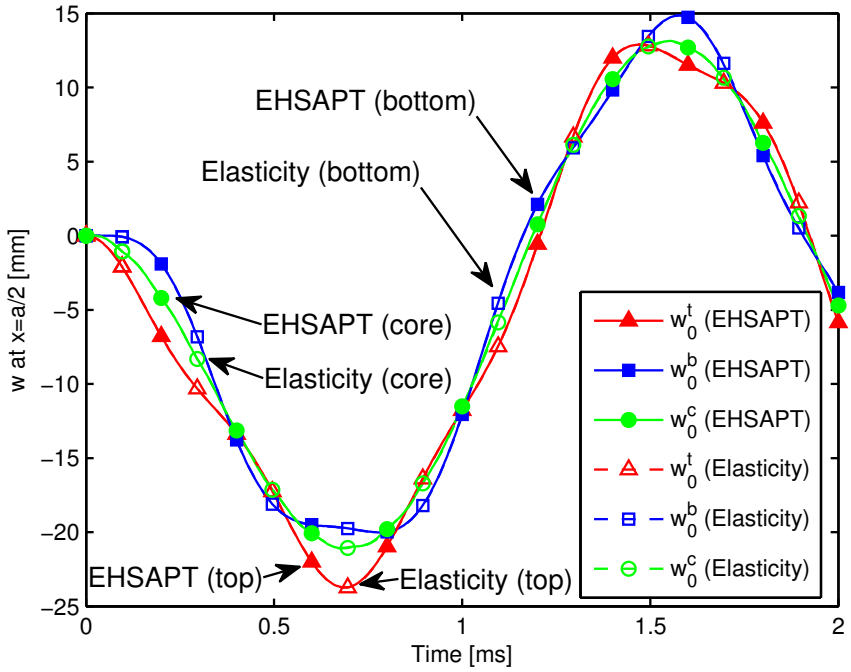

Figure 4.2: Transverse displacement w of the top face, bottom face, and core at middle span of linear EHSAPT and elasticity

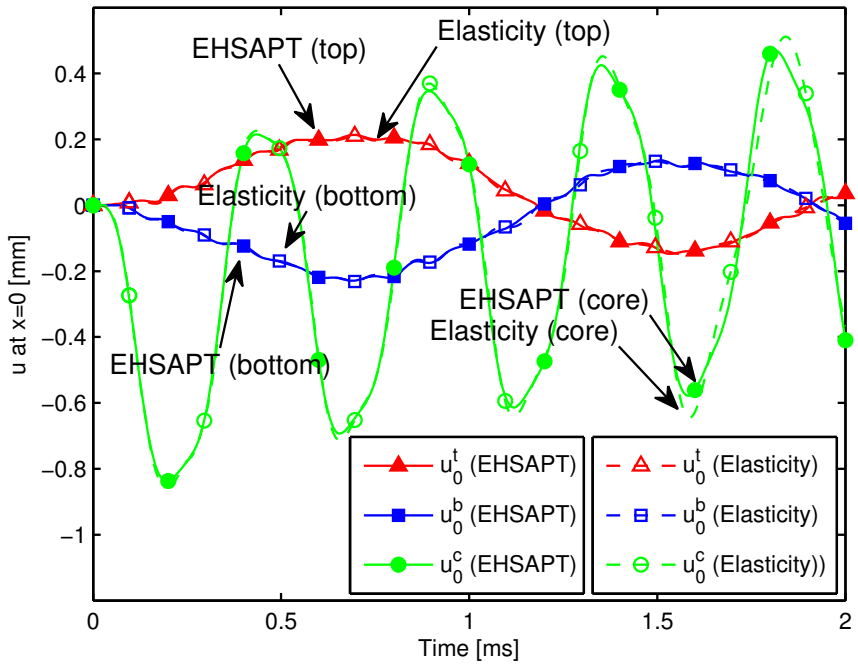

Figure 4.3: Axial displacement u of the top face , bottom face, and core at left edge of linear EHSAPT and elasticity

and relatively larger amplitude cyclic behavior compared to the faces, while the vibration frequency of $u_0^{t,b}$ is similar to $w_0^{t,b}$.

Besides the displacements, the stresses obtained by the linear EHSAPT and linear elasticity also agree quite well. The interface transverse normal stress σ_{zz} at mid-span, $x = a/2$, is shown in Fig. 4.4. It follows a similar cyclic behavior as in the core axial displacement. Again, some phase difference between the EHSAPT and elasticity, which was observed in Ref. [58], is no longer. The interface shear stress, τ_{xz}, at $x = 0$ is shown in Fig. 4.5. The solid lines and dash lines agree perfectly and follow a similar cyclic response as for the transverse displacement, shown in Fig. 4.2.

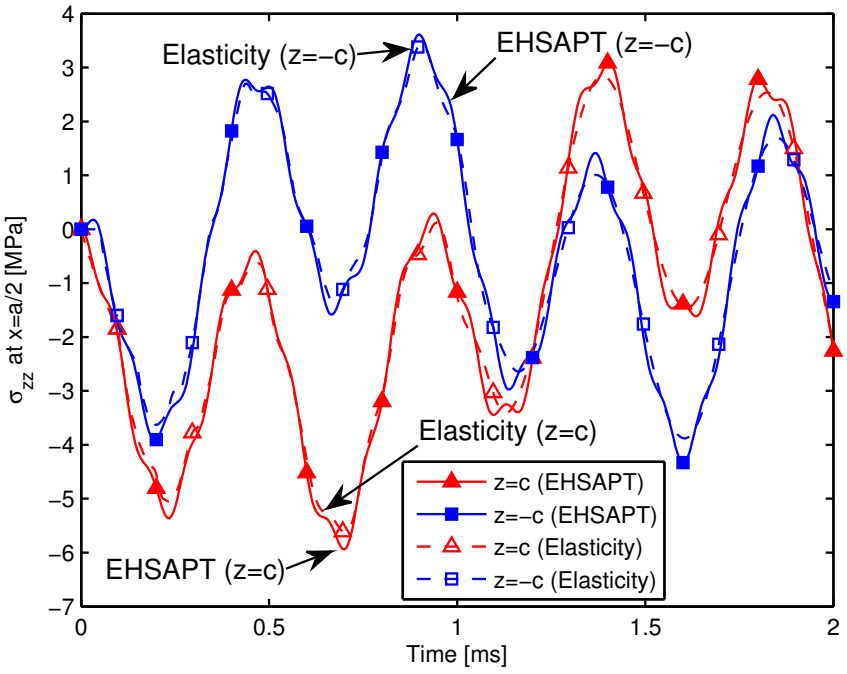

Figure 4.4: Transverse normal stress σ_{zz} of the interface between the faces and core at middle span of linear EHSAPT and elasticity

Fig. 4.6 plots the axial normal stresses in the top face at mid-span of sandwich panel $(x = a/2)$. The axial stresses at the upper surface $z = c + f_t$ and the lower surface $z = c$, which is also the interface with the core, are both given. A good agreement between the linear elasticity and linear EHSAPT is observed. The peak value occurs at around 0.7 ms.

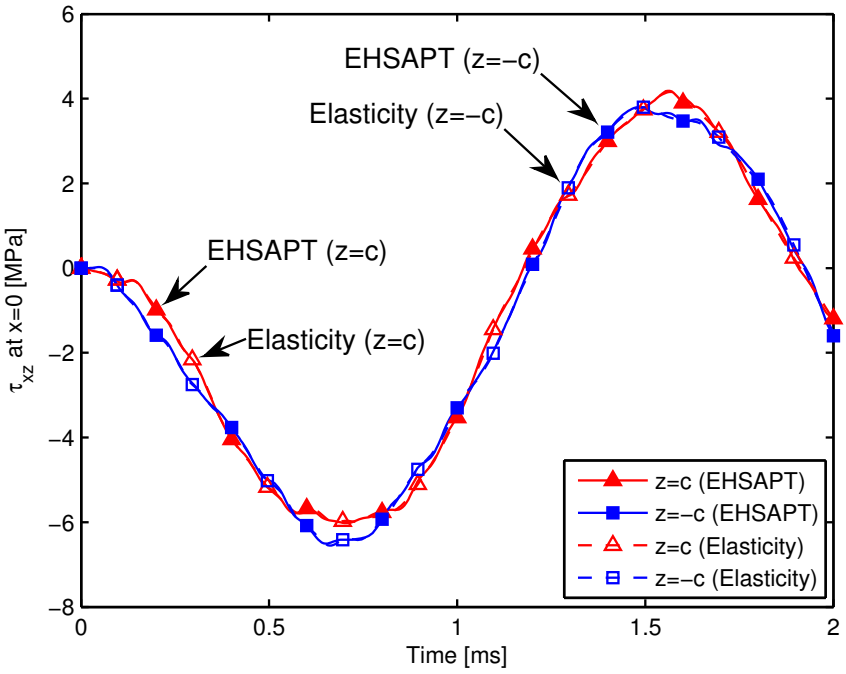

Figure 4.5: Shear stress τ_{xz} of the interface between the faces and core at left edge of linear EHSAPT and elasticity

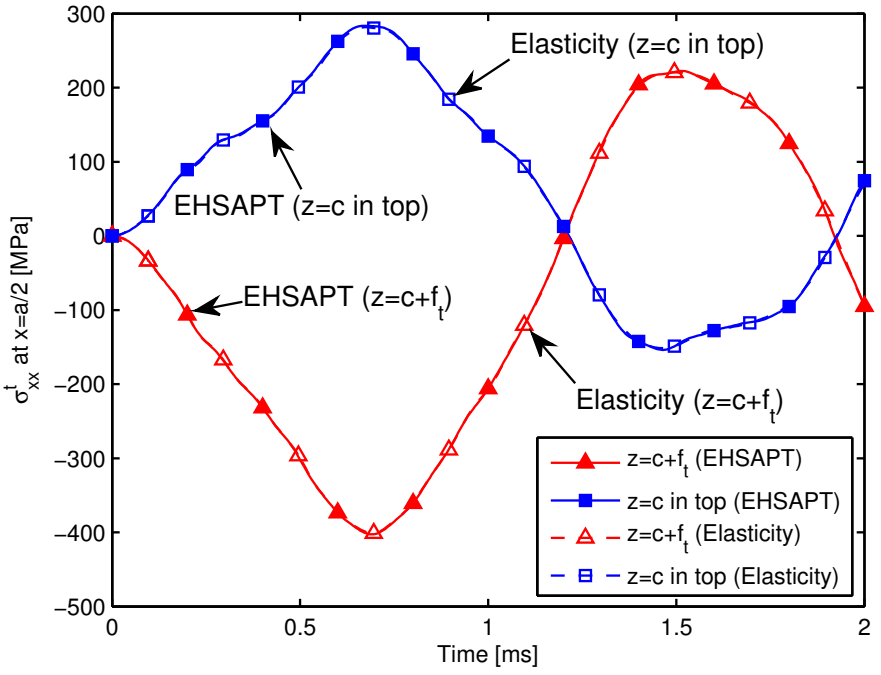

Figure 4.6: Top face axial normal stress σ^t_{xx} at middle span of linear EHSAPT and elasticity

The comparisons show that the EHSAPT can accurately predict the linear dynamic response. The Euler-Bernoulli assumptions used in the face sheets are verified and the solution yields accurate displacements and stresses, as verified by the linear elasticity solution. In the early study, some divergences and phase differences were observed. This issue is solved by imposing the same constitutive equations for the core in these two approaches. The elasticity solution has several limitations. Due to the limitation of the numerical inverse Laplace transform, the elasticity solution is only valid for a few milliseconds. For longer durations, other numerical inverse Laplace transform methods need to be used. Also, the elasticity solution is only available for simply supported boundary conditions. Moreover, it is a linear solution. The proposed dynamic analysis based on the EHSAPT is based on the finite element method. It can easily handle arbitrary boundary conditions and loads. In the time domain, the direct time integration is robust and capable of longer time duration. A most important feature is that, as shown in the next section, it can also provide results that include geometric nonlinearities.

4.2.2 The Effects of Geometric Nonlinearities

The same sandwich panel with the same loading and boundary conditions is analyzed with nonlinear kinematic relations included. In the literature, different simplifications are used in the nonlinear dynamic analysis of sandwich structures. In Chapter 3, it is seen that the geometric nonlinearity has a great effect on the static behavior, and the simplifications about the nonlinear terms may lead to inaccurate results. In this part, various simplifications will be considered to further examine the nonlinearity effects on the dynamic response of sandwich structures. Several scenarios are considered, namely:

- NL1: $\alpha_2 = 1$, and $\alpha_1 = \beta_j = 0$, $(j = 1...6)$; The nonlinear kinematic term $(w_{,x})^2$ is used in the faces only (not in the core). In the core, linear strain is used.

- NL2: $\alpha_2 = \beta_2 = 1$, and $\alpha_1 = \beta_j = 0$, $(j = 1, 3, 4, 5, 6)$; It comes from the Von Kármán strain assumption that only the $(w_{,x})^2$ terms are used in all three layers (only

terms considered not negligible, compared to $u_{,x}$) [67, 101].

- NL3: $\alpha_2 = \beta_2 = \beta_4 = \beta_6 = 1$, and $\alpha_1 = \beta_j = 0$, $(j = 1, 3, 5)$; In this assumption, we consider all the nonlinear terms related to the transverse displacement w in all layers, i.e., in addition to the $(w_{,x})^2$ terms, we also include the $(w_{,z})^2$ and $w_{,x}w_{,z}$ terms.

- NL4: $\alpha_2 = \beta_j = 1, (j = 1...6)$, and $\alpha_1 = 0$; The faces include nonlinear terms related to w, i.e., the $(w_{,x})^2$ term only, the one considered in Euler-Bernoulli beam, while the core contains all nonlinear terms.

- NL5: $\alpha_i = \beta_j = 1$, $(i = 1, 2,\ j = 1...6)$; The nonlinear terms appearing in the kinematic equations are all included in all theree layers.

The first two are the most used assumptions in the nonlinear dynamic analysis of sandwich structures. In the following nonlinear analysis, the same finite element model and time step size as used in the linear analysis are used, i.e., 50 2-node EHSAPT-based elements and $\Delta t = 0.5 \times 10^{-4}$ ms. In order to examine the geometric nonlinear effects on the dynamic response, the linear dynamic results are also provided for comparison. Considering the limitation of numerical inverse Laplace transform, the elasticity solution is unstable for a long duration, and the linear EHSAPT has been verified that it is accurate enough to serve as the benchmark. Thus, the linear EHSAPT dynamic results are used instead for comparison. It is known that the conventional FEM may have numerical difficulties in analyzing sandwich structures when considering geometric nonlinearities. Indeed, in nonlinear static analysis, commercial FEM software was aborted due to the large distortions of the elements of the core (observed in Chapter 3 and Ref. [48]), which was caused by the large differences in the material properties of the faces and the core. Same numerical difficulties are observed in the nonlinear dynamic analysis when using commercial FEA software. In the EHSAPT-based element, a displacement assumption in the thickness direction is embedded through the EHSAPT, and only one element is placed along the thickness direction. With

the EHSAPT-based element, the nonlinear dynamic analysis was successfully performed in all cases examined.

Fig. 4.7 plots the transverse displacement at the midtop, w_0^t, at the middle span ($x = a/2$). The responses obtained by different nonlinear assumptions and the linear result are given. In the figure, the results considering the nonlinear terms are marked with "NL1" to "NL5", which contain different nonlinear terms, and are defined as above. The linear result using linear kinematic relation is marked with "Linear". Same notation is applied to all figures. In Fig. 4.7, it can be seen that different assumptions yield similar transverse displacement response, with small phase difference. When the nonlinear kinematic relation is only used in the faces, i.e., the $(w^{t,b}_{,x})^2$ term only "NL1", the transverse displacement is very close to the linear result. When more nonlinear terms are considered, the results have higher peak value and larger phase difference. The effect caused by the geometric nonlinearity is cumulative. The phase difference increases with time. Three cases that include the nonlinear terms related to the w^c yield almost identical response. Similar comparisons are observed in the transverse displacement response of the bottom face and the core, and thus are omitted for conciseness. The geometric nonlinearity affects the phase and the magnitude of transverse displacement response. It makes the period longer. Thus, it can be concluded that the geometric nonlinearity makes the sandwich panel soften. It agrees with the observations reported in the nonlinear static analysis, shown in Chapter 3. Moreover, the general trends of the transverse displacement response of the linear dynamic and nonlinear dynamic are similar.

The axial displacements at mid-top, mid-core, and mid-bot of the left edge are plotted in Figs. 4.8-4.10. The geometric nonlinearity has a very significant effect on the axial displacement response. The vibration patterns, including the frequency and peak value, are completely different. In the linear dynamic response, the behaviors of the top and bottom faces are symmetric, as shown in Fig. 4.3. The moving directions of the top edge and the bottom edge are opposite to each other, in other words rotating around the center

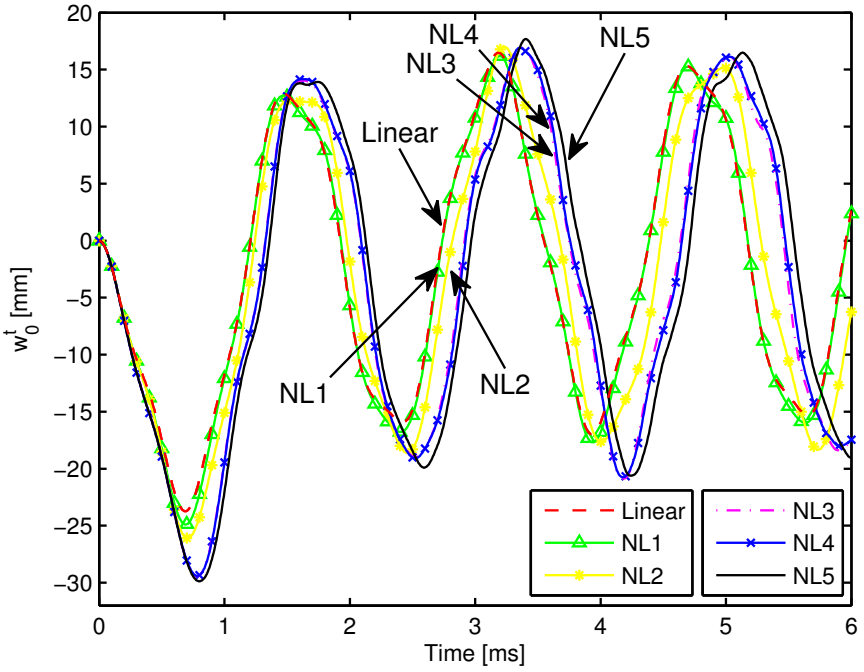

Figure 4.7: Transverse displacement response of the midtop w_0^c at middle span of nonlinear dynamic analysis

of the core, is the major movement of the top edge and the bottom edge in the linear analysis. The neutral positions of the top edge and the bottom edge are the corresponding initial positions approximately. However, when considering the geometric nonlinearity, the moving directions of the top and the bottom are the same. The peak value is much higher than the linear dynamic case, and the period is halved. In the nonlinear dynamic analysis, the highest peak value of the mid-top axial deformation is around 7 mm and occurs at $t = 0.8$ ms. After that, in the axial direction, the top face experiences a cyclic oscillation with a peak value around 3 mm with a period around 1 ms. The neutral position is around $x = 1.5$ mm. The axial response of the bottom sheet is similar to the steady state of top sheet, and the peak value is around 3 mm. On the other hand, the linear dynamic response shows the top edge and bottom edge oscillating between ± 0.2 mm with a period of 2 ms.

The axial movement of the mid-core ($z = 0$, $x = 0$) is plotted in Fig. 4.10. Only before the first 1 ms, the linear dynamic and nonlinear dynamic agree with each other. After that,

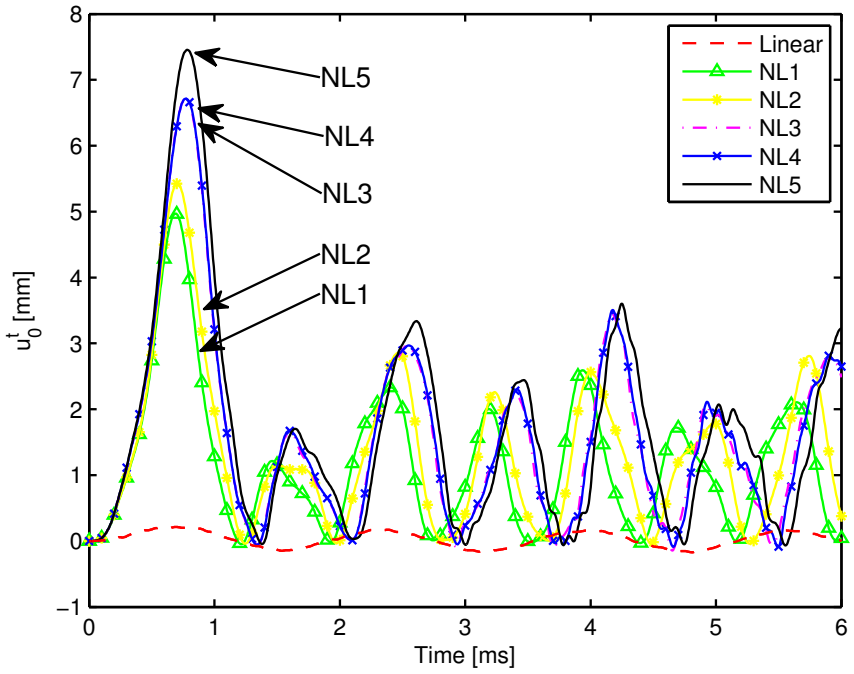

Figure 4.8: Axial displacement of the top face u_0^t at left edge of nonlinear dynamic analysis

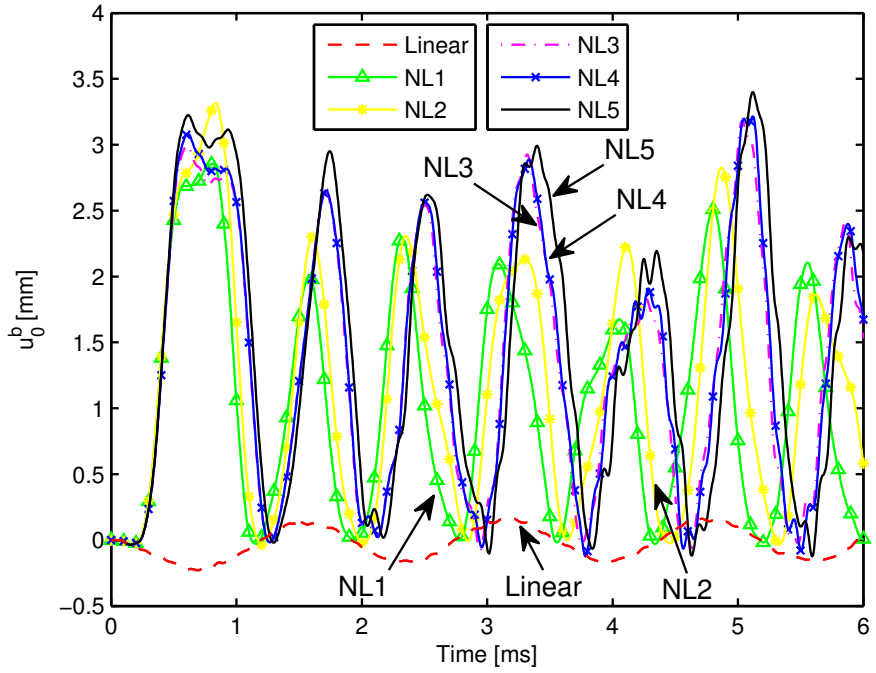

Figure 4.9: Axial displacement of the bottom face u_0^b at left edge of nonlinear dynamic analysis

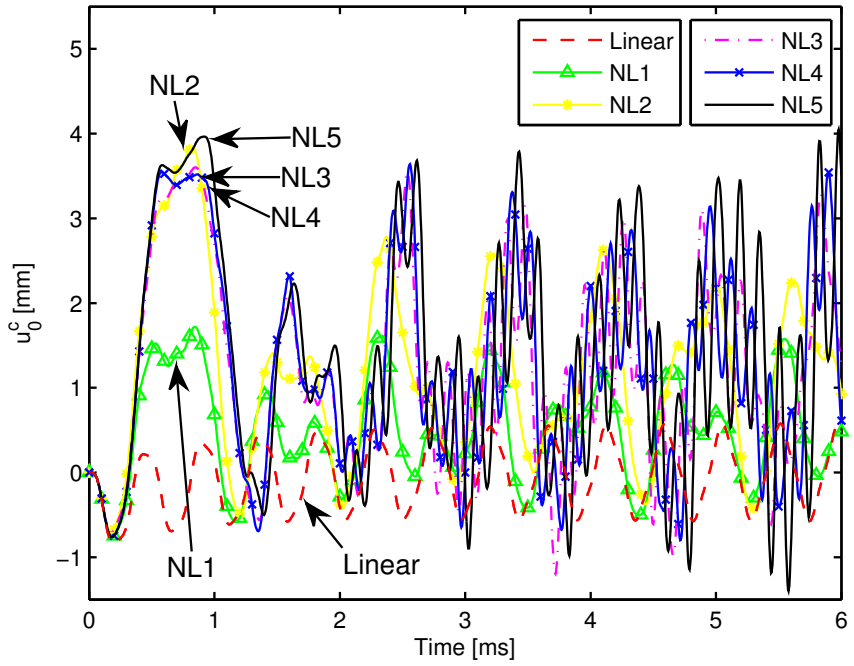

Figure 4.10: Axial displacement of the core u_0^c at left edge of nonlinear dynamic analysis

the linear kinematic relations are not valid due to the large deformation. The peak value when including nonlinear terms is around 3 mm and the period is around 1 ms, similar to the face edges. But the linear dynamic shows that the core undergoes relatively larger amplitude with relatively higher frequency cyclic behavior than the faces. Another important phenomenon observed in the nonlinear dynamic analysis is that there exists high frequency in-plane vibration along axial direction after 2 ms, as shown by the curve that includes only the w nonlinear terms in all three layers (i.e., $(w^{t,b}_{,x})^2$, $(w^c_{,x})^2$, $(w^c_{,z})^2$ and $w^c_{,x}w^c_{,z}$) "NL3", the curve that includes $(w^{t,b}_{,x})^2$ and all nonlinear terms in the core "NL4", and the curve that includes all nonlinear terms in all three layers "NL5". Due to the nonlinear terms in the core kinematic relation, the axial displacement u and transverse displacement w are coupled. Hence, it can capture the in-plane vibration initiated by the transverse blast loading when wave propagates in the sandwich panel. The dynamic response of the sandwich panel is a combination of low-frequency out-plane transverse vibration, and in-plane high-frequency axial vibration. However, the linear dynamic analysis cannot capture this, since the kine-

matic relation only retains the linear part. The curves of only the $(w^{t,b}_{,x})^2$ "NL1" and only the $(w^{t,b}_{,x})^2$ and $(w^{c}_{,x})^2$ "NL2" also cannot show this phenomenon.

From the axial displacement response, it can be seen that the most commonly used assumption, i.e., only including the nonlinear term in the faces, does improve the results. However, there are still noticeable differences when further including more nonlinear terms of the core. In Fig. 4.10, the peak value of the curve that includes only the the $(w^{t,b}_{,x})^2$ "NL1" is only half that in the other curves that include the nonlinear terms of the core. Regarding the results, adopting Von Kármán strains in the core is inadequate. At least the nonlinear terms related to the transverse displacement w need to be included, namely $\beta_2 = \beta_4 = \beta_6 = 1$ (i.e. the $(w^{c}_{,x})^2$, $(w^{c}_{,z})^2$ and $w^{c}_{,x}w^{c}_{,z}$ terms). The effect of the nonlinear term $(u^{t,b}_{,x})^2$ in the faces is small.

The transverse normal stress σ_{zz} at the face/core interfaces and at mid-span is shown in Figs. 4.11-4.12. Fig. 4.11 plots the stress at the interface between the top face and the core ($z = c$), and Fig. 4.12 plots the same at the interface located at $z = -c$. When only including the nonlinear term of faces, $(w^{t,b}_{,x})^2$, "NL1", and when using Von Kàrmàn strain that only includes $(w^{t,b}_{,x})^2$ and $(w^{c}_{,x})^2$ in the face and core axial strain, "NL2", they both yield similar results to the linear dynamic. The curves obtained by the other three nonlinear cases are close to each other, and show higher amplitude and phase difference to the linear results. These cases include all the nonlinear terms related to w^c at least. The peak value of normal transverse stress occurs at the interface between top face and core at $t = 0.8$ ms. The peak value given by "NL3" (i.e. the $(w^{t,b}_{,x})^2$ in the faces and $(w^{c}_{,x})^2$, $(w^{c}_{,z})^2$ and $w^{c}_{,x}w^{c}_{,z}$ terms in the core), "NL4" (i.e., the $(w^{t,b}_{,x})^2$ in the faces and all nonlinear terms in the core) and "NL5" (i.e., all nonlinear terms in the faces and core) is about 11 MPa, while the "NL2" (i.e., only $(w^{t,b}_{,x})^2$ in the faces and only $(w^{c}_{,x})^2$ in the core) gives 8.6 MPa; "NL1" (i.e., only $(w^{t,b}_{,x})^2$ in the faces) gives 8 MPa, and the linear dynamic analysis only gives 6 MPa. The differences between the nonlinear dynamic and linear dynamic can be 83%. Thus, it is important to consider the geometric nonlinearity, and the nonlinear terms

in the core should be included. The transverse normal stress changes rapidly and the period of sign change is around 0.5 ms.

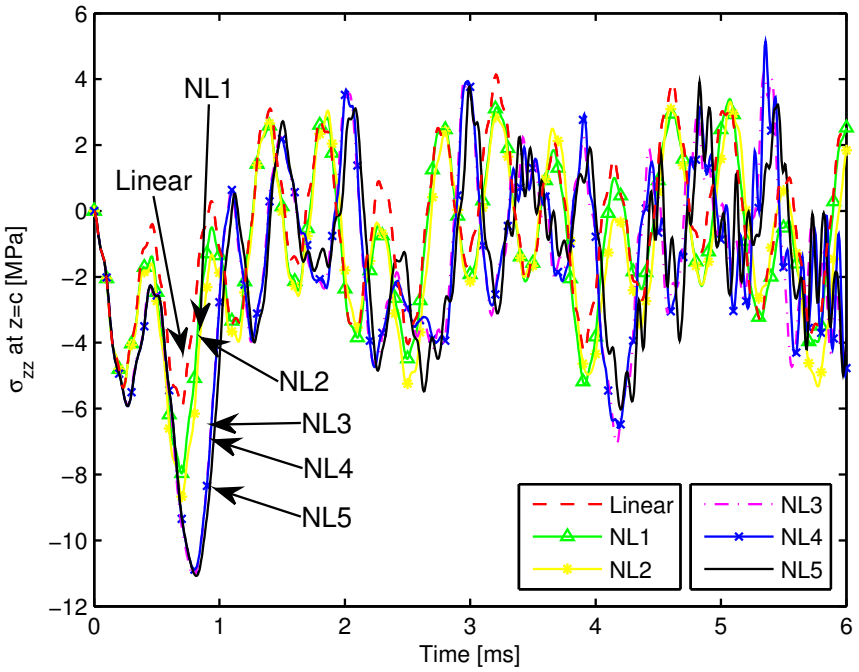

Figure 4.11: Transverse normal stress σ_{zz} of the interface between the top face and the core at middle span of nonlinear dynamic analysis

Fig.4.13 and Fig. 4.14 plot the shear stress at the interfaces between the faces and the core at the left edge, $z = 0$. The observation is similar to the transverse normal stress, σ_{zz}. When only considering the nonlinear terms in the face, even with one more nonlinear term in the core axial strain, the $(w^c_{,x})^2$, the dynamic response is close to the linear dynamic response. When considering all the nonlinear terms in the core, or at least all the nonlinear terms related to the transverse displacement, it captures the phase difference to the linear dynamic and the high frequency oscillation due to the in-plane movement. As shown in Figs. 4.8-4.10, the edges experience high frequency and noticeable amplitude in axial movement, especially the core after 2 ms. Part of the shear stress is caused by this axial movement. The period of sign change of the shear stress is around 2 ms, and is about four times that of the transverse normal stress.

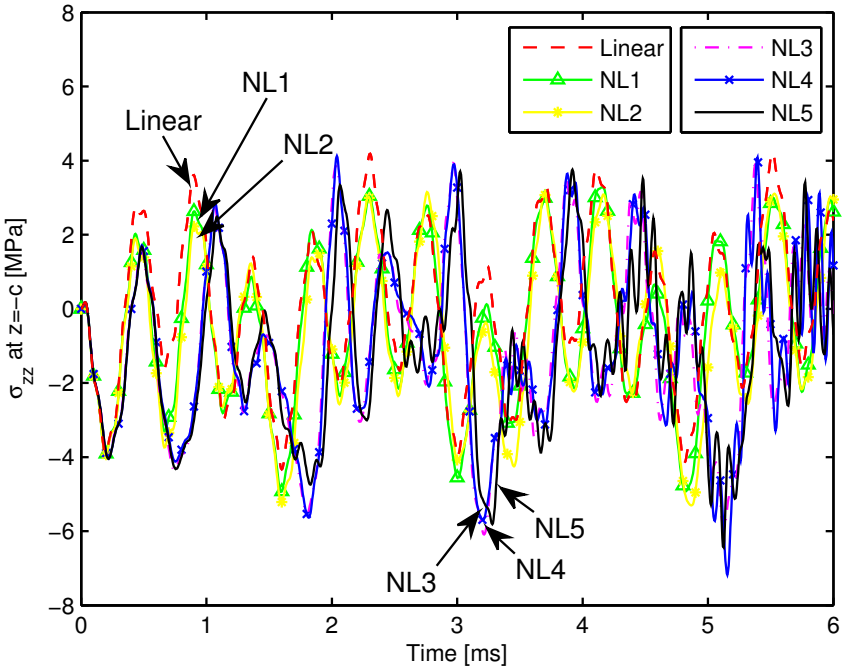

Figure 4.12: Transverse normal stress σ_{zz} of the interface between the bottom face and the core at middle span of nonlinear dynamic analysis

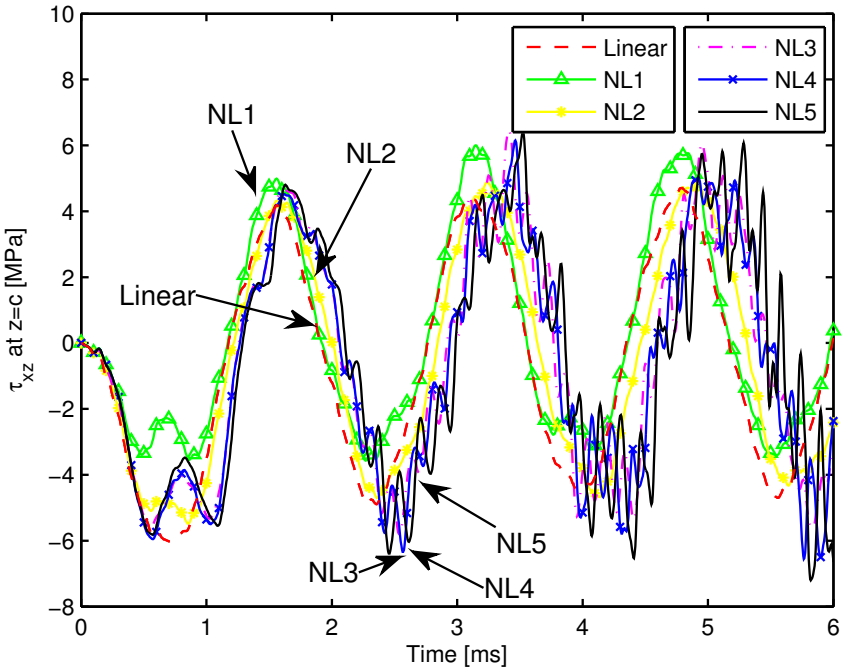

Figure 4.13: Shear stress τ_{xz} of the interface between the top face and the core at left edge of nonlinear dynamic analysis

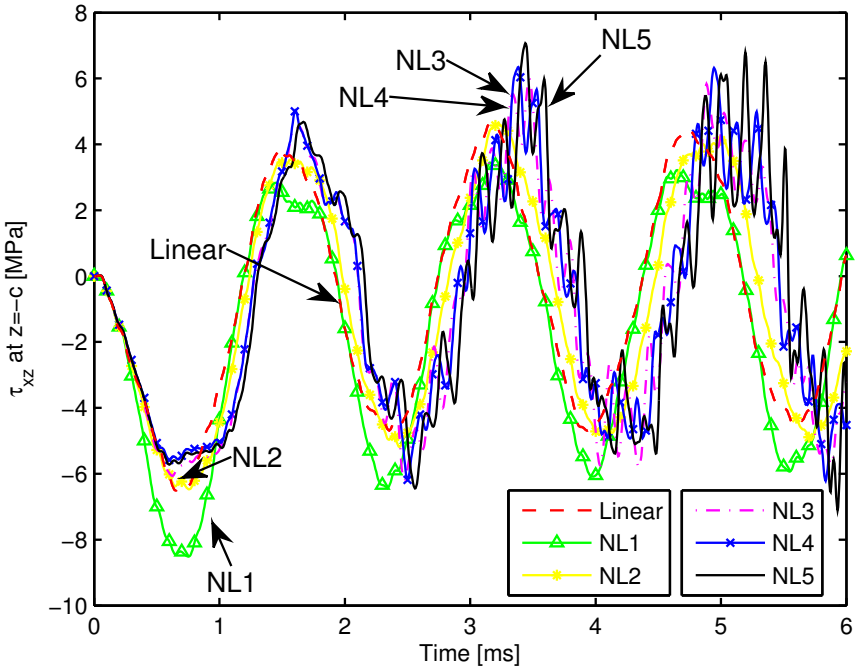

Figure 4.14: Shear stress τ_{xz} of the interface between the bottom face and the core at left edge of nonlinear dynamic analysis

Fig. 4.15 and Fig. 4.16 plot the axial normal stress in the top face at mid-span ($x = a/2$). Fig. 4.15 is the axial stress at the upper surface of the top face, $z = c + f_t$, and Fig. 4.16 is the corresponding one at the lower surface of the top face, $z = c$, which is also the interface with the core. It shows that the linear dynamic analysis underestimates significantly the peak values. The difference of the peak value can be about 50%. The peak value occurs at around 1 ms. Due to the in-plane vibration, the axial stress response also shows small oscillations on the major tendency.

The deformed shape of the sandwich panel within the first 2 ms is given in Fig. 4.17. The plots correspond to the nonlinear kinematic relation with $\alpha_2 = \beta_j = 1, (j = 1...6)$. It reflects the true ratio of geometry and deformation, and no scaling is applied. Fig. 4.17 also illustrates the wave propagation in the sandwich panel. The wave from the blast is initiated from the loaded top face. Initially, it is seen that the top face moves towards the core due to the blast loading, At $t = 0.2$ ms, the deformation of the lower part of the

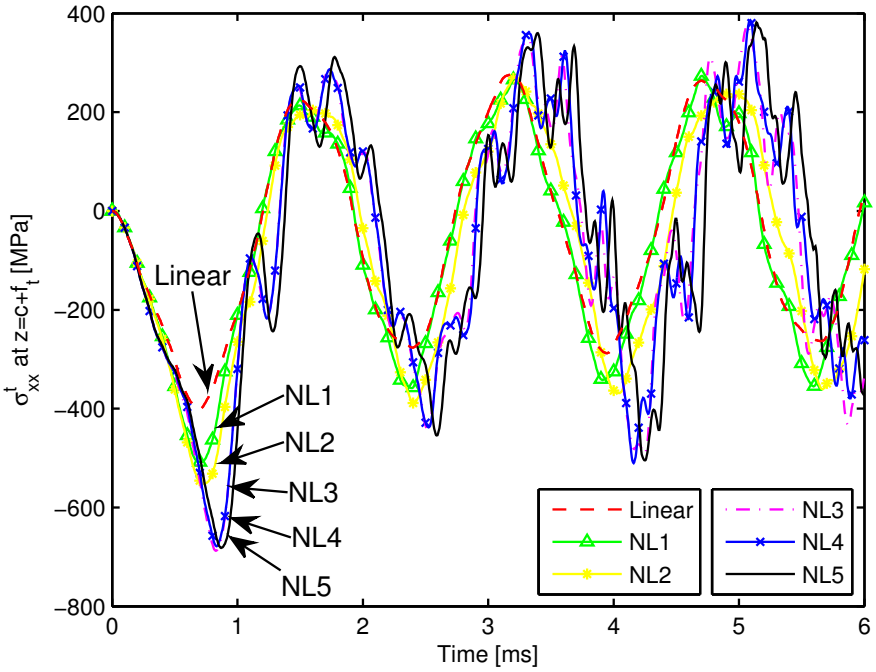

Figure 4.15: Top face axial normal stress σ^t_{xx} of the surface ($z = c + f_t$) at middle span of nonlinear dynamic analysis

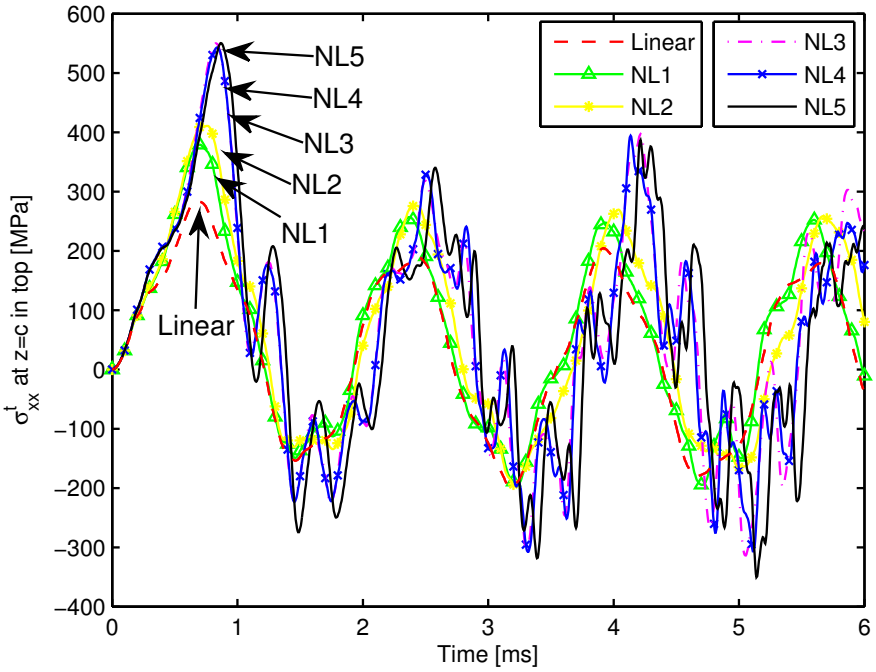

Figure 4.16: Top face axial normal stress σ^t_{xx} of the interface with core ($z = c$) at middle span of nonlinear dynamic analysis

sandwich panel is much smaller than that of the upper part due to inertia and the fact that wave reaches the bottom face later than the top face. Therefore, the core is compressed in the thickness direction and expands along the axial direction at the edges. This is attributed to wave travelling from the top face to the bottom face through the core. After the wave reaches the bottom face, both top face and bottom face move downward, the material in the middle span drags the edges to move towards the center, as shown from $t = 0.4$ ms to $t = 0.8$ ms. When the sandwich panel reaches the maximum transverse deformation, the center of the panel begins to reverse the moving direction and the edges move back to the initial position, as shown from $t = 0.8$ ms to $t = 1.2$ ms. Then, the sandwich panel moves upward in an analogous manner. Thus, despite the out-of-plane vibration along the thickness direction, the sandwich panel also experiences the in-plane oscillation. The edges move along the axial direction with higher frequency than the out-of-plane vibration. This in-plane oscillation can only be captured by the nonlinear dynamic analysis. When ignoring the geometric nonlinearity, the linear dynamic response only predicts that the edges oscillate around the initial position, see Ref. [59]. The corresponding deformed shape of the first 2 ms by the linear EHSAPT dynamic is given in Fig. 4.18. The phase difference between the nonlinear dynamic response and linear dynamic response can be clearly observed by comparing to Fig. 4.17. The movements of edges are much smaller than that when considering geometric nonlinearities.

In general, the geometric nonlinearity has a significant effect on the dynamic response of a sandwich panel subjected to blast loading. Differences in magnitude and shifting in time are both observed. The linear dynamic analysis is only valid for small deformations when the infinitesimal kinematic relations hold. When introducing geometric nonlinearities, the displacements and stresses are no longer proportional to the load intensity and have nonlinear relations to the load intensity. Therefore, the differences between the linear dynamic analysis and the nonlinear dynamic analysis depend on the load intensity.

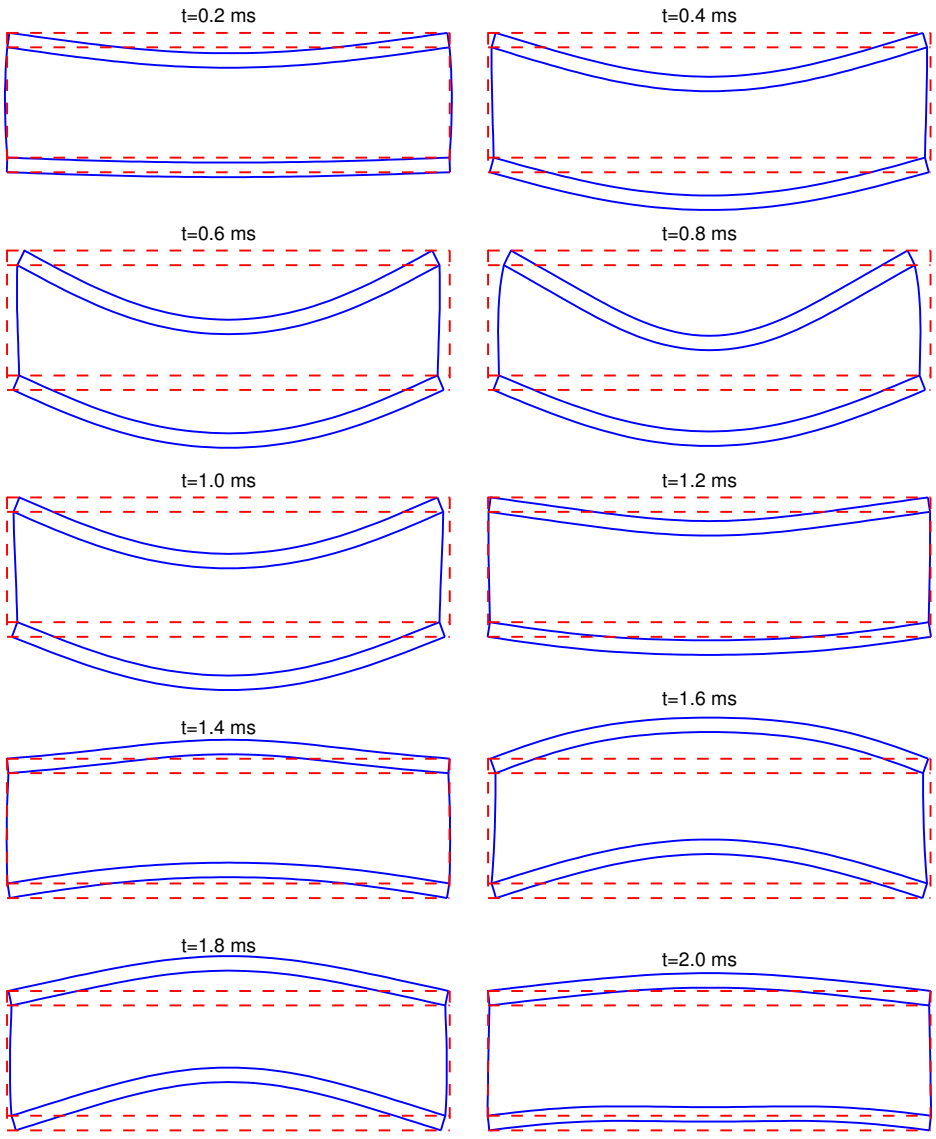

Figure 4.17: The deformed shape of sandwich panel in first 2 ms (nonlinear EHSAPT dynamic analysis)

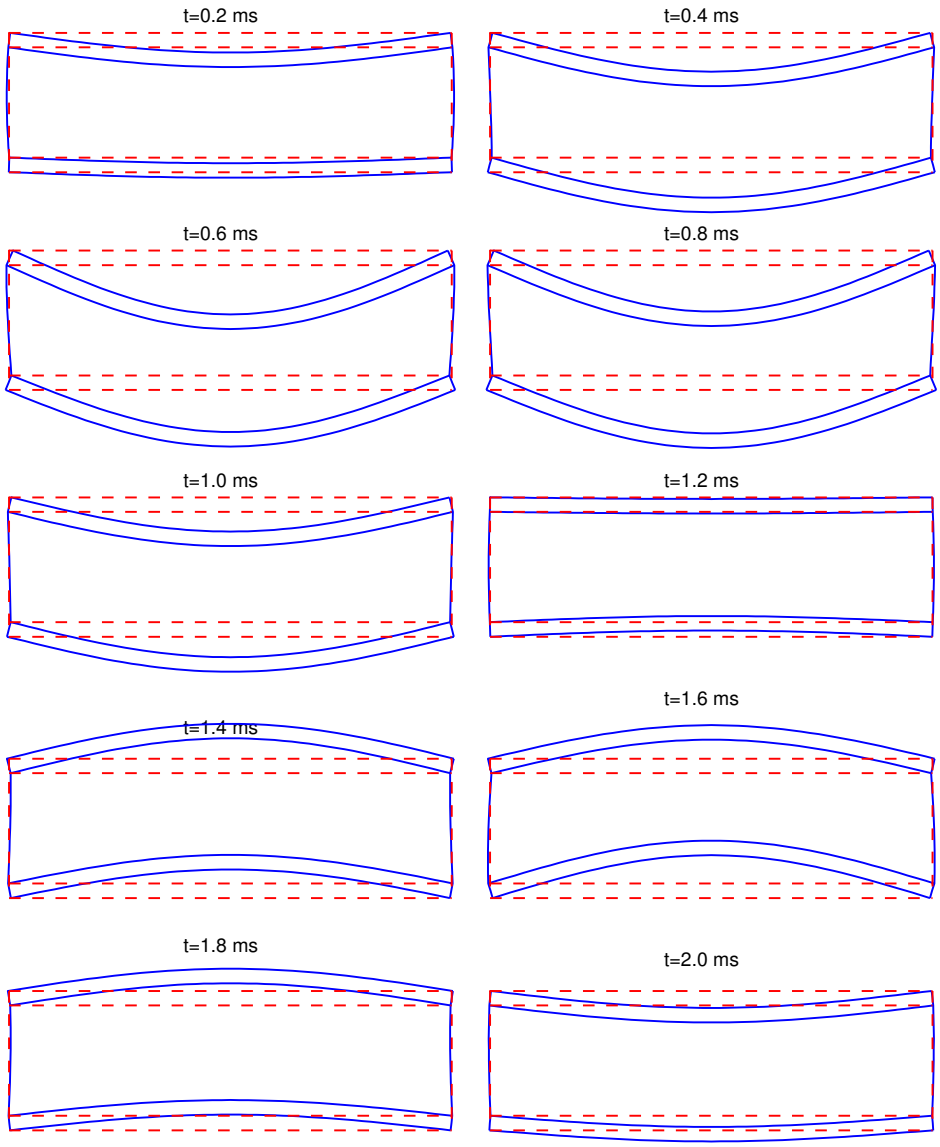

Figure 4.18: The deformed shape of sandwich panel in first 2 ms (linear EHSAPT dynamic analysis)

4.3 Conclusions

A systematic nonlinear dynamic analysis strategy is presented. In the spatial domain, the sandwich panel is modeled with the EHSAPT-based finite element. The central difference method is used in the time domain to obtain the dynamic response.

A sandwich panel subjected to blast loading is analyzed with the proposed method. The linear dynamic results are first compared with the linear elasto-dynamic solution. In the earlier study, some divergences and phase differences were observed between the linear EHSAPT dynamic and the linear elasticity dynamic. It is shown that these differences are no longer present if the same constitutive equations are imposed in the core. The results show that the linear EHSAPT can accurately predict the linear dynamic response of sandwich panels. The displacements and stresses are identical to the closed form linear elasticity solution. Benefiting from the time integral method, the proposed EHSAPT approach can accurately predict the dynamic response over a long duration while the elastic solution is restricted by the limitation of the inverse Laplace transform method used to only the short duration transient response.

Subsequently, the geometric nonlinearity effects are investigated. Five nonlinear models, including commonly used simplifications, are used to perform the nonlinear dynamic analysis. Numerical results indicate that the geometric nonlinearities have a significant effect on the dynamic response of sandwich structures. The linear dynamic response coincides with the nonlinear one only at the very beginning. The effects caused by the geometric nonlinearities are cumulative. Thus, the difference between the linear dynamic and nonlinear dynamic increases over time. When the sandwich panel is subjected to a transverse blast loading, the transverse displacement shows similar trends either with or without geometric nonlinearities, but higher amplitudes and phase changes are observed when considering the geometric nonlinearities. The nonlinear dynamic response of the axial displacement and that of the stresses are much different from the corresponding linear

results. The edge movement and in-plane vibration can only be captured when considering the geometric nonlinearities. The comparison between different nonlinear models reveals that the nonlinear terms appearing in the core kinematic relations are important. The simplifications that only include the nonlinear terms of the faces, or these referring to Von Kàrmàn relations in the faces and core can improve the accuracy of the results, but still are inadequate. It is suggested to include the full nonlinear terms of the core, or at least all the nonlinear terms related to the transverse displacement.

CHAPTER 5

GLOBAL BUCKLING AND WRINKLING OF SANDWICH STRUCTURES

In sandwich composites, two high stiffness thin face sheets are typically bonded to a low density soft core. Benefiting from this configuration, sandwich composites have been known as high efficient structures comprising high stiffness and strength with low resultant weight. This configuration leads sandwich structures to have more complicated stability behavior than ordinary beams. The compressibility of the core significantly affects the stability response and contributes to the local instability phenomenon. The stability of sandwich structures is extremely important since the compressive strength can be realized only if they are stabilized against buckling. The buckling behavior of sandwich panels can be divided in to two types. One is the global buckling (Euler buckling) and the other is the short-wave wrinkling of the faces. The buckling mode shape of sandwich panels can also be a combination of the global buckling and wrinkling.

5.1 Buckling Analysis

In Chapter 3, the weak form nonlinear governing equations are derived based on the EHSAPT. They describe the equilibrium state of sandwich panels. As suggested in Chapter 3 and Chapter 4, we only consider the case with $\alpha_2 = \beta_j = 1, (j = 1...6)$, and $\alpha_1 = 0$, namely the faces include nonlinear terms related to w, i.e., the $(w_{,x})^2$ term only, the one considered in Euler-Bernoulli beam, while the core contains all nonlinear terms.

Loads are usually applied proportionally when considering the stability problem. Thus, the external force vector is further written as $\lambda\{\boldsymbol{R}\}$, in which $\{\boldsymbol{R}\}$ is a unit load vector and λ is a load scalar. Therefore, the governing equations Eq. (3.10) are rewritten as,

$$\{\boldsymbol{G}(\{\boldsymbol{U}\}, \lambda)\} = [\boldsymbol{K}]\{\boldsymbol{U}\} - \lambda\{\boldsymbol{R}\} = \{\boldsymbol{0}\} \tag{5.1}$$

Regarding the buckling behavior, we are seeking for bifurcation points at which there are multiple equilibrium states under same loading. Thus, it requires the determinant of the Jacobian matrix of Eq. (5.1) equals to zero [94], namely,

$$\det\left([\boldsymbol{K}_T]\right) = \left|\frac{\partial\{\boldsymbol{G}\left(\{\boldsymbol{U}\},\lambda\right)\}}{\partial\{\boldsymbol{U}\}}\right| = 0 \tag{5.2}$$

The tangent stiffness matrix is given by Eq. (3.12). Solving Eq. (5.2) yields the critical buckling load and corresponding buckling mode. Since $[\boldsymbol{K}_T]$ depends on the displacement $\{\boldsymbol{U}\}$ which is related to the deformation of sandwich panels, it is not easy to solve Eq. (5.2) directly. By linearization, the critical buckling load and mode shape can be determined at a convenience manner.

The tangent stiffness matrix includes a linear part, that is independent of the deformation, and the rest part depends on the deformation, as shown Eq. (3.12a). When it is loaded with reference load scaler λ_r, the tangent stiffness matrix is collected as

$$[{}^r\boldsymbol{K}_T] = [\boldsymbol{K}_L] + [{}^r\boldsymbol{K}_{T_{NL}}] \tag{5.3}$$

where $[\boldsymbol{K}_L]$ is the linear part and $[{}^r\boldsymbol{K}_{T_{NL}}]$ is the nonlinear part under load scaler λ_r.

It is assumed that the nonlinear part is proportional to the load scalar λ. Therefore, the tangent stiffness matrix subjected to critical load λ_c is approximated as

$$[\boldsymbol{K}_T] = [\boldsymbol{K}_L] + \frac{\lambda_c}{\lambda_r}[{}^r\boldsymbol{K}_{T_{NL}}] \tag{5.4}$$

Substituting Eq. (5.4) into Eq. (5.2), it becomes

$$\det\left([\boldsymbol{K}_L] + \frac{\lambda_c}{\lambda_r}[{}^r\boldsymbol{K}_{T_{NL}}]\right) = 0 \tag{5.5}$$

The nonlinear equations of buckling analysis given by Eq. (5.2) is turned into a standard

eigen-value problem. Solving Eq. (5.5) yields λ_c/λ_r, and the corresponding eigen-vector is the buckling mode shape. When formulating $[^r\boldsymbol{K}_{T_{NL}}]$, the deformation of sandwich panel in pre-buckling state is required. It is determined by the nonlinear static analysis of the sandwich panel under load λ_r. The detailed buckling analysis procedures are given as follows:

1. For a given reference load λ_r, an initial guess $\{\boldsymbol{U}\}_0$ is calculated as the linear static response, which neglects the nonlinear terms appearing in the stiffness matrix, namely

$$[\boldsymbol{K}_L]\{\boldsymbol{U}\}_0 = \lambda_r\{\boldsymbol{R}\} \tag{5.6}$$

   where $[\boldsymbol{K}_L]$ is the linear stiffness matrix that only includes $[\boldsymbol{K}_{e_L}]$ in each element. $[\boldsymbol{K}_L]$ is also the same as the linear part of the tangent stiffness matrix.

2. Starting from the initial guess $\{\boldsymbol{U}\}_0$ and $i = 0$, $\{\boldsymbol{U}\}_{i+1}$ is obtained by using the Newton-Raphson method, namely

$$\{\boldsymbol{U}\}_{i+1} = \{\boldsymbol{U}\}_i - [\boldsymbol{K}_T(\{\boldsymbol{U}\}_i, \lambda_r)]^{-1}\{\boldsymbol{G}(\{\boldsymbol{U}\}_i, \lambda_r)\} \tag{5.7}$$

   Usually, $\{\boldsymbol{U}\}_{i+1} \neq \{\boldsymbol{U}\}_i$. Repeat Eq. (5.7) until the results are within a prescribe tolerance,

$$\text{Error} = \sqrt{\frac{(\{\boldsymbol{U}\}_{i+1} - \{\boldsymbol{U}\}_i)^T(\{\boldsymbol{U}\}_{i+1} - \{\boldsymbol{U}\}_i)}{\{\boldsymbol{U}\}_i^T\{\boldsymbol{U}\}_i}} \tag{5.8}$$

3. The nonlinear part of the tangent stiffness matrix at reference load λ_r, $[^r\boldsymbol{K}_{T_{NL}}]$, is computed with the converged displacement vector $\{\boldsymbol{U}\}_{i+1}$. Then Eq. (5.5) can be solved by a generalized eigen-value solver.

The above are the general procedures of the buckling analysis of sandwich panels based on the EHSAPT. The critical buckling load and buckling mode shape are determined. It can be seen that, the pre-buckling state when sandwich panels subjected to reference load

λ_r is determined by a nonlinear static analysis, and the geometric nonlinearities of both faces and core are considered. Therefore, the pre-buckling state is not constrained to have membrane state only. The buckling mode shape is determined as the corresponding eigenvector. So, there is no additional constraint on the mode shape either. The results given by this buckling analysis will be further used as the preliminary results for the nonlinear post-buckling analysis to increase the computational efficiency.

5.2 Numerical Results and Discussion

Numerical studies are carried out to investigate the stability of sandwich panels subjected to axial compressive loads. Sandwich panel is a compound structure that has layered configuration. The constraints at different layers should be considered separately to reflect the true boundary conditions. In present work, the boundary conditions, as shown in Fig. 5.1, are considered. The left edge and right edge of three layers are constrained in transverse direction. The axial movement of the right edge of the bottom face is constrained. The left edge of the bottom face, both edges of the top face, and both edges of the core can move freely along x direction.

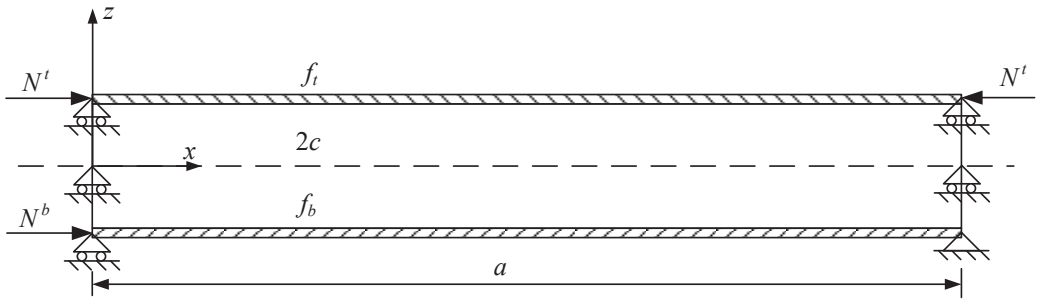

Figure 5.1: Sketch of a sandwich panel subjected to axial compressive loads

The geometric and material parameters are taken from Ref. [79]. The sandwich panel has faces with thickness $f_t = f_b = 0.5$ mm, and core with thickness $2c = 19.05$ mm. The width is $b = 60$ mm. Different lengths are considered. The elasticity modulus of the top

face and the bottom face are $E_1^t = E_1^b = 26900.0$ MPa. In core, it has $E_1^c = E_2^c = E_3^c = E^c = 52.0$ MPa, $G_{12}^c = G_{31}^c = G_{31}^c = G^c = 21.0$ MPa. The Poisson's ratio is calculated as $\nu_{12}^c = \nu_{13}^c = \nu_{32}^c = E^c/2G^c - 1$.

Typically, the axial rigidity of the core is two or three orders smaller than that of faces, e.g., $E_1^c/E_1^t = 0.0019$ for the sandwich panel we considered here. Therefore, the axial rigidity of the core is usually neglected [43, 79]. This assumption is justified in the static response of sandwich panels either considering the geometric nonlinearity effects or not, and yields acceptable results. To evaluate the effect of the core sheet axial rigidity, same sandwich panels with $E_1^c = 52.0 \times 10^{-5}$ MPa is also considered. By this taken, the axial rigidity of the core is neglected and the EHSAPT is deduced to the HSAPT. It can also be regarded as a sandwich panel made with a core material that has zero axial rigidity.

5.2.1 Sandwich Panels Subjected to Equal Axial Compressive Loads

Consider a sandwich panel with length $a = 300$ mm subjected to equal axial force at top and bottom, namely, $N^t = N^b = P/2$. A convergence study is performed first. To ensure the accuracy and also well capture the wrinkling that has multiple short waves, results are presented with 450 uniform length 2-node EHSAPT-based elements.

Sandwich panels subjected to equal axial loads are often assumed to have membrane pre-buckling state [43, 81, 82], i.e., the lateral deformation is zero . Thus, the pre-buckling state is studied first. The transverse displacement of three layers of the sandwich panel in pre-buckling state with $P = 9000$ N are plotted in Fig. 5.2. It is seen that the axial rigidity of the core has a significant effect on the transverse deformation. When the core sheet axial rigidity is included, the maximum transverse displacement is about 0.12 mm, and the transverse displacement is constant at the regions away from edges, as shown in Fig. 5.2a. The sign of transverse displacement of the faces only changes twice and it happens near edges. The edge effect is observed. However, when neglecting the axial rigidity of the core, or for the sandwich panel made with zero axial rigidity core material, the

transverse displacement pattern is different, and the maximum value is only 6×10^{-6} mm, as shown in Fig. 5.2b. Thus, only the transverse displacement when neglecting the core axial rigidity can be regarded as negligible, and the membrane pre-buckling state approximation is valid. For this sandwich panel we considered, although the ratio of the axial rigidity of the core over the that of faces is very small, i.e., $E_1^c/E_1^t = 0.0019$, the small magnitude axial rigidity of the core affects the axial load transfer mechanism. Therefore, it influences the deformation of pre-buckling state and further alters the critical buckling load and the buckling mode shape.

Table 5.1 lists the critical loads of the first 6 buckling modes of the 300 mm sandwich panel subjected to equal axial compressive loads at the top and bottom faces. The buckling type, i.e., global buckling (G) or wrinkling (W), is included. For comparison and verification, same sandwich panel is analyzed by commercial FEA software ADINA. A two-dimensional model with fine mesh is built in ADINA. Both faces and core are modelled with 9-node plane stress element, 4 elements are placed in the thickness direction of the top face and bottom face, respectively, and 15 elements are in the thickness direction of the core. There are 4600 elements totally. The result in the literature obtained by the HSAPT is included. The results in row of "EHSAPT" are the solutions obtained by the proposed approach with the axial rigidity of the core and the geometric nonlinearities of the faces and core included. The critical loads of neglecting the core sheet axial rigidity by setting $E_1^c = 52.0 \times 10^{-5}$ MPa are marked with "$E_1^c \approx 0$". Besides, a simplified geometric nonlinear model that only considers the geometric nonlinearity in the faces is also used to perform the stability analysis. This model is achieved by only including the nonlinear stiffness matrix and nonlinear tangent stiffness matrix of the faces and neglecting those of the core, i.e., $\alpha_2 = 1$, and $\alpha_i = \beta_j = 0$, $(i \neq 2,\ j = 1...6)$. The corresponding results are marked with "NL face".

In Table 5.1, it is seen that the wrinkling critical loads are very close to each other. In a small range of load magnitude, there exist several wrinkling modes. The axial rigidity

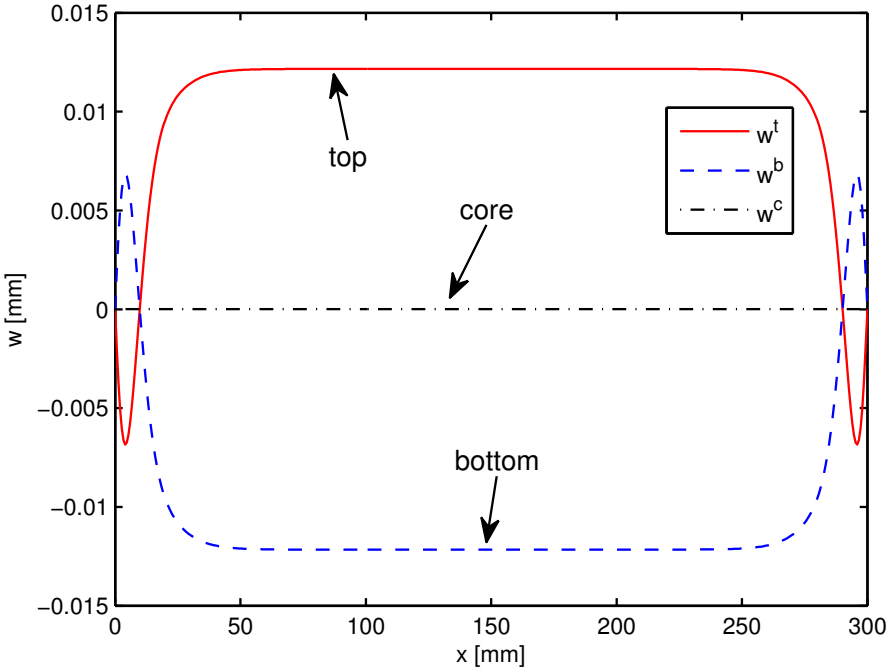

(a)

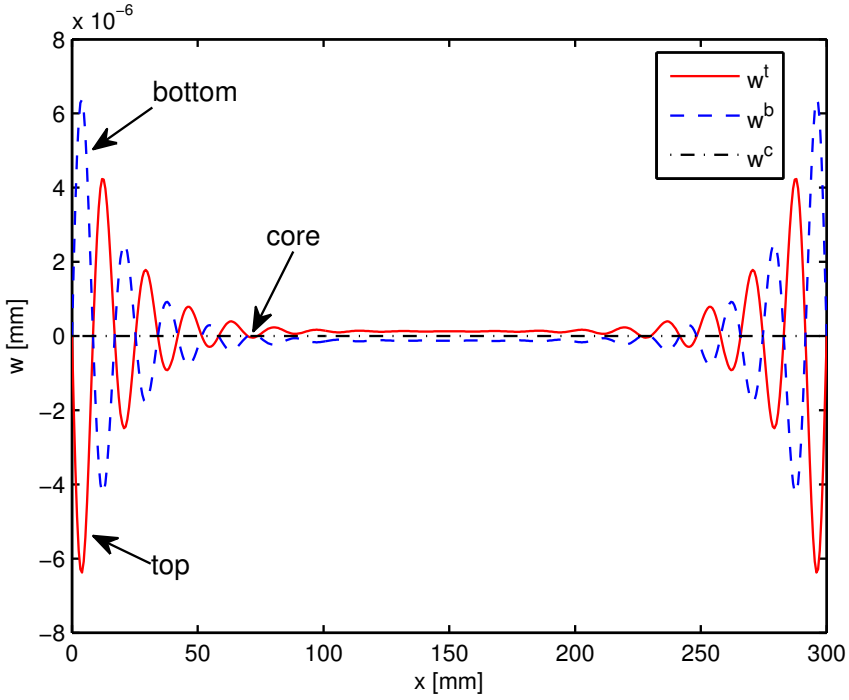

(b)

Figure 5.2: Transverse displacement in pre-buckling state of $a = 300$ mm sandwich panel subjected to equal axial compressive loads $N^t = N^b = P/2$ with $P = 9000$ N: (a) $E_1^c = 52.0$ MPa ; (b) $E_1^c = 52.0 \times 10^{-5}$ MPa

Table 5.1: Critical buckling loads of $a = 300$ mm sandwich panel, $N^t = N^b = P/2$ (N)

Mode	1	2	3	4	5	6
EHSAPT	10292.78 (G)	15633.34 (W)	15633.43 (W)	15770.31 (W)	15773.35 (W)	15804.63 (W)
EHSAPT (NL face)	10554.70 (G)	15763.30 (W)	15763.39 (W)	15882.62 (W)	15887.84 (W)	15916.08 (W)
EHSAPT ($E_1^c \approx 0$)	9389.66 (W)	9394.95 (W)	9413.12 (W)	9431.53 (W)	9463.10 (W)	9502.35 (W)
EHSAPT ($E_1^c \approx 0$, NL face)	9389.55 (W)	9394.83 (W)	9413.01 (W)	9431.42 (W)	9462.99 (W)	9502.24 (W)
ADINA	10126.89 (G)	15342.48 (W)	15342.84 (W)	15469.38 (W)	15469.56 (W)	15504.12 (W)
HSAPT [80]	9387.14 (W)					

(G): Global buckling
(W): Wrinkling

of the core has a significant effect on the critical load of wrinkling. When including the axial rigidity of the core, the wrinkling critical load is around 15600 N. However, when neglecting the axial rigidity of the core, or for sandwich panels made with zero axial rigidity core material, the wrinkling critical load is around 9400 N. It is reduced by around 50%. When neglecting the axial rigidity of the core, the first critical buckling load given by the EHSAPT is 9389.66 N, while the HSAPT gives 9387.14 N [80]. In the HSAPT, the geometric nonlinearity is only considered in the faces. The geometric nonlinearity effect of the core has a very small effect on the prediction of critical buckling load. It is because the deformation is small when the panel is buckled initially. A good agreement is observed between the EHSAPT and ADINA. When only considering the axial rigidity of the core, the first buckling mode is global buckling, which agrees with ADINA. In contrast, neglecting the core axial rigidity leads to wrinkling as the first buckling mode.

The first buckling mode shape given by the EHSAPT, when including the core axial rigidity or neglecting the core axial rigidity, and the mode shape obtained by ADINA are plotted in Fig. 5.3. It is seen that the proposed approach agree well ADINA, and the global

buckling mode shape is similar to that of ordinary beams, i.e., there is one half sine wave over the panel. When neglecting the core axial rigidity, marked with $E_1^c = 52.0 \times 10^{-5}$ MPa, it has wrinkling as the first buckling mode instead. There are approximately 36 half sine waves with uniform magnitude, which agrees with the observation given by the HSAPT [45].

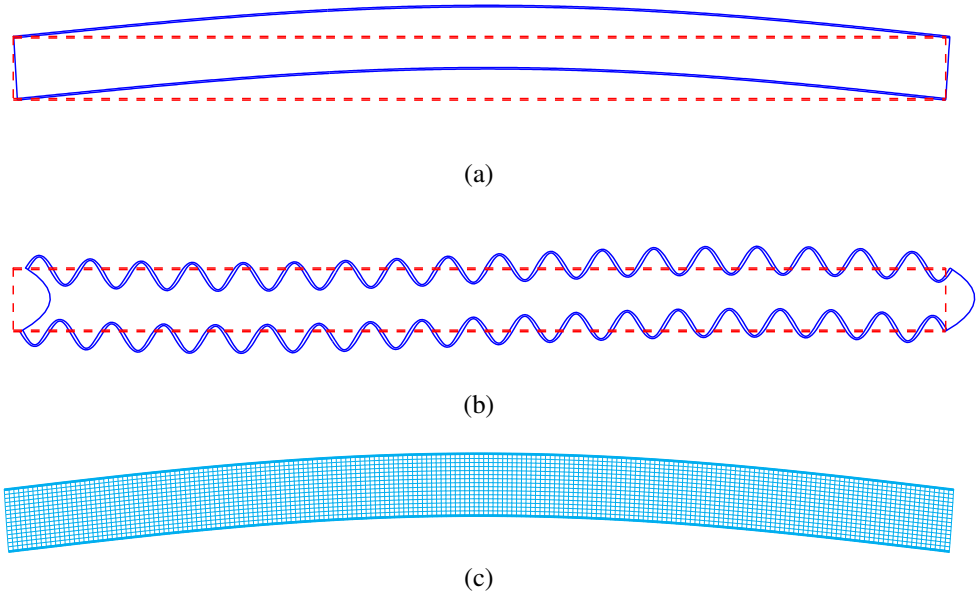

(a)

(b)

(c)

Figure 5.3: First buckling mode shape of $a = 300$ mm sandwich panel: (a) EHSAPT, $E_1^c = 52.0$ MPa; (b) EHSAPT, $E_1^c = 52.0 \times 10^{-5}$ MPa; (c) ADINA

The second and third buckling modes predicted by the EHSAPT and ADINA are shown in Fig. 5.4 and Fig. 5.5. The mode shapes given by the EHSAPT agree well with ADINA's. It should be noted that ADINA requires a two-dimensional model while the model used by the EHSAPT-based element is only one-dimension. The one-dimensional EHSAPT-based element can well capture wrinkling that has multiple non-uniform short waves in faces. Both the second and the third buckling modes are wrinkling. Due to the edge effect in the pre-buckling state, the waves near edges have higher amplitude, and the buckling mode shape can be regarded as anti-symmetric type, instead of the symmetric wrinkling given by the HSAPT, shown in Fig. 5.3b.

The first six buckling loads of sandwich panels with different lengths subjected to equal

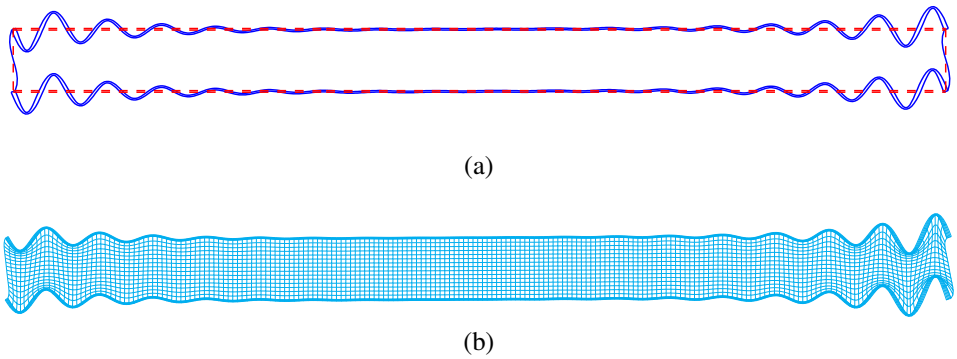

(a)

(b)

Figure 5.4: Second buckling mode shape of $a = 300$ mm sandwich panel: (a) EHSAPT, $E_1^c = 52.0$ MPa; (b) ADINA

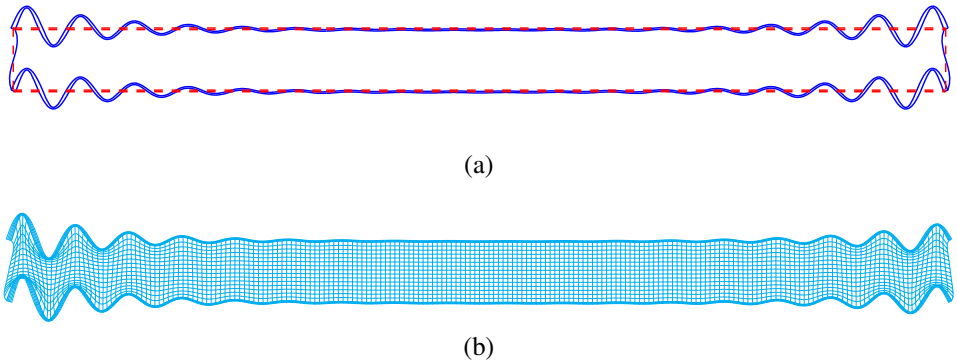

(a)

(b)

Figure 5.5: Third buckling mode shape of $a = 300$ mm sandwich panel: (a) EHSAPT, $E_1^c = 52.0$ MPa; (b) ADINA

loads are given in Table 5.2. The type of buckling mode, global buckling (G) or wrinkling (W), is also listed in the table. The results agree with ADINA's, given by Table 5.3. It is seen that the critical load corresponding to wrinkling is around 15600 N, and remains in the same range when sandwich panels have different lengths. However, the critical load of global buckling changes with the length of sandwich panel, which is similar to ordinary beams. A longer sandwich panel is much easier to be buckled globally. It can be concluded that the overall length of sandwich panel determines the sequence of the buckling mode type. When sandwich panels have different lengths, once the critical load of the global buckling is lower than that of wrinkling, the global buckling is sorted as the first buckling mode, and vise versa.

Table 5.2: Critical buckling loads of sandwich panel of different lengths by EHSAPT with $E_1^c = 52.0$ MPa, $N^t = N^b = P/2$ (N)

Mode	1	2	3	4	5	6
$a = 150$ mm	15617.30 (W)	15620.59 (W)	15802.41 (W)	15825.84 (W)	15955.57 (W)	15997.91 (W)
$a = 300$ mm	10292.78 (G)	15633.34 (W)	15633.43 (W)	15770.31 (W)	15773.35 (W)	15804.63 (W)
$a = 600$ mm	3673.90 (G)	10300.93 (W)	15414.70 (W)	15656.23 (W)	15656.52 (W)	15775.78 (W)
$a = 900$ mm	1771.96 (G)	5885.35 (G)	10303.61 (G)	13952.37 (G)	15677.84 (W)	15677.88 (W)
$a = 1200$ mm	1027.29 (G)	3675.35 (G)	7025.36 (G)	10305.02 (G)	13132.49 (G)	15420.40 (G)

(G): Global buckling
(W): Wrinkling

The first 4 buckling mode shapes of $a = 600$ mm sandwich panel are given by Fig. 5.6. The first three are the global buckling mode with one, two, and three half sine waves, respectively, and the fourth is the wrinkling mode since its critical load is between than that of the global buckling mode with three and four half sine waves. The global buckling mode shape is the same as the ordinary beam's, and the wrinkling mode shape has multiple short waves. The wrinkling mode has localized buckling pattern rather than uniform waves.

Table 5.3: Critical buckling loads of sandwich panel of different lengths by ADINA, $N^t = N^b = P/2$ (N)

Mode	1	2	3	4	5	6
$a = 150$ mm	15358.80 (W)	15367.08 (W)	15469.08 (W)	15473.04 (W)	15480.00 (W)	15525.48 (W)
$a = 300$ mm	10126.89 (G)	15342.48 (W)	15342.84 (W)	15469.38 (W)	15469.56 (W)	15504.12 (W)
$a = 600$ mm	3646.59 (G)	10156.92 (G)	15181.56 (G)	15385.23 (W)	15386.16 (W)	15510.24 (W)
$a = 900$ mm	1764.81 (G)	5827.01 (G)	10162.38 (G)	13744.50 (G)	15436.35 (W)	15437.70 (W)
$a = 1200$ mm	1024.67 (G)	3649.96 (G)	6947.78 (G)	10164.51 (G)	12938.94 (G)	15196.50 (G)

(G): Global buckling
(W): Wrinkling

Same global buckling and wrinkling mode shapes are observed by ADINA.

The first two buckling modes of $a = 150$ mm sandwich panel are plotted in Fig. 5.7. Again, wrinkling with non-uninform buckling waves are observed. When the length is 150 mm, the lowest global buckling critical load, whose mode shape has one half sine wave, is much higher than that of wrinkling. Thus, the wrinkling comes first. Same buckling mode shapes are observed by ADINA. Comparing Fig. 5.4, Fig. 5.5, Fig. 5.6d, and Fig. 5.7, it is seen that the wrinkling mode shapes are similar although the length of sandwich panel varies. Due to the edge effect, the buckling waves at the edges have higher relative amplitude compared to that at center. It further demonstrates the inadequate of using presumed sinusoidal buckling pattern with uniform amplitude to estimate the buckling load. This approximation might be acceptable for sandwich panels made with zero core axial rigidity, as shown in Fig. 5.3b.

In Table 5.2, it is seen that the critical buckling loads of different wrinkling modes are very close, which is a notable feature and is different from the global buckling. It implies that when considering the wrinkling, it should not be limited to one wrinkling mode with the lowest critical load. Since the critical loads of other wrinkling modes are so close that

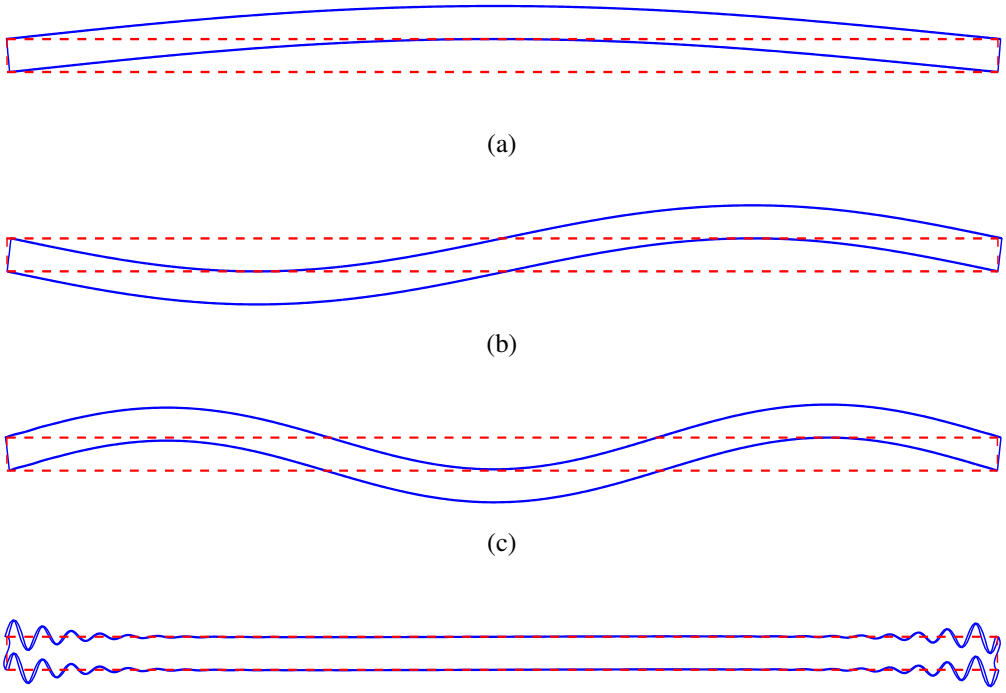

(a)

(b)

(c)

(d)

Figure 5.6: Buckling mode shapes of $a = 600$ mm sandwich panel: (a) Mode 1; (b) Mode 2; (c) Mode 3; (d) Mode 4

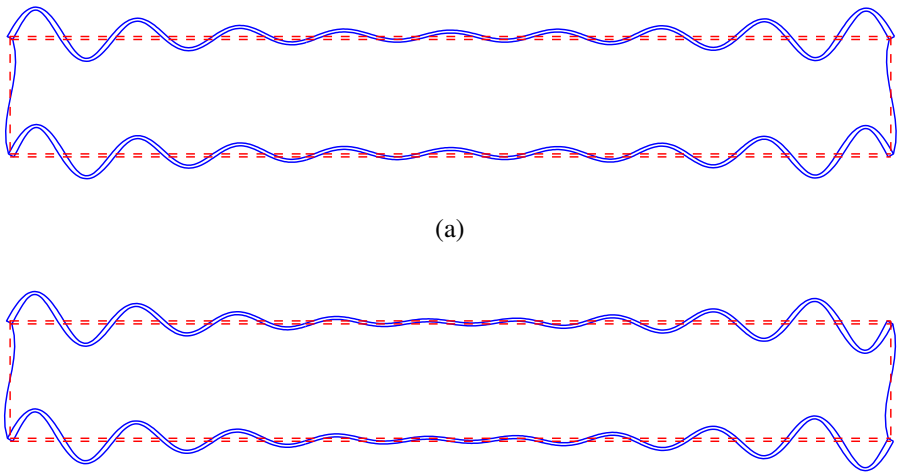

(a)

(b)

Figure 5.7: Buckling mode shapes of $a = 150$ mm sandwich panel: (a) Mode 1; (b) Mode 2

other modes might also be initiated. This feature will be further discussed in terms of the the nonlinear post-buckling response in the Chapter 6.

Same buckling analysis is performed on sandwich panels neglecting core sheet axial rigidity, namely by setting $E_1^c = 52.0 \times 10^{-5}$ MPa. It can also be regarded as the stability property of sandwich panels made with core material that has zero axial rigidity. The critical buckling loads of sandwich panels with various lengths subjected to equal axial compressive loads are listed in Table 5.4. Same as Table 5.2, for sandwich panels made with zero core axial rigidity, the global buckling critical load depends on the length of the sandwich panel, while the wrinkling critical load remains similar when the sandwich panel has different lengths. For a sandwich panel with a specific length, critical load difference between different global buckling modes, e.g., the one has one half sine wave, two half sine waves, or three, are large, while the wrinkling critical loads are very vlose.

Table 5.4: Critical buckling loads of sandwich panel of different lengths by EHSAPT with $E_1^c = 52.0 \times 10^{-5}$ MPa, $N^t = N^b = P/2$ (N)

Mode	1	2	3	4	5	6
$a = 150$ mm	9389.58 (W)	9431.47 (W)	9463.00 (W)	9610.77 (W)	9635.01 (W)	9892.76 (W)
$a = 300$ mm	9389.66 (W)	9394.95 (W)	9413.12 (W)	9431.53 (W)	9463.10 (W)	9502.35 (W)
$a = 600$ mm	3636.57 (G)	9389.43 (W)	9390.61 (W)	9395.74 (W)	9398.97 (W)	9409.88 (W)
$a = 900$ mm	1752.94 (G)	5825.84 (G)	9394.25 (W)	9395.69 (W)	9396.09 (W)	9400.52 (W)
$a = 1200$ mm	1016.00 (G)	3636.53 (G)	6954.50 (G)	9409.78 (W)	9410.18 (W)	9411.28 (W)

(G): Global buckling
(W): Wrinkling

Comparing Table 5.2 and Table 5.4, it is seen that the axial rigidity of the core has almost no effect on the global buckling critical load, but it reduces the wrinkling critical load significantly, around 50%. Since the buckling mode is sequenced with the magnitude of the correspond critical load, the wrinkling mode with lower critical load might come

ahead of the global buckling mode when sandwich panel has zero core axial rigidity. Take $a = 600$ mm sandwich panel as an example. When including the core axial rigidity, the first three buckling modes are all global buckling since the critical loads of these three global buckling modes are lower than that of wrinkling, however, when neglecting the core axial rigidity, the wrinkling mode comes as the second buckling mode since it has lower critical load, although both cases have very close global buckling critical load. The first and second buckling mode shapes of $a = 600$ mm sandwich panel neglecting core axial rigidity are plotted in Fig. 5.8. It shows that neglecting the axial rigidity of the core does not change the global buckling mode shape, as seeb in Fig. 5.8a and Fig. 5.6a, both cases have one half sine wave over the panel. But the wrinkling buckling mode shape is different from the one considering the axial rigidity of the core, shown by Fig. 5.8b and Fig. 5.6d. Neglecting axial rigidity leads wrinkling to have multiple uniform sine waves. It is similar to the wrinkling mode shape of $a = 300$ mm sandwich panel with zero axial rigidity, shown in Fig. 5.3b. Similar wrinkling mode shape with multiple uniform sine waves is observed for sandwich panels with other lengths. The buckling waves numbers are related to the length of the sandwich panel. Only for such cases, the presumed sinusoidal wrinkling mode patterns can yield good estimations.

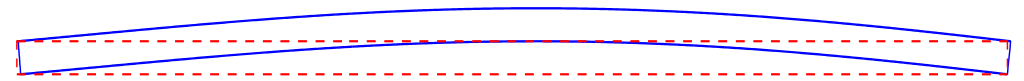

(a)

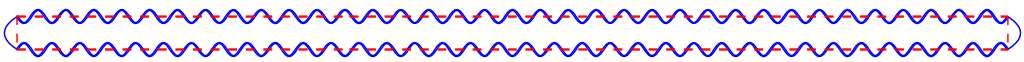

(b)

Figure 5.8: Buckling mode shapes of $a = 600$ mm sandwich panel with $E_1^c = 52.0 \times 10^{-5}$ MPa: (a) Mode 1; (b) Mode 2

5.2.2 Sandwich Panels Subjected to Unequal Axial Compressive Loads

In practice, the compressive loads applied to the top face and the bottom face are not essential to be equal. Due to imperfections or the loads transferred from other structures, the loads might have unequal magnitudes. As a result, a sandwich panel is possible to have a curved shape in the pre-buckling state.

A sandwich panel subjected to unequal axial compressive loads, namely $N^t = 0.3P$ and $N^b = 0.7P$, is considered. The length of the sandwich panel is $a = 300$ mm, other geometric and material parameters are the same as the ones in the case subjected to equal axial compressive loads. To ensure the accuracy and well capture the wrinkling, results are presented with 450 uniform length 2-node EHSAPT-based elements. The transverse displacements of three layers in pre-buckling state with $P = 6600$ N are plotted in Fig. 5.9. Three curves coincide with each other. Due to the unequal loading, the sandwich panel is bent, and the transverse displacement is more significant than the equal compressive loading case. The pre-buckling state is no longer membrane.

The first two buckling modes obtained by the EHSAPT have same critical load and it is 8499.63 N. ADINA also have same critical load for the first two buckling modes and it is 7908.65 N. Fig. 5.10 plots the first two buckling mode shapes given by the EHSAPT. These two mode shapes are close to each other and are the same as the ones given by ADINA. There are multiple short waves at the center region of the bottom face since the bottom face is subjected higher compressive loads. The short waves have non-uniform amplitudes and the deformation of the bottom face is larger than that of top face.

Comparing Fig. 5.9 with Figs. 5.3a and 5.6a, it is seen that the first global buckling mode of the sandwich panel subjected to equal axial loads is similar to the pre-buckling state of the sandwich panels subjected to unequal axial loads. Therefore, it raises the possibility that sandwich panels may be further buckled into the buckling mode shown in Fig. 5.10 after they are buckled globally.

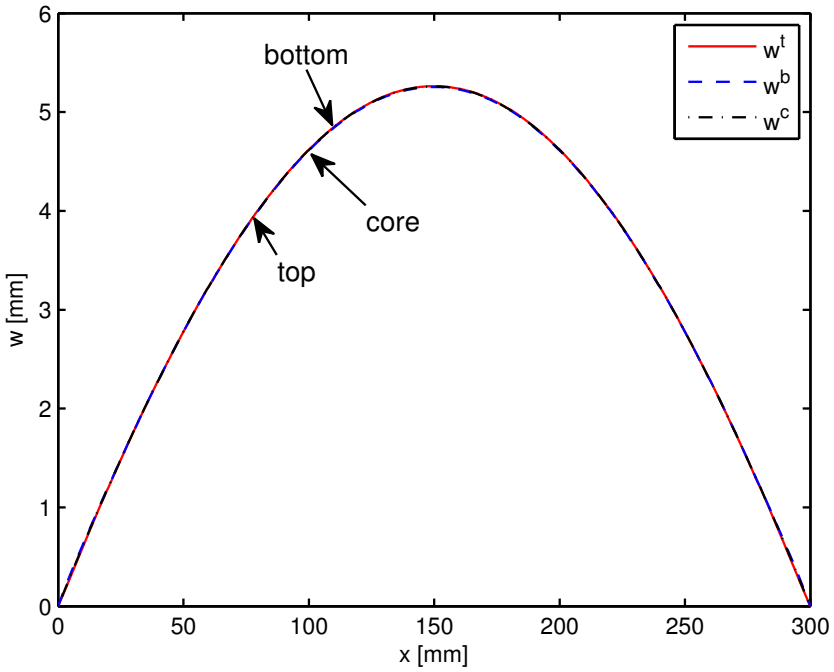

Figure 5.9: Transverse displacement in pre-buckling state of $a = 300$ mm sandwich panel subjected to unequal axial compressive loads $N^t = 0.3P$, $N^b = 0.7P$ with $P = 6600$ N

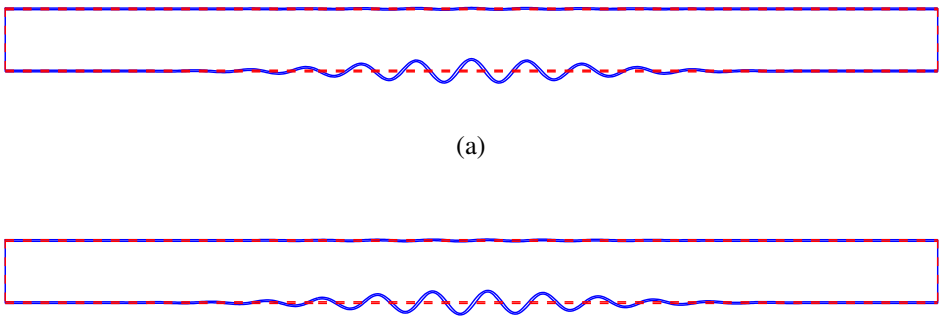

(a)

(b)

Figure 5.10: Buckling mode shapes of $a = 300$ mm sandwich panel subjected to unequal axial compressive loads $N^t = 0.3P$, $N^b = 0.7P$: (a) Mode 1; (b) Mode 2

5.3 Conclusions

The buckling behavior of sandwich panels, including the critical buckling load and buckling mode shape, is investigated. Both faces and core are considered undergoing large displacements with moderate rotations. A general buckling analysis, that can predict the critical buckling load and give buckling mode shape of sandwich panels is outlined.

Results show that the pre-buckling state is not essential to have membrane state, and the buckling mode shape may also have non-uniform sine wave pattern, although the membrane pre-buckling state and uniform sine wave buckling mode are very common for ordinary beams. Due to the edge effect or the bending response in the pre-buckling state, the wrinkling buckling mode shape has non-uniform sine waves. The localized effect plays an important role in the wrinkling mode shape. The global buckling mode shape of sandwich panels has one or several half sine waves with same amplitude, which is the same as ordinary beams.

Sandwich panels with different lengths are studied. For verifications, results are compared with commercial FEA software ADINA. A good agreement is observed. Both global buckling and wrinkling (local buckling) may occur for the sandwich panels subjected to axial compressive loads. For a specific sandwich panel, different global buckling modes have quite different critical loads. The global buckling critical load is related to the length of sandwich panels. In contrast, the wrinkling usually has multiple short waves, and there exist many wrinkling modes in a very narrow load intensity range. That means the wrinkling mode with lowest critical load is not essential to occur first since the critical loads of other wrinkling modes are very close, and other wrinkling modes may be initiated by imperfections or other reasons in practice. The length of sandwich panel has very little effects on the critical load of wrinkling. For a sandwich panel with a specific length, the first buckling mode is characterized as the one with the lowest critical load. Therefore, the longer sandwich panel is more easy to experience global buckling since the critical global buckling

load of longer sandwich panel is lower than that of shorter one, and the critical buckling load of wrinkling remains almost similar for sandwich panels with different lengths.

Axial rigidity of the core has a significant effect on the stability response, although it is usually negligible in static analysis. For the sandwich panels we considered, although $E_1^c/E_1^t = 0.0019$, neglecting the core axial rigidity reduces the wrinkling critical load by around 50%. The wrinkling mode shape becomes multiple short waves with uniform amplitude instead, and the wrinkling wave number is changed with the length of the sandwich panel.

CHAPTER 6

NONLINEAR POST-BUCKLING RESPONSE OF SANDWICH STRUCTURES

The buckling analysis can provide a basic understanding about the stability property of sandwich structures, including the critical load and buckling mode shape at a convenient manner. However, it cannot give further information about the behavior after sandwich structures are buckled. The buckling behavior does not essentially mean that sandwich structures lost the load carrying capability, especially in the case with a stable post-buckling response. Therefore, the post-buckling response of sandwich panels is investigated in this chapter.

6.1 Solution Approach

6.1.1 Path Following Procedure

The weak form governing equations Eq. (5.1) describe the equilibrium of sandwich panels in arbitrary state. The solution points compose the equilibrium path. These nonlinear equations are solved by the iterative method together with a path following procedure. The equilibrium path is divided into several increments. The converged solution of current increment is calculated iteratively from that of the previous one.

Denote the solution of Eq. (5.1) at the end of previous increment as $(\{\boldsymbol{U}\}_0, \lambda_0)$. The relation between two iterative steps are,

$$\{\boldsymbol{U}\}_{i+1} = \{\boldsymbol{U}\}_i + \{\Delta\boldsymbol{U}\}_i \tag{6.1a}$$

$$\lambda_{i+1} = \lambda_i + \Delta\lambda_i \tag{6.1b}$$

where $\{\Delta\boldsymbol{U}\}_i$ and $\Delta\lambda_i$ are the displacement corrector and load level corrector of i-th iterative step.

Apply Taylor expansion to $\{\boldsymbol{G}(\{\boldsymbol{U}\}_{i+1}, \lambda_{i+1})\}$ and retain linear terms only,

$$\begin{aligned}\{\boldsymbol{G}(\{\boldsymbol{U}\}_{i+1}, \lambda_{i+1})\} \approx &\{\boldsymbol{G}(\{\boldsymbol{U}\}_i, \lambda_i)\} + \left.\frac{\partial\{\boldsymbol{G}(\{\boldsymbol{U}\}, \lambda)\}}{\partial\{\boldsymbol{U}\}}\right|_{(\{\boldsymbol{U}\}_i, \lambda_i)} \{\Delta\boldsymbol{U}\}_i + \\ &+ \left.\frac{\partial\{\boldsymbol{G}(\{\boldsymbol{U}\}, \lambda)\}}{\partial\lambda}\right|_{(\{\boldsymbol{U}\}_i, \lambda_i)} \Delta\lambda_i\end{aligned} \tag{6.2}$$

where the subscript $(\{\boldsymbol{U}\}_i, \lambda_i)$ denotes the value is evaluated at $(\{\boldsymbol{U}\}, \lambda) = (\{\boldsymbol{U}\}_i, \lambda_i)$.

For easy presentation, the tangent stiffness $[\boldsymbol{K}_T(\{\boldsymbol{U}\}_i, \lambda_i)]$ and $\{\boldsymbol{G}(\{\boldsymbol{U}\}_i, \lambda_i)\}$, which are values evaluated at $(\{\boldsymbol{U}\}_i, \lambda_i)$, are denoted as $[\boldsymbol{K}_T]_i$ and $\{\boldsymbol{G}\}_i$ for short, respectively. We are seeking for solutions of $\{\boldsymbol{G}(\{\boldsymbol{U}\}_{i+1}, \lambda_{i+1})\} = \{\boldsymbol{0}\}$. Note that

$$\frac{\partial\{\boldsymbol{G}(\{\boldsymbol{U}\}, \lambda)\}}{\partial\lambda} = -\{\boldsymbol{R}\} \tag{6.3}$$

Thus, Eq.(6.2) gives

$$[\boldsymbol{K}_T]_i\{\Delta\boldsymbol{U}\}_i - \{\boldsymbol{R}\}\Delta\lambda_i = -\{\boldsymbol{G}\}_i \tag{6.4}$$

If the load increment $\Delta\lambda_i$ is manually given, then Eq. (6.4) is the well known Newton-Raphson method. However, the change of load sometimes is not easy to be determined ahead, especially the case with snap through, in which exists a limit for the load level. This issue can be solved by adding one more constraint equation to determine the change of load level $\Delta\lambda_i$. The additional constraint may be given in terms of the arc-length, such as the "spherical constraint" used by Crifield [92, 93].

$$(\{\boldsymbol{U}\} - \{\boldsymbol{U}\}_0)^T(\{\boldsymbol{U}\} - \{\boldsymbol{U}\}_0) + (\lambda - \lambda_0)^2\{\boldsymbol{R}\}^T\{\boldsymbol{R}\} - \Delta s^2 = 0 \tag{6.5}$$

where Δs is called arc-length and is an input parameter.

Although the "spherical constraint" shown in Eq. (6.5) can capture the snap-through phenomenon and is widely used in the nonlinear static analysis. But the quadratic constraint equation gives two solutions, and only one of them gives the correct direction that

follows the path. For the case involving bifurcation points, the solution may double back to the existing path. Hence, the pseduoarclength continuation using tangent vector [96] is considered. The additional constraint equation is introduced as

$$\Gamma\left(\{\boldsymbol{U}\},\lambda\right)=\frac{d\{\boldsymbol{U}\}_0^T}{ds}(\{\boldsymbol{U}\}-\{\boldsymbol{U}\}_0)+\frac{d\lambda_0}{ds}(\lambda-\lambda_0)-\Delta s=0 \tag{6.6}$$

where $\left(\frac{d\{\boldsymbol{U}\}_0^T}{ds},\frac{d\lambda_0}{ds}\right)$ is the tangent vector at the end of last increment, and Δs is the input parameter arc-length.

Plugging $(\{\boldsymbol{U}\},\lambda)=(\{\boldsymbol{U}\}_i+\{\Delta\boldsymbol{U}\}_i,\lambda_i+\Delta\lambda_i)$ for step $i+1$, it has,

$$\frac{d\{\boldsymbol{U}\}_0^T}{ds}\{\Delta\boldsymbol{U}\}_i+\frac{d\lambda_0}{ds}\Delta\lambda_i=-\Gamma\left(\{\boldsymbol{U}\}_i,\lambda_i\right) \tag{6.7}$$

Solving Eq. (6.4) and Eq. (6.7) simultaneously obtains $(\{\Delta\boldsymbol{U}\}_i,\Delta\lambda_i)$. It can be written in a matrix form,

$$\begin{bmatrix}[\boldsymbol{K}_T]_i & -\{\boldsymbol{R}\}\\ \frac{d\{\boldsymbol{U}\}_0^T}{ds} & \frac{d\lambda_0}{ds}\end{bmatrix}\begin{Bmatrix}\{\Delta\boldsymbol{U}\}_i\\ \Delta\lambda_i\end{Bmatrix}=\begin{Bmatrix}-\{\boldsymbol{G}\}_i\\ -\Gamma_i\end{Bmatrix} \tag{6.8}$$

where Γ_i stands for $\Gamma\left(\{\boldsymbol{U}\}_i,\lambda_i\right)$ for short.

It is seen that, although the tangent stiffness $[\boldsymbol{K}_T]$ is singular at bifurcation points and limit points, the coefficient matrix of Eq. (6.8) remains nonsingular and is invertible.

Once $(\{\Delta\boldsymbol{U}\}_i,\Delta\lambda_i)$ is obtained, $(\{\boldsymbol{U}\}_{i+1},\lambda_{i+1})$ is calculated by adding the correctors, given by Eq. (6.1). Repeat this procedure until it yields prescribed tolerance,

$$\text{ErrTol}=\sqrt{\frac{\{\Delta\boldsymbol{U}\}_i^T\{\Delta\boldsymbol{U}\}_i+\Delta\lambda_i^2}{\{\boldsymbol{U}\}_0^T\{\boldsymbol{U}\}_0+\lambda_0^2}} \tag{6.9}$$

$(\{\boldsymbol{U}\}_{i+1},\lambda_{i+1})$ is the converged result at end of this increment and is used as the initial iterative value for the next increment. Repeating the same procedure, then points located at the equilibrium path can be determined successively. Since the path is obtained as discrete points instead of a continue path, it is crucial to choose appropriate arc-length Δs to balance

the computational efficiency and the accuracy. Δs with too small value requires extra computational time, while too large Δs may skip some details and fail to detect bifurcation points and limit points.

The total number of nodes in the sandwich panel model is n. Since the EHSAPT-based element has 10 DOFs each nodes, $\{\boldsymbol{U}\}$ is a vector with $10n$ terms. At the end of each increment, two scalars are defined as,

$$\delta_{\text{load}} = |\lambda_{i+1} - \lambda_0| \tag{6.10a}$$

$$\delta_{\text{displ}} = \sqrt{\frac{\left(\{\boldsymbol{U}\}_{i+1} - \{\boldsymbol{U}\}_0\right)^T \left(\{\boldsymbol{U}\}_{i+1} - \{\boldsymbol{U}\}_0\right)}{10n}} \tag{6.10b}$$

where δ_{load} and δ_{disp} are the change of the load level and the change of the displacements, respectively.

Denote the accuracy requirement for displacements and loads δ^c_{displ} and δ^c_{load}. If $\delta_{\text{load}} > \delta^c_{\text{load}}$ and/or $\delta_{\text{displ}} > \delta^c_{\text{displ}}$, solution of this increment is discard and this increment is recalculated with new arc-length Δs, which is given as,

$$\Delta s_{\text{new}} = \frac{\Delta s_{\text{old}}}{2} \min\left(\frac{\delta^c_{\text{load}}}{\delta_{\text{load}}}, \frac{\delta^c_{\text{displ}}}{\delta_{\text{displ}}}\right) \tag{6.11}$$

If $\delta_{\text{load}} < \delta^c_{\text{load}}$ and $\delta_{\text{displ}} < \delta^c_{\text{displ}}$, the solution is taken as the converged solution of this increment. Then, the next increment is calculated in the same way. To adjust the arc-length according to iterative steps used in current increment, Δs of next increment is updated as

$$\Delta s_{\text{new}} = 2^{\frac{6-\gamma}{4}} \Delta s_{\text{old}} \tag{6.12}$$

where γ is the number of iteration to get converged solution in current increment. Eq. (6.12) aims to get converged iterative solutions with desired iterative steps, and it is 6 steps herein.

6.1.2 Tangent Vector at Regular Points

Recall the arc-length constraint equation given by Eq. (6.6), the arc-length is calculated as the inner product of the tangent vector at the end of last increment with the current increment size. The tangent vector is required and is obtained by taking the derivative with respective to s to Eq. (5.1). After plugging into $(\{\boldsymbol{U}\}, \lambda) = (\{\boldsymbol{U}\}_0, \lambda_0)$, it yields,

$$[\boldsymbol{K}_T]_0 \frac{d\{\boldsymbol{U}\}_0}{ds} - \{\boldsymbol{R}\} \frac{d\lambda_0}{ds} = 0 \tag{6.13}$$

As a unit vector is considered, it has,

$$\frac{d\{\boldsymbol{U}\}_0^T}{ds} \frac{d\{\boldsymbol{U}\}_0}{ds} + \left(\frac{d\lambda_0}{ds}\right)^2 = 1 \tag{6.14}$$

Therefore, Eq. (6.13) and Eq. (6.14) shows the unit tangent vector at the end of last increment is

$$\left(\frac{d\{\boldsymbol{U}\}_0^T}{ds}, \frac{d\lambda_0}{ds}\right) = (\eta\{\boldsymbol{\Psi}\}_0, \eta) \tag{6.15}$$

with

$$[\boldsymbol{K}_T]_0\{\boldsymbol{\Psi}\}_0 = \{\boldsymbol{R}\}, \qquad \eta = \frac{\pm 1}{\sqrt{1 + \{\boldsymbol{\Psi}\}_0^T\{\boldsymbol{\Psi}\}_0}} \tag{6.16}$$

To follow the path direction instead of double back, the sign of η is chosen as the one that has an acute angle to the previous tangent vector, namely,

$$\eta \left(\frac{d\{\boldsymbol{U}\}_{-1}^T}{ds}\{\boldsymbol{\Psi}\}_0 + \frac{d\lambda_{-1}}{ds}\right) > 0 \tag{6.17}$$

where $\left(\frac{d\{\boldsymbol{U}\}_{-1}^T}{ds}, \frac{d\lambda_{-1}}{ds}\right)$ is the previous tangent vector.

Applying the strategy discussed in Section 6.1.1 and Section 6.1.2, the equilibrium path of nonlinear behavior can be tracked.

6.1.3 Bifurcation Points and Branch Switching

In the stability response of sandwich panels, the bifurcation phenomenon may be observed. Once the load level exceeds a critical value, there exist multiple solution paths. We are interested in these alterative solutions, in which sandwich panels have remarkable deformations. The deformed shape is also different from that in the primary state. Following the incremental procedure as describe above, the step-by-step solutions are most likely to follow the primary path starting from the initial deformation under very small load intensity, even when the load is higher the critical value. Thus, solutions need to be switched from one branch to another in order to yield other solutions.

Before that, the bifurcation points, at which two or more equilibrium branches corresponding to solutions of Eq. (5.1) intersect, are determined first. One of the feature of these bifurcation points is that the tangent stiffness matrix is singular at these points. Therefore, the determinant sign of the tangent stiffness can be used as the test function to determinate the simple bifurcation points, at which only two branches intersect [97].

At the end of each increment, the determinant sign of the tangent stiffness is calculated and is compared with that of the previous increment. If the sign is changed, then there might exist one bifurcation point within current increment. Apply bisection method in terms of Δs determines the point with zero value. Denote the point $(\{\boldsymbol{U}\}_*, \lambda_*)$ and the corresponding tangent stiffness matrix at that point $[\boldsymbol{K}_T]_*$. Since the tangent stiffness is singular at both limit point (no branch behavior) and bifurcation point, verification is applied to determine the type of the singular point. According to the properties of these two type of points, i.e., the bifurcation point has $\{\boldsymbol{R}\} \in range[\boldsymbol{K}_T]_*$ whereas the limit point has $\{\boldsymbol{R}\} \notin range[\boldsymbol{K}_T]_*$ [97], therefore it implies that [102],

$$\{\boldsymbol{\psi}\}^T[\boldsymbol{R}] \begin{cases} \approx 0 & \text{for bifurcation points} \\ \neq 0 & \text{for limit points} \end{cases} \tag{6.18}$$

where $\{\boldsymbol{\psi}\}$ is the left null vector of $[\boldsymbol{K}_T]_*$, namely

$$\{\boldsymbol{\psi}\}^T[\boldsymbol{K}_T]_* = \{\boldsymbol{0}\}^T \tag{6.19}$$

Once the bifurcation point is determined, the branch is switched based on the method suggested by Keller [96, 102]. As a simply bifurcation point is considered, two smooth branches intersect at the bifurcation point. The corresponding tangents lie on a plane spanned by $(\{\boldsymbol{\varphi}_1\}, 0)$ and $(\{\boldsymbol{\varphi}_0\}, 1)$, where $\{\boldsymbol{\varphi}_1\}$ is the right null vector of the tangent stiffness matrix at the singular point, namely

$$[\boldsymbol{K}_T]_*\{\boldsymbol{\varphi}_1\} = \{\boldsymbol{0}\} \tag{6.20}$$

and $\{\boldsymbol{\varphi}_0\}$ is a vector defined by,

$$[\boldsymbol{K}_T]_*\{\boldsymbol{\varphi}_0\} = \{\boldsymbol{R}\}\ ; \qquad \{\boldsymbol{\psi}\}^T\{\boldsymbol{\varphi}_0\} = 0 \tag{6.21}$$

where $\{\boldsymbol{\psi}\}$ is the left null vector of the singular tangent stiffness matrix given by Eq. (6.19).

Since one branch and its tangent direction are known, we can seek one vector which is orthogonal to known tangent vector and lies in the plane spanned by $(\{\boldsymbol{\varphi}_1\}, 0)$ and $(\{\boldsymbol{\varphi}_0\}, 1)$. A point off the original path is obtained by moving the bifurcation point in the orthogonal direction. Then, starting a new iterative procedure from the new point and taking the orthogonal direction as the approximate new tangent direction can switch the solution to the other branch. The detailed branch switching procedure is given as following.

Denote the known tangent vector on original branch $\left(\frac{d\{\boldsymbol{U}\}_*^T}{ds}, \frac{d\lambda_*}{ds}\right)$, and it can be written as,

$$\frac{d\{\boldsymbol{U}\}_*^T}{ds} = C_0\{\boldsymbol{\varphi}_0\} + C_1\{\boldsymbol{\varphi}_1\}\ ; \qquad \frac{d\lambda_*}{ds} = C_0 \tag{6.22}$$

Considering the relation in Eq. (6.21b), coefficients C_0, C_1, and vector $\{\boldsymbol{\varphi}_0\}$ are determined

as,

$$C_0 = \frac{d\lambda_*}{ds} \tag{6.23a}$$

$$C_1 = \frac{\{\boldsymbol{\psi}\}^T \frac{d\{\boldsymbol{U}\}_*}{ds}}{\{\boldsymbol{\psi}\}^T\{\boldsymbol{\varphi}_1\}} \tag{6.23b}$$

$$\{\boldsymbol{\varphi}_0\} = \frac{1}{C_0}\left(\frac{d\{\boldsymbol{U}\}_*^T}{ds} - C_1\{\boldsymbol{\varphi}_1\}\right) \tag{6.23c}$$

An orthogonal vector to the known tangent in plane is $\left(\hat{C}_0\{\boldsymbol{\varphi}_0\} + \hat{C}_1\{\boldsymbol{\varphi}_1\}, \hat{C}_0\right)$, with

$$\hat{C}_0 = -C_1\{\boldsymbol{\varphi}_1\}^T\{\boldsymbol{\varphi}_1\}\,; \qquad \hat{C}_1 = C_0(1 + \{\boldsymbol{\varphi}_0\}^T\{\boldsymbol{\varphi}_0\}) \tag{6.24}$$

So, a new point away from the original path is given by moving the bifurcation point along the orthogonal direction, namely

$$\{\boldsymbol{U}\}_{*1} = \{\boldsymbol{U}\}_* + \xi\left(\hat{C}_0\{\boldsymbol{\varphi}_0\} + \hat{C}_1\{\boldsymbol{\varphi}_1\}\right) \tag{6.25a}$$

$$\lambda_{*1} = \lambda_* + \xi\hat{C}_0 \tag{6.25b}$$

where ξ is a small scaler that controls how far that point is away from the bifurcation point. ξ should has an intermediate magnitude, since a too small value will lead solution to return to the original path and a too big value will make the point move too far away from the new branch and increase the difficulty in getting the converged solution.

Applying the iterative method described in Section 6.1.1 from point $(\{\boldsymbol{U}\}_{*1}, \lambda_{*1})$ and using $(\hat{C}_0\{\boldsymbol{\varphi}_0\} + \hat{C}_1\{\boldsymbol{\varphi}_1\}, \hat{C}_0)$ as the tangent vector in the arc-length constraint equation , the solution in new branch can be obtained. Reversing the tangent vector direction can get the other part of the new bifurcation branch.

6.1.4 Perturbed Bifurcation

Sandwich panels with perfect conditions, i.e., symmetric geometry and loading, usually require to consider the branch switching technique in order to obtain other equilibrium branches. Another way to evaluate the post-buckling response can be done by applying artificial imperfections to obtain perturbed bifurcations. With appropriate perturbations, smooth curves approaching to different branches can be evaluated. The smaller imperfections are applied, the closer curves are to the branches of the perfect structure. Instead of passing the bifurcation point, perturbed curves pass the neighbourhood of bifurcation points. Both geometric imperfections and loading imperfections can be applied. Loading imperfection can be easily applied by adding imperfection loads to the equilibrium equations. The only modification in the solve procedure is to add imperfection loads vector to $\{\boldsymbol{G}\}_i$ in Eq. (6.8).

6.2 Numerical Results and Discussion

Numerical studies are carried out to investigate the post-buckling response of sandwich panels subjected to axial compressive loads. Sandwich panels whose buckling response were analyzed in Chapter 5 are further studied here.

Sandwich panels are simply supported at left edge and right edge, as shown in Fig. 5.1. The transverse displacement of both edges are constrained. One additional constraint is applied to the right edge of the bottom face to constrain the axial movement. Sandwich panels with two different lengths, namely $a = 300$ mm and $a = 150$ mm, are considered. Other geometric parameters and material properties are the same as that in Chapter 5. The thicknesses of the top face, bottom face, and core are $f_t = f_b = 0.5$ mm, and $2c = 19.05$ mm, respectively. The width is $b = 60$ mm. The elasticity modulus of the top face and bottom face are $E_1^t = E_1^b = 26900.0$ MPa. In core, it has $E_1^c = E_2^c = E_3^c = E^c = 52.0$ MPa, $G_{12}^c = G_{31}^c = G_{31}^c = G^c = 21.0$ MPa. The Poisson's ratio is calculated as $\nu_{12}^c =$

$\nu_{13}^c = \nu_{32}^c = E^c/2G^c - 1$

6.2.1 Sandwich Panel of 300 mm Length

A sandwich panel with length $a = 300$ mm is considered first. The panel is subjected to equal axial compressive loads $N^t = N^b = P/2$. A preliminary convergence study is carried out and results are presented with 450 uniform length 2-node EHSAPT-based elements. The equilibrium path is plotted in Fig. 6.1, where Fig. 6.1a is the transverse displacement of the top face middle point (w^t at $x = a/2$) versus applied load P curve and Fig. 6.1b is the axial displacement of the top face left edge (u^t at $x = 0$) versus applied load P curve. Both branch switching technique and perturbed bifurcation are considered. The solid line stands for the equilibrium path of a perfect sandwich panel. Two different load imperfections are applied to yield perturbed bifurcation. Uniform distributed loads with magnitude of 1.0×10^{-5} MPa applied to the top face and bottom face are considered as the first imperfection loads. The imperfection loads are both applied along z direction or both along $-z$ direction. Different loading directions lead to two similar equilibrium paths with sandwich panels bent towards top or bottom. The results are marked as "Imperfection 1" and plotted with dashed line in Fig. 6.1. The curves when consider another imperfection loads are marked as "Imperfection 2" and plotted with dashdotted line. "Imperfection 2" has uniform distributed loads of 1.0×10^{-5} MPa applied to both top face and bottom face, and concentrated loads of 0.1 N per unit width applied to the middle point of both top face and bottom face. When these loads are along z direction, it yields the right curve in Fig. 6.1a, and the $-z$ direction loads yield the left curve Fig. 6.1a. Since the axial displacement of the top face left edge (u_0^t at $x = 0$) are the same when sandwich panel bent towards top or bottom, the curves corresponding different bending direction coincide together in Fig. 6.1b.

Same sandwich panel is studied in Chapter 5. The buckling analysis predicts global buckling mode as the first buckling mode and the critical load is 10292.78 N. In present

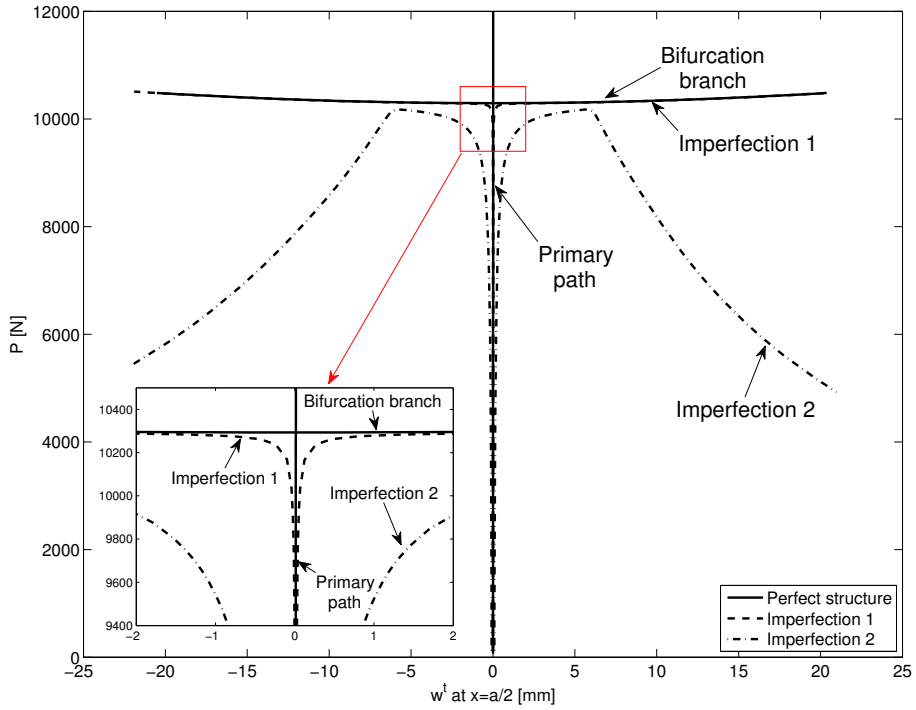

(a)

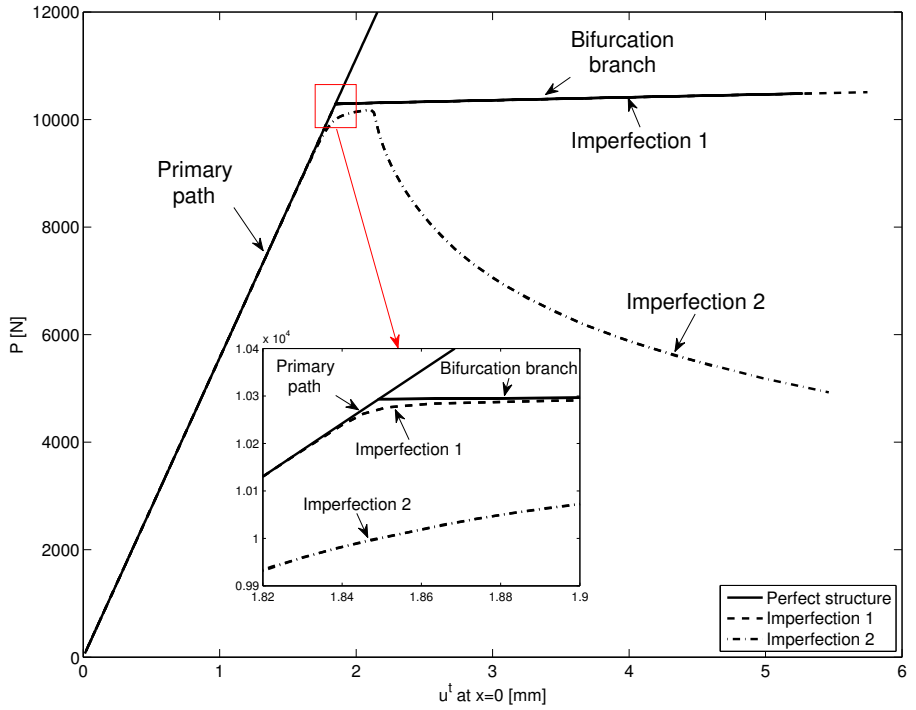

(b)

Figure 6.1: Equilibrium path of $a = 300$ mm sandwich panel: (a) w^t versus load P at middle ($x = a/2$); (b) u^t versus load P at left edge ($x = 0$)

post-buckling analysis of the perfect sandwich panel, the first singular point is determined as 10292.41 N and agrees well with the one given by the buckling analysis. After switching branch, it has a stable post-buckling response in which a higher load level is required in order to have a larger deformation. Performing the perturbed analysis with "Imperfection 1", similar result is obtained. Since the magnitude of the imperfection loads is very small, the perturbed curves are very close to the equilibrium path of perfect sandwich panel. They are almost identical and very small differences can only be observed in the zoom in plots.

The transverse displacement of the top and bottom faces corresponding to the right branch of "Imprefection 1" is plotted in Fig. 6.2. Different curves correspond to the deformations at different increments. It is clearly seen that the sandwich panel is buckled globally. There is one half sine wave over the panel, and it is the same as the buckled shape of ordinary beams. Same global buckling mode shape is given by the buckling analysis.

Sandwich panels are compound structures. The interaction between different layers may result in complicated post-buckling behavior. Although it has a stable post-buckling response with global buckling mode shape at the beginning, the localized effect can cause the interaction between the global buckling and local wrinkling and lead to an unstable post-buckling response. By implementing "Imperfection 2" in the imperfection analysis, the sandwich panel shows such a post-buckling response. It should be noted that the only difference between "Imperfection 2" and "Imperfection 1" is that there are two concentrated loads with 0.1 N per unit width along transverse direction applied to the middle points of both top and bottom faces. In the primary equilibrium path, where the load is lower than the critical load, curves obtained by different methods are close to each other. At the region near to the bifurcation point, curves of "Imperfection 2" are farther away to curves of prefect sandwich panel than that of "Imperfection 1" since "Imperfection 2" has larger resultant transverse imperfection load. The equilibrium paths approach to that of perfect structure. However, when the top face middle point transverse displacement reaches around 6 mm, the load shows a sudden drop while the deformation keeps increasing. The localized

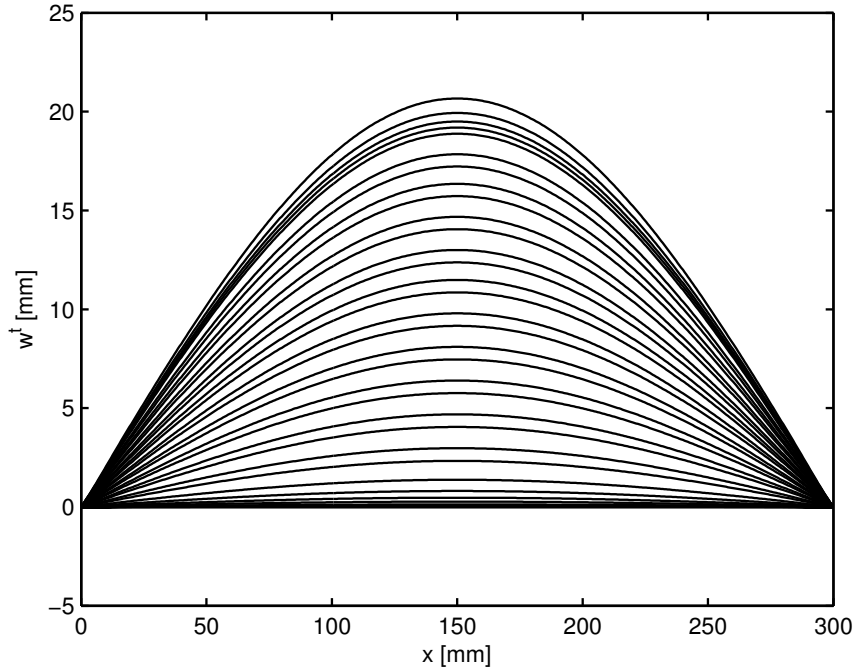

(a)

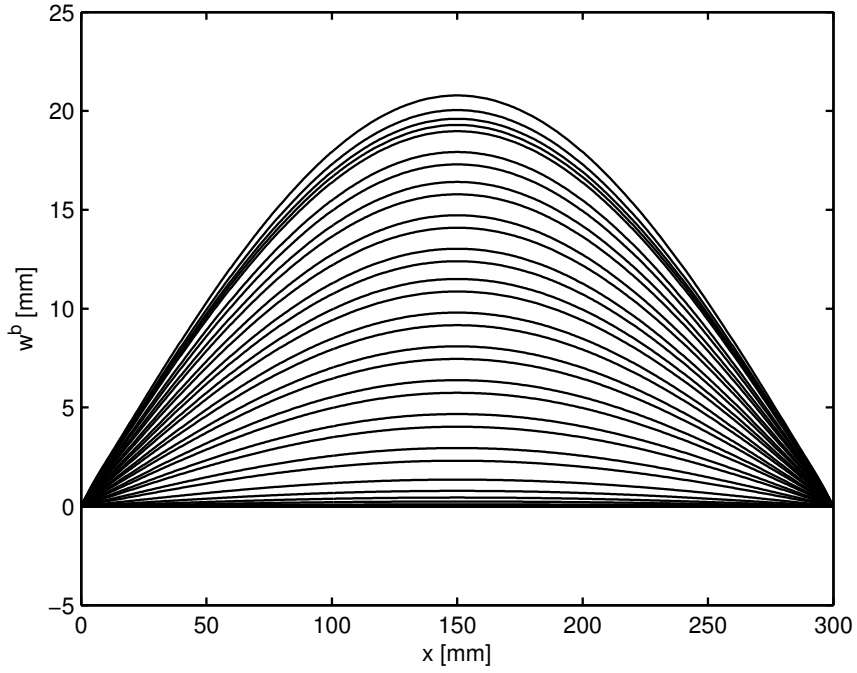

(b)

Figure 6.2: Variations of transverse displacement at various axial compressive loads ($a = 300$ mm sandwich panel with uniform distributed load imperfection): (a) top face w^t; (b) bottom face w^b

effect causes the destabilization. To illustrate the reason, the variation of the transverse displacement of the top face and bottom face at different increments when "Imperfection 2" are applied are given in Fig. 6.3.

Fig. 6.3 shows that the sandwich panel is buckled globally at the beginning, and has similar buckling shape as that of "Imperfection 1", although there are concentrated loads applying to the middle points. Therefore, the perturbed equilibrium path has same tendency as that of "Imperfection 1" and that of perfect system. Then, the center area of the bottom face is wrinkled locally. After that, the local wrinkling grows as the deformation is aggravated, and the required load level for larger deformation is lower that the load required to maintain current deformation. The initial appearance of bottom face local wrinkling corresponds to the turning point from the stable post-buckling response to the unstable post-buckling response in Fig. 6.1 "Imperfection 2" curves. It is seen that the localized effect has a destabilization effect on the post-buckling response of sandwich panels.

The imperfections are unavoidable in practice, and the prefect structure is only idealized. Therefore, even when sandwich panels show global buckling behavior as ordinary beams initially , they may experience localized wrinkling at some point. After that, it cannot retain the stable post-buckling response any more. Due to the localized wrinkling, sandwich panels lost their load carrying capability. This is a important factor need to be considered in the design of sandwich structures.

6.2.2 Sandwich Panel of 300 mm Length Neglecting Core Axial Rigidity

Recall that the axial rigidity of the core has a significant effect on the buckling critical load and buckling mode shape, thus its effect on the post-buckling response is analyzed further. Same 300 mm sandwich panel used in the previous example is re-analyzed by setting core axial rigidity to be $E_1^c = 1.0 \times 10^{-5}$ MPa. This approach degenerates the EHSAPT to HSAPT, in which the core axial rigidity is neglected. It can also be regarded as a sandwich panel made of a core material that has zero axial rigidity.

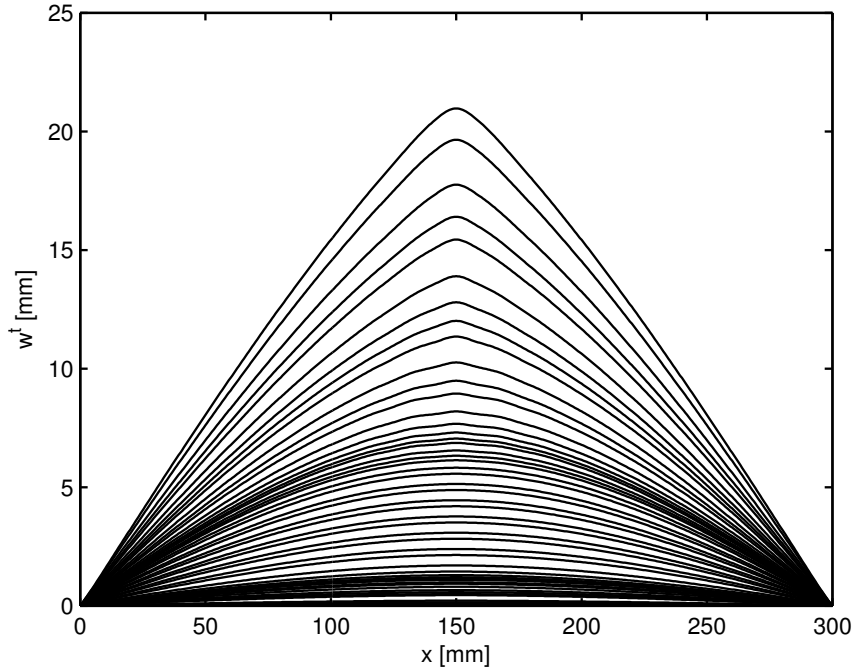

(a)

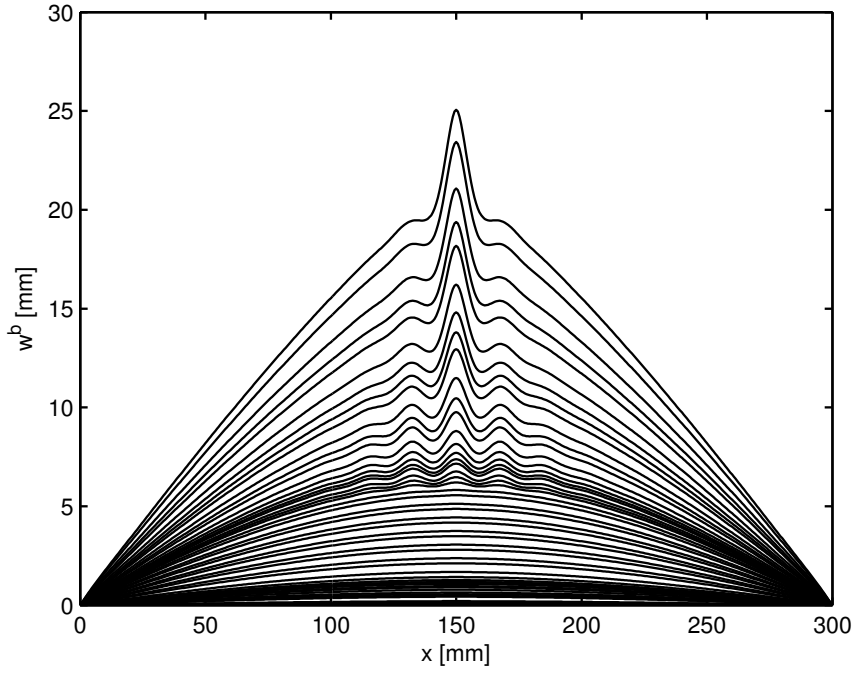

(b)

Figure 6.3: Variations of transverse displacement at various axial compressive loads ($a = 300$ mm sandwich panel with uniform distributed load imperfection and concentrated load imperfection): (a) top face w^t; (b) bottom face w^b

In the previous buckling analysis, neglecting the core axial rigidity results a 300 mm sandwich panel has a wrinkling mode as the first buckling mode shape instead of the global buckling mode. The wrinkling mode shape has multiple uniform sine waves over the panel. The imperfection analysis is performed with the fictitious imperfection load "Imperfection 1", namely uniform distributed loads of 1.0×10^{-5} MPa applied to both top face and bottom face. The top face middle point transverse displacement w^t versus axial compressive load level P is plotted in Fig. 6.4. Different from the "Imperfection 1" path shown in Fig. 6.1a, when neglecting the core axial rigidity, the sandwich panel has a unstable post-buckling response. The required axial compressive loads are decreased to maintain the equilibrium.

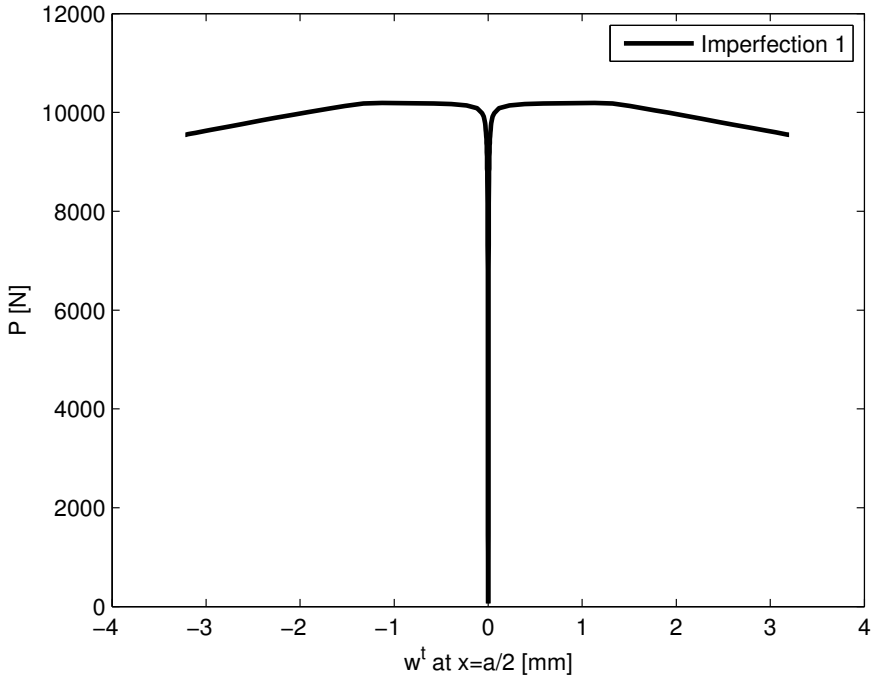

Figure 6.4: Equilibrium path of $a = 300$ mm sandwich panel with $E_1^c = 1.0 \times 10^{-5}$ MPa, w^t versus load P at middle ($x = a/2$)

Fig. 6.5 plots the top face and bottom face transverse displacement at various increments when imperfection loads applied along z direction. It corresponds to the right branch of Fig. 6.4. The post-buckling deformations are different from that considering the core axial rigidity as $E_1^c = 52$ MPa, given by Fig. 6.2. It is seen that due to the transverse

imperfection loads, the center region is bulged towards the loading direction. At the very begin when significant transverse deformation is observed, the deformation is a half sine wave shape. To this point, the post-buckling is similar to that including core axial rigidity. However, wrinkling with multiple short waves distributed over the whole panel is observed later on. Considering the direction of imperfection loads considered in Fig. 6.5, since the bottom face takes higher resultant compressive loads due to the bending, the wrinkling waves have higher amplitude at the bottom face.

The deformed shape in the post-buckling region agrees with the buckling mode shape predicted by the linearized buckling analysis. Comparing the buckling behavior and the post-buckling response between sandwich panels including core axial rigidity and sandwich panels neglecting that, it can be concluded that the axial rigidity of the core should be considered when analyze the stability of sandwich structures. Although it is usually two or three orders smaller that of faces, i.e., $E_1^c/E_1^t = 0.0019$ for the case considered here, and it has very little effect on the static response, the effect on buckling mode shape and post-buckling response is significant.

6.2.3 Sandwich Panel of 150 mm Length

Next, a sandwich panel which has wrinkling mode as the first buckling mode is discussed. Consider a sandwich panel of 150 mm length, and other geometric and material properties are the same as the one used in Section 6.2.1. Same boundary conditions are applied, as shown in Fig. 5.1. Equal axial compressive loads are applied to both top face and bottom face, $N^t = N^b = P/2$. A convergency study is carried out and results presented are modelled with 450 uniform 2-node EHSAPT-based elements. Both branch switching technique and perturbed bifurcation are considered. In the perturbed bifurcation analysis, uniform distributed loads with magnitude of 1.0×10^{-5} MPa are applied to the top face and bottom face. The fictitious imperfection loads are applied along z direction or $-z$ direction to yield solutions approaching to both sides of bifurcations. The equilibrium paths are plotted in

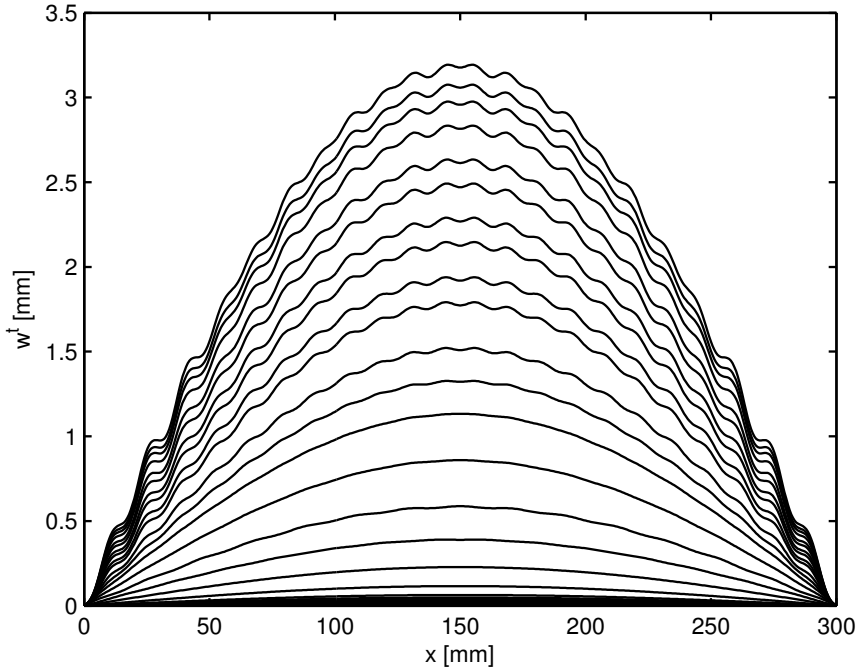

(a)

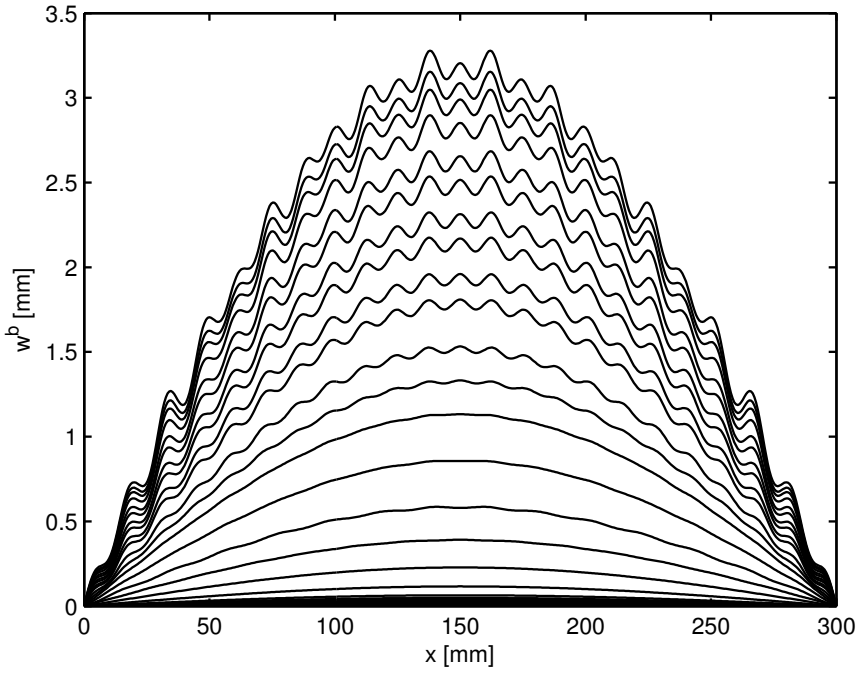

(b)

Figure 6.5: Variations of transverse displacement at various axial compressive loads ($a = 300$ mm sandwich panel with uniform distributed load imperfection and $E_1^c = 1.0 \times 10^{-5}$ MPa): (a) top face w^t; (b) bottom face w^b

Fig. 6.6. Both the transverse displacement of top face point at $x = 5$ mm ($x = a/30$) versus axial compressive load level P, and the axial displacement of the top face left edge ($x = 0$) versus P are given. The solid line represents the result of perfect sandwich panel using branch switching technique, and the dashed lines are the results by imposing imperfection loads.

For the perfect structure, the first bifurcation point is found with a load level $P_{cr1} = 15573.05$ N. The second bifurcation point is not far from the first one. The load level of the second one is $P_{cr2} = 15576.20$ N, and it is only 3 N higher than the first one. Thus, a very small accuracy should be considered in the post-buckling analysis. Otherwise some buckling modes might be ignored. The accuracy requirement can be determined by the critical buckling load given by the previous buckling analysis. Same sandwich panel was analyzed in Chapter 5, and the buckling analysis gives 15617.30 N and 15620.59 N as the critical loads of the first and second buckling modes. A good agreement is observed. Unstable post-buckling response is observed in both branches. The required axial compressive load level is decreased to have a larger deformation. A significant load dropping is observed right after bifurcation happens. Since the sandwich panel has different deformed shapes in the first and second branch, w^t output point ($x = a/30$) happens to have same displacement at the left part of the plot, and w^t versus P curves cross to each other at the right part. When applied imperfection loads, the perturbed curves are close to the first branch. Due the small magnitude of imperfection loads, the perturbed curves are almost identical to results of perfect structures, and very small differences can be observed in zoom in plot. Considering the fact that there exist several winkling modes in a very narrow range of load level, it raises the possibility that sandwich panels may be buckled into the other bifurcation branch instead of the first one with lowest critical load when there are appropriate imperfections.

The transverse displacement of the top face and bottom face at various increments of the first and second bifurcated branches are given in Fig. 6.7 and Fig. 6.8. Only the results corresponding to the right part of the branches of Fig. 6.6a are plotted. Fig. 6.7 and Fig.

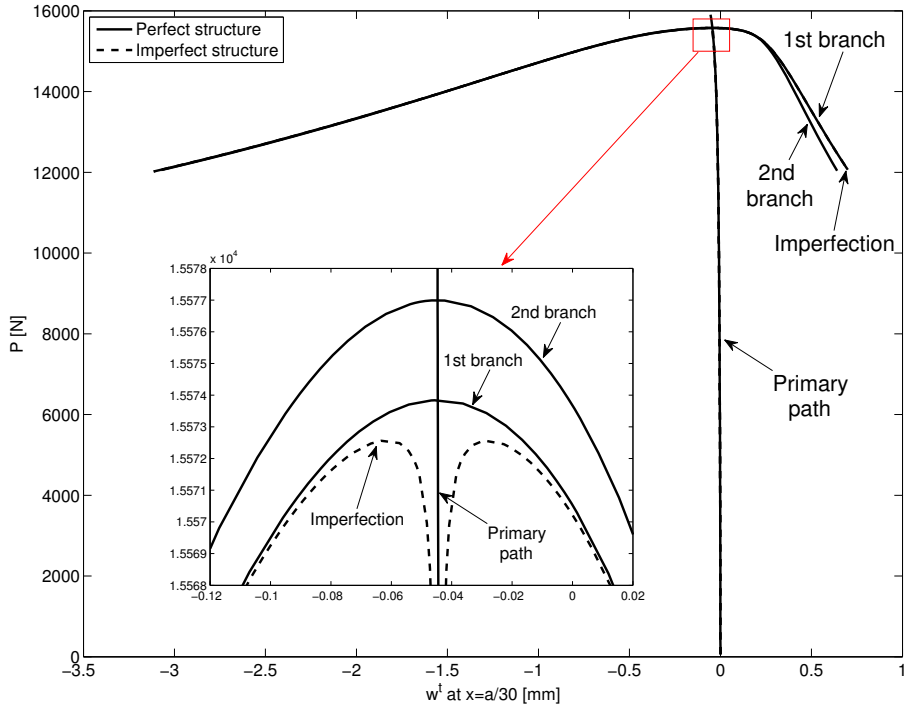

(a)

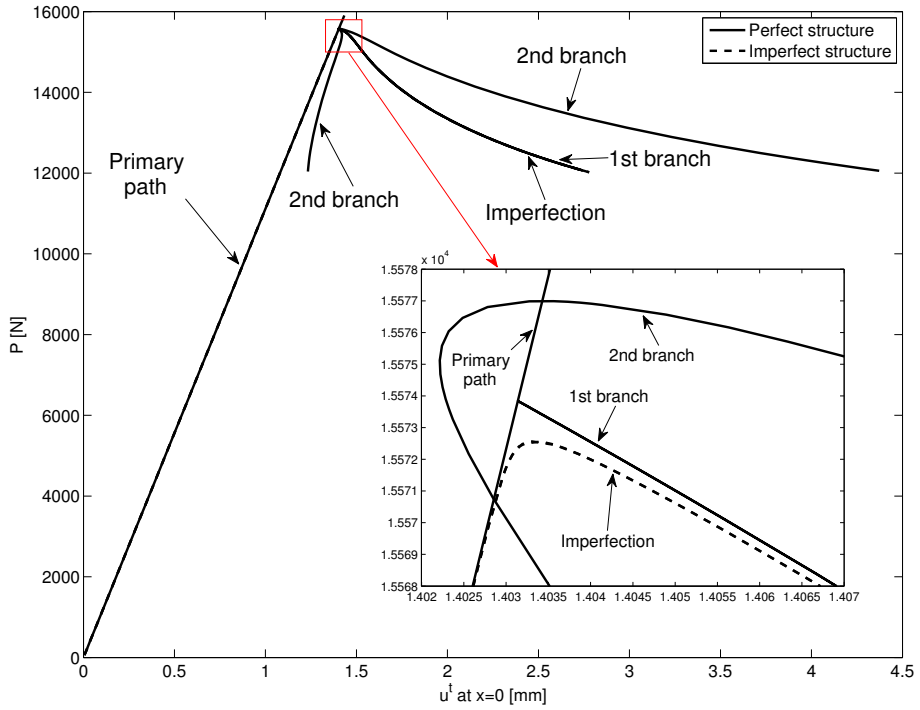

(b)

Figure 6.6: Equilibrium path of $a = 150$ mm sandwich panel: (a) w^t versus load P at $x = a/30$; (b) u^t versus load P at left edge ($x = 0$)

6.8 both show that the sandwich panel is wrinkled. The maximum transverse deformation happens at regions near edges. The edge effect is observed. The deformed shape when considering imperfection is the same as that of the first branch. The deformations verify the buckling mode shapes given by the buckling analysis in Fig. 5.7. In the buckling analysis, the first two buckling mode shapes are wrinkling mode with non-uniform short waves and the waves near edges have higher amplitude. It is seen that in the post-buckling response, the deformation of each part of sandwich panel is not increased at the same rate. In other words, the deformation at some regions grows faster than other parts. So, using uniform sine waves to describe the buckled shape is inappropriate. It might lead to inaccurate predictions.

Different from the global buckling, when sandwich panels experience wrinkling, they lose the load carrying capability at very beginning. Thus, for such kind of sandwich panels, it should be avoided to enter the post-buckling region.

6.3 Conclusions

Several sandwich panels which were studied in Chapter 5 are studied as examples to investigate the post-buckling response of sandwich panels. The results obtained by the linear buckling analysis are used as the primary results to determine the accuracy requirement to increase the computation efficiency in the nonlinear post-buckling analysis. In terms of the buckling mode shape and the critical load, a good agreement is observed between the nonlinear post-buckling analysis and the buckling analysis.

The post-buckling response further proves that the axial rigidity of the core has significant effects on the stability of sandwich panels, including the post-buckling response. The numerical examples demonstrate that the wrinkling has non-sinusoidal shape after the critical load. The edge effect and localized effect both affect the deformation. Therefore, it might lead to inaccurate results if assuming sandwich panels have uniform sine wave modes.

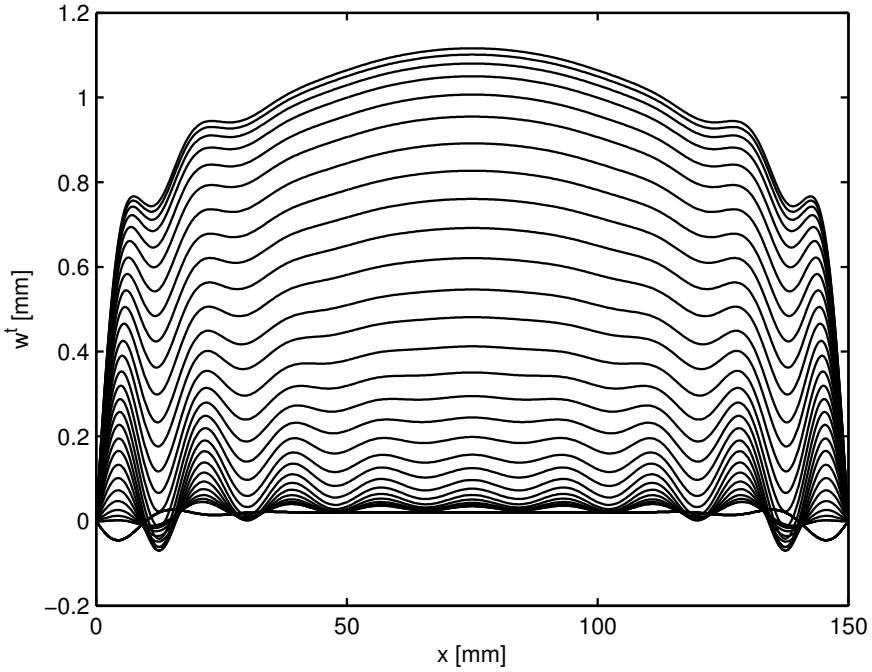

(a)

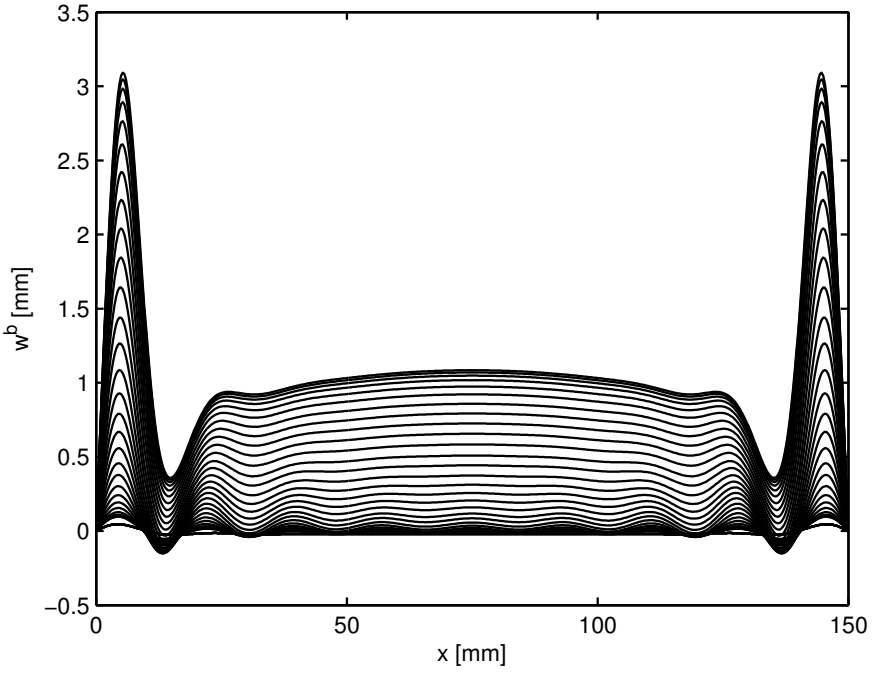

(b)

Figure 6.7: Variations of transverse displacement at various axial compressive loads of $a = 150$ mm sandwich panel of the right part of first branch: (a) top face, w^t; (b) bottom face, w^b

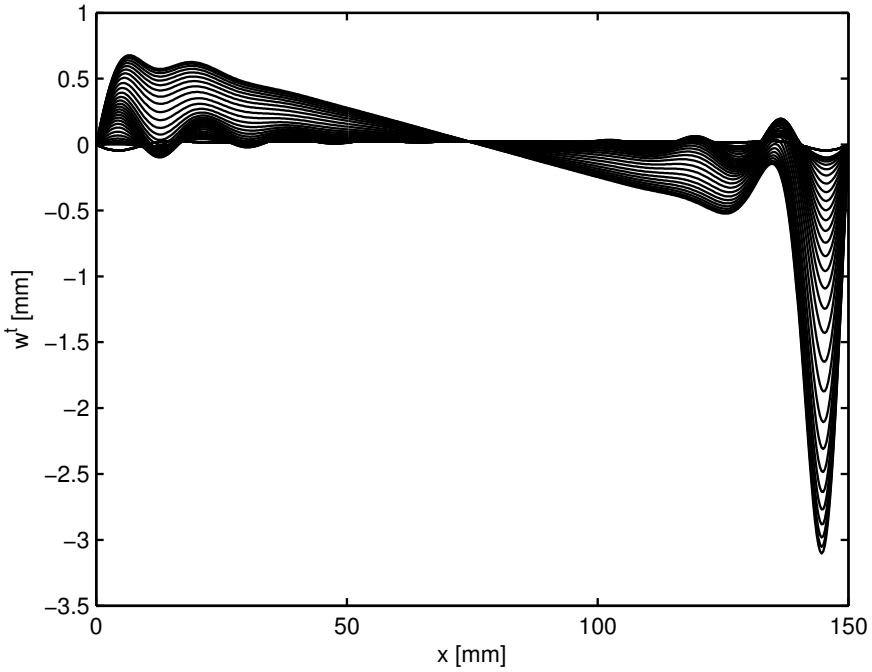

(a)

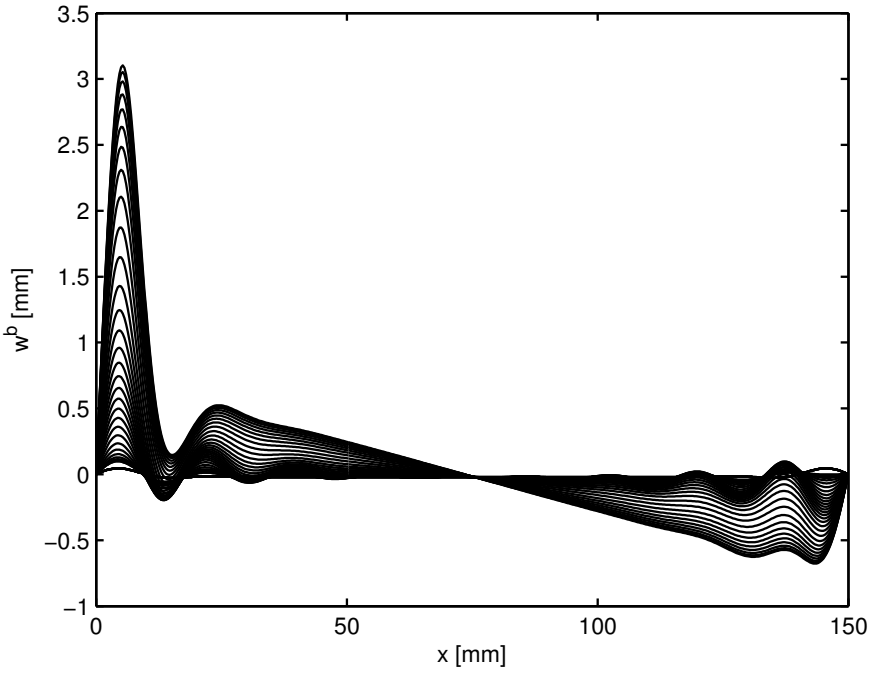

(b)

Figure 6.8: Variations of transverse displacement at various axial compressive loads $a = 150$ mm sandwich panel of the right part of second branch: (a) top face, w^t; (b) bottom face, w^b

The perturbed bifurcation analysis and the branch switching technique work well for the post-buckling analysis of sandwich panels. A good agreement between these two methods is observed. Due to the interaction of different layers and high divergency in material properties, the localized effect may be initialized by imperfection loads with very small magnitude during the post-buckling response. Thus, different imperfections may lead to different post-buckling responses in which the load carrying capabilities are completely different. Special care is required when performing the post-buckling analysis in terms of sandwich structures. Both branch switching of the perfect structure and perturbed bifurcation should be considered.

Sandwich panels have different post-buckling responses when they experience global buckling and wrinkling. Although they may have similar global buckling shape as ordinary beams, they cannot retain the stable post-buckling response for a long duration as ordinary beams. When global buckling occurs, the post-buckling response is stable at begin. However, with the growing of the deformation, sandwich panels may be destabilized due to the imperfections and localized effects. When wrinkling occurs, sandwich panels lose their load carrying capability immediately, and the required axial compressive load level for further deformation is lower than that to maintain current deformation. Same to the buckling analysis, it is seen that there exist several winkling modes in a very narrow range of load level. Thus, it raises the possibility that sandwich panels may be buckled into other bifurcation branches instead of the first one with the lowest critical load when there are appropriate imperfections.

CHAPTER 7
CONCLUSIONS AND FUTURE WORK

7.1 Conclusions

The geometric nonlinearity effects on the behavior of sandwich structures have been investigated and presented. It follows the Extended High-order Sandwich Panel Theory (EHSAPT) in which the axial rigidity, transverse compressibility, and shear effect of the core are all considered. Thus, it is suitable for a wide range of core materials, including both stiff core and soft core. The EHSAPT, originally proposed under small deformation, is further developed to take geometric nonlinearities into account.

A special finite element is proposed to implement the EHSAPT with the finite element method. The proposed method extends the application ranges of the EHSAPT, since its analytical solution is only available to sandwich panels with simple supported edges and subjected to sinusoidally distributed loads. Validation of the proposed EHSAPT-based element is performed by comparison with the benchmark elasticity solution. The EHSAPT-based element can yield exactly the same displacements and stresses to the elasticity solutions with very small amount of 2-node elements. It can easily handle arbitrary combinations of boundary conditions and loads. Each node of the EHSAPT-based element has 10 DOFs, which contain the displacement information of the top face, bottom face, and core. Thus, only one element is required in the thickness direction, and the corresponding finite element model is a one-dimensional model. The modelling effort is significantly reduced compared to a two-dimensional model or a three-dimensional model required by the conventional finite elements. The EHSAPT-based finite element method can serve as the analysis tool to seek numerical solutions when considering the geometric nonlinearities.

A comprehensive investigation about the geometric nonlinearity effects on both sta-

tic behavior and dynamic response are carried out. Both faces and core are considered undergoing large displacements with moderate rotations. There are various simplifications scatted in the literature when considering the geometric nonlinearities of sandwich structures. These simplifications are compared and verified for the first time. When the deformation is small, the geometric nonlinearities have very little effect on the behavior of sandwich structures. The deformation has a nearly linear relation to the load intensity. Therefore, these simplifications are all acceptable and can yield similar results even ignoring the geometric nonlinearities. When large deformation occurs, sandwich structures have a nonlinear behavior. Then, divergences are observed when considering different simplifications. It shows that the nonlinearity of the core sheet has a significant effect. However, the core is usually assumed undergoing small deformation and adopts infinitesimal strains in most of the available nonlinear analysis. By considering only the geometric nonlinearities in faces, meaningless results may be obtained. But, there is one exception. The HSAPT, in which the core axial rigidity is also neglected, can yield correct nonlinear response tendency, although only faces are considered undergoing large deformation. The absence of the core axial rigidity in the HSAPT can compensate part of the error caused by neglecting the geometric nonlinearities of the core. However, a softer behavior is always obtained by the HSAPT since part of the rigidity is neglected.

The geometric nonlinearity of sandwich structures plays an important role in the mechanical response of sandwich structures. Some phenomena can be captured only when the geometric nonlinearity is included in the formulation, e.g., the localized effect, and the high frequency in-plane vibration when sandwich panels subjected to transverse blast loading. Both nonlinear static behavior and nonlinear dynamic response suggest that the geometric nonlinearities of the core should be considered, and the nonlinear terms appeared in the core kinematic relations should be included. At least the nonlinear terms related to the transverse displacement must be included. It should be noted that, when the Euler-Bernoulli assumptions are applied to the faces of sandwich structures, transverse strain and

shear strain vanish automatically when considering the infinitesimal strain. However, these two strains have nonlinear terms when applying the displacement expressions of Euler-Bernoulli assumptions directly into the Green-Lagrange strains. These non-zero transverse strain and shear strain should be discarded since they conflict with the Euler-Bernoulli assumptions.

The propose EHSAPT-based finite element method successfully analyzed both nonlinear static behavior and nonlinear dynamic response of sandwich structures, while numerical difficulties are always observed in conventional finite element method. In conventional finite element method, the faces and core need to be modelled separately. Thus, low convergency and element with large distortion are more likely happen due to the high divergence in material properties and geometric characteristics. Since the proposed EHSAPT-based element is a one-dimensional element, the computational cost is significantly reduced when compared to two-dimensional models even three-dimensional models used by the conventional finite element method.

The investigation about the stability of sandwich panels, including the pre-buckling state, buckling mode shape, critical buckling load, and nonlinear post-buckling response, is carried out. Both buckling analysis, which can determine the buckling mode shape and critical buckling load, and nonlinear post-buckling analysis, which can evaluate the post-buckling response of sandwich structures with or without imperfections, are both presented. The branch switching technique and perturbed bifurcation analysis are both considered in the post-buckling analysis.

In the buckling analysis, the pre-buckling state is determined by a nonlinear static analysis. Applying the linearization to the tangent stiffness, the critical buckling load and mode shape are conveniently determined by an eigen-value solver. Since the faces and core are made with different materials and have different geometric sizes, thus there are interactions between faces and core. The pre-buckling state of sandwich structures does not essentially have a membrane state even when a symmetric sandwich panel is subjected to symmetric

axial compressive loads. Due to the edge effect and localized effect, the buckling mode shape is not necessary to have uniform multiple sine waves, especially when winkling occurs. Therefore, the buckling behavior of sandwich structures are much complicated. The estimations based on the membrane pre-buckling state and presume uniform sine wave buckling mode shape may lead to inaccurate conclusions.

Both global buckling and wrinkling are observed in numerical examples. Slender sandwich structures are much easier to have global buckling. Sandwich panels which are buckled globally have similar deformed shapes as ordinary beams. The post-buckling response is also close to that of ordinary beams until they reach certain deformation. Before sandwich panels reach that deformation, they still have load carrying capability and a higher load level is required to have a larger deformation. However, due the interaction between the faces and core, localized effect may be easily initiated after sandwich structures are buckled globally. It destabilizes the post-buckling response. After that, sandwich structures lost their load carrying capability.

Wrinkling happens more often on short sandwich structures. It have multiple short waves, and sandwich structures lost load carrying capability once the wrinkling happens. It is observed that there exist multiple wrinkling modes in a narrow range of load level. Thus, it shows the possibility that wrinkling with different deformed shapes may happen due to the imperfections in practice.

The axial rigidity of the core shows a significant influence on the stability behavior of sandwich structures. Although it is usually negligible in most static cases due to its small magnitude compared to that of faces, it affects the buckling behavior and post-buckling response. The wrinkling mode shape is quite different when considering or ignoring the axial rigidity of the core. The wrinkling critical load is also reduced by a large amount if neglecting the axial rigidity of the core in the analysis. Since the first buckling mode is usually taken as the one with the lowest critical load, if the wrinkling has a lower critical load due to ignoring the core axial rigidity, it might be mistaken as the first buckling

mode. Therefore, the axial rigidity of the core should be always considered in the buckling analysis although it is rather small compared to that of faces.

7.2 Future Work

It is seen that the EHSAPT and EHSAPT-based finite element method are very promising sandwich structure theory and sandwich structure analysis tool. The geometric nonlinearity effects on sandwich structures can be analyzed by the proposed method. In the future, other sources of nonlinearity, such as the material nonlinearity, can be studied. Beside, the discontinuities in sandwich structures, e.g., cracks and delamination, can be considered. In present study, a one-dimensional EHSAPT-based element is developed. Its two-dimensional version can also be developed for sandwich plates.

APPENDIX A

ELEMENT INTERPOLATION MATRIX OF 2-NODE EHSAPT-BASED ELEMENT

The element displacement vector of a 2-node EHSAPT-based element is

$$\{\boldsymbol{U}_e\} = \begin{Bmatrix} \{\boldsymbol{U}_1\} \\ \{\boldsymbol{U}_2\} \end{Bmatrix} \tag{A.1}$$

The displacement interpolation matrix $[\boldsymbol{N}(s)]$ of a 2-node EHSAPT-based element is a 7×20 matrix, and is given as

$$\Big[\boldsymbol{N}(s)\Big] = \begin{bmatrix} N_1 & 0 & 0 & 0 & 0 & 0 & 0 & 0 & 0 & 0 & N_2 & 0 & 0 & 0 & 0 & 0 & 0 & 0 & 0 & 0 \\ 0 & N_3 & N_4 & 0 & 0 & 0 & 0 & 0 & 0 & 0 & 0 & N_5 & N_6 & 0 & 0 & 0 & 0 & 0 & 0 & 0 \\ 0 & 0 & 0 & N_1 & 0 & 0 & 0 & 0 & 0 & 0 & 0 & 0 & 0 & N_2 & 0 & 0 & 0 & 0 & 0 & 0 \\ 0 & 0 & 0 & 0 & N_3 & N_4 & 0 & 0 & 0 & 0 & 0 & 0 & 0 & 0 & N_5 & N_6 & 0 & 0 & 0 & 0 \\ 0 & 0 & 0 & 0 & 0 & 0 & N_1 & 0 & 0 & 0 & 0 & 0 & 0 & 0 & 0 & 0 & N_2 & 0 & 0 & 0 \\ 0 & 0 & 0 & 0 & 0 & 0 & 0 & N_3 & N_4 & 0 & 0 & 0 & 0 & 0 & 0 & 0 & 0 & N_5 & N_6 & 0 \\ 0 & 0 & 0 & 0 & 0 & 0 & 0 & 0 & 0 & N_1 & 0 & 0 & 0 & 0 & 0 & 0 & 0 & 0 & 0 & N_2 \end{bmatrix} \tag{A.2}$$

In the above matrix, the shape functions $N_k (k = 1...6)$ are in terms of the local coordinate, $s = x - x_i$, where x_i is the x coordinate of the i-th node (Fig. 2.3); also in the following equations for the shape functions, $h_i = x_{i+1} - x_i$ is the length of the i-th element:

$$N_1 = 1 - \frac{s}{h_i}\,; \qquad N_2 = \frac{s}{h_i}$$

$$N_3 = 1 - 3\frac{s^2}{h_i^2} + 2\frac{s^3}{h_i^3}\,; \qquad N_4 = s - 2\frac{s^2}{h_i} + \frac{s^3}{h_i^2}$$

$$N_5 = 3\frac{s^2}{h_i^2} - 2\frac{s^3}{h_i^3}\,; \qquad N_6 = -\frac{s^2}{h_i} + \frac{s^3}{h_i^2}$$

REFERENCES

[1] F. J. Plantema, *Sandwich Constrction*. New York: Wiley, 1966.

[2] H. G. Allen, *Analysis and Design of Structural Sandwich Panels*. Oxford: Pergamon, 1969.

[3] D. Zenkert, *An Introduction to Sandwich Structures*. Chamelon, Oxford, 1995.

[4] L. A. Carlsson and G. A. Kardomateas, *Structural and Failure Mechanics of Sandwich Composites*. New York: Springer, 2011.

[5] J. R. Vinson, *The Behavior of Sandwich Structures of Isotropic and Composite Materials*. Lancaster, PA: CRC Press, 1999.

[6] A. K. Noor, W. S. Burton, and C. W. Bert, "Computational models for sandwich panels and shells," *Applied Mechanics Reviews*, vol. 49, no. 3, pp. 155–199, 1996.

[7] H. Altenbach, "Theories for laminated and sandwich plates. A review," *Mechanics of Composite Materials*, vol. 34, no. 3, pp. 243–252, 1998.

[8] E. Carrera and S. Brischetto, "A survey with numerical assessment of classical and refined theories for the analysis of sandwich plates," *Applied Mechanics Reviews*, vol. 62, no. 1, pp. 010 803–010 803, 2008.

[9] E. Carrera and S. Brischetto, "A comparison of various kinematic models for sandwich shell panels with soft core," *Journal of Composite Materials*, 2009.

[10] L. Librescu and T. Hause, "Recent developments in the modeling and behavior of advanced sandwich constructions: A survey," *Composite Structures*, vol. 48, no. 1-3, pp. 1–17, 2000.

[11] N. Pagano, "Exact solutions for composite laminates in cylindrical bending," *Journal of Composite Materials*, vol. 3, no. 3, pp. 398–411, 1969.

[12] N. Pagano, "Exact solutions for rectangular bidirectional composites and sandwich plates," *Journal of Composite Materials*, vol. 4, no. 1, pp. 20–34, 1970.

[13] G. A. Kardomateas and C. N. Phan, "Three-dimensional elasticity solution for sandwich beams/wide plates with orthotropic phases: The negative discriminant case," *Journal of Sandwich Structures and Materials*, vol. 13, no. 6, pp. 641–661, 2011.

[14] S. K. Malhotra and B. J. C. Babu, "A study on GRP skin/foam core sandwich structures," *Composites*, vol. 14, no. 4, pp. 383–386, 1983.

[15] J. M. Whitney, "Stress analysis of thick laminated composite and sandwich plates," *Journal of Composite Materials*, vol. 6, no. 3, pp. 426–440, 1972.

[16] E. Reissner, "A consistent treatment of transverse shear deformations in laminated anisotropic plates," *AIAA Journal*, vol. 10, no. 5, pp. 716–718, 1972.

[17] A. M. Lush, "An equivalent layer sandwich panel model," *Computers & Structures*, vol. 21, no. 5, pp. 861–868, 1985.

[18] W. S. Burton and A. K. Noor, "Assessment of computational models for sandwich panels and shells," *Computer Methods in Applied Mechanics and Engineering*, vol. 124, no. 1, pp. 125–151, 1995.

[19] S. B. Dong and C. K. Chun, "Shear constitutive relations for laminated anisotropic shells and plates: Part iłmethodology," *Journal of Applied Mechanics*, vol. 59, no. 2, pp. 372–379, 1992.

[20] Y. Frostig, M. Baruch, O. Vilnay, and I. Sheinman, "High-order theory for sandwich-beam behavior with transversely flexible core," *Journal of Engineering Mechanics*, vol. 118, no. 5, pp. 1026–1043, 1992.

[21] C. N. Phan, Y. Frostig, and G. A. Kardomateas, "Analysis of sandwich beams with a compliant core and with in-plane rigidity – extended high-order sandwich panel theory versus elasticity," *Journal of Applied Mechanics*, vol. 79, no. 4, pp. 041 001–041 001, 2012.

[22] C. N. Phan, "The extended high-order sandwich panel theory," PhD thesis, School of Aerospace Engineering, Georgia Institute of Technology, 2012.

[23] F. K. Siddiqui, "Extended higher order theory for sandwich plates of arbitrary aspect ratio," PhD thesis, School of Aerospace Engineering, Georgia Institute of Technology, 2015.

[24] N. Rodcheuy, "Advanced high order theories and elasticity solutions for curved sandwich composite panels," PhD thesis, School of Aerospace Engineering, Georgia Institute of Technology, 2017.

[25] H. Murakami, "Laminated composite plate theory with improved in-plane responses," *Journal of Applied Mechanics*, vol. 53, no. 3, pp. 661–666, 1986.

[26] Y. B. Cho and R. C. Averill, "First-order zig-zag sublaminate plate theory and finite element model for laminated composite and sandwich panels," *Composite Structures*, vol. 50, no. 1, pp. 1–15, 2000.

[27] A. Tessler, M. D. Sciuva, and M. Gherlone, "A refined zigzag beam theory for composite and sandwich beams," *Journal of Composite Materials*, vol. 43, no. 9, pp. 1051–1081, 2009.

[28] E. Carrera, "Historical review of zig-zag theories for multilayered plates and shells," *Applied Mechanics Reviews*, vol. 56, no. 3, pp. 287–308, 2003.

[29] J. N. Reddy, "An evaluation of equivalent-single-layer and layerwise theories of composite laminates," *Composite Structures*, vol. 25, no. 1, pp. 21–35, 1993.

[30] D. H. Robbins and J. N. Reddy, "Modelling of thick composites using a layerwise laminate theory," *International Journal for Numerical Methods in Engineering*, vol. 36, no. 4, pp. 655–677, 1993.

[31] M. Tahani, "Analysis of laminated composite beams using layerwise displacement theories," *Composite Structures*, vol. 79, no. 4, pp. 535–547, 2007.

[32] A. Barut, E. Madenci, and A. Tessler, "A refined zigzag theory for laminated composite and sandwich plates incorporating thickness stretch deformation," in *53rd AIAA/ASME/ASCE/AHS/ASC Structures, Structural Dynamics and Materials Conference*, ser. Structures, Structural Dynamics, and Materials and Co-located Conferences. American Institute of Aeronautics and Astronautics, 2012.

[33] L. Iurlaro, M. Gherlone, and M. Di Sciuva, "A mixed cubic zigzag model for multilayered composite and sandwich plates including transverse normal deformability," in *Proceedings of the 11th World Congress on Computational Mechanics (WCCM XI)*, 2014.

[34] A. R. Atilgan and D. H. Hodges, "On the strain energy of laminated composite plates," *International Journal of Solids and Structures*, vol. 29, no. 20, pp. 2527–2543, 1992.

[35] V. G. Sutyrin and D. H. Hodges, "On asymptotically correct linear laminated plate theory," *International Journal of Solids and Structures*, vol. 33, no. 25, pp. 3649–3671, 1996.

[36] W. Yu, J.-S. Kim, D. H. Hodges, and M. Cho, "A critical evaluation of two reissnercmindlin type models for composite laminated plates," *Aerospace Science and Technology*, vol. 12, no. 5, pp. 408–417, 2008.

[37] M. V. Peereswara Rao, D. Harursampath, and K. Renji, "Prediction of inter-laminar stresses in composite honeycomb sandwich panels under mechanical loading using variational asymptotic method," *Composite Structures*, vol. 94, no. 8, pp. 2523–2537, 2012.

[38] V. S. Sokolinsky, H. Shen, L. Vaikhanski, and S. R. Nutt, "Experimental and analytical study of nonlinear bending response of sandwich beams," *Composite Structures*, vol. 60, no. 2, pp. 219–229, 2003.

[39] E. Reissner, "Finite deflections of sandwich plates," *Journal of the Aeronautical Sciences*, vol. 15, no. 7, pp. 435–440, 1948.

[40] A. M. Alwan, "Large deflection of sandwich plates with orthotropic cores," *AIAA Journal*, vol. 2, no. 10, pp. 1820–1822, 1964.

[41] S. Dutta and B. Banerjee, "Large deflections of sandwich plates with orthotropic cores - a new approach," *AIAA Journal*, vol. 30, no. 3, pp. 845–847, 1992.

[42] E. Wang, N. Gardner, and A. Shukla, "The blast resistance of sandwich composites with stepwise graded cores," *International Journal of Solids and Structures*, vol. 46, no. 18C19, pp. 3492–3502, 2009.

[43] Y. Frostig and M. Baruch, "High-order buckling analysis of sandwich beams with transversely flexible core," *Journal of Engineering Mechanics*, vol. 119, no. 3, pp. 476–495, 1993.

[44] V. Sokolinsky and Y. Frostig, "Nonlinear behavior of sandwich panels with a transversely flexible core," *AIAA Journal*, vol. 37, no. 11, pp. 1474–1482, 1999.

[45] V. Sokolinsky and Y. Frostig, "Branching behavior in the nonlinear response of sandwich panels with a transversely flexible core," *International Journal of Solids and Structures*, vol. 37, no. 40, pp. 5745–5772, 2000.

[46] R. Li and G. A. Kardomateas, "Nonlinear high-order core theory for sandwich plates with orthotropic phases," *AIAA Journal*, vol. 46, no. 11, pp. 2926–2934, 2008.

[47] J. Hohe and L. Librescu, "A nonlinear theory for doubly curved anisotropic sandwich shells with transversely compressible core," *International Journal of Solids and Structures*, vol. 40, no. 5, pp. 1059–1088, 2003.

[48] Y. Frostig, O. T. Thomsen, and I. Sheinman, "On the non-linear high-order theory of unidirectional sandwich panels with a transversely flexible core," *International Journal of Solids and Structures*, vol. 42, no. 5-6, pp. 1443–1463, 2005.

[49] S. Dariushi and M. Sadighi, "A new nonlinear high order theory for sandwich beams: An analytical and experimental investigation," *Composite Structures*, vol. 108, pp. 779–788, 2014.

[50] G. A. Kardomateas, Y. Frostig, and C. N. Phan, "Dynamic elasticity solution for the transient blast response of sandwich beams/wide plates," *AIAA Journal*, vol. 51, no. 2, pp. 485–491, 2013.

[51] G. A. Kardomateas, N. Rodcheuy, and Y. Frostig, "Transient blast response of sandwich plates by dynamic elasticity," *AIAA Journal*, vol. 53, no. 6, pp. 1424–1432, 2015.

[52] M. Ganapathi, B. P. Patel, and D. P. Makhecha, "Nonlinear dynamic analysis of thick composite/sandwich laminates using an accurate higher-order theory," *Composites Part B: Engineering*, vol. 35, no. 4, pp. 345–355, 2004.

[53] R. A. S. Moreira and J. D. Rodrigues, "Static and dynamic analysis of soft core sandwich panels with through-thickness deformation," *Composite Structures*, vol. 92, no. 2, pp. 201–215, 2010.

[54] M. A. R. Loja, J. I. Barbosa, and C. M. Mota Soares, "Dynamic behaviour of soft core sandwich beam structures using kriging-based layerwise models," *Composite Structures*, vol. 134, pp. 883–894, 2015.

[55] B. R. Sekhar, S Gopalakrishnan, and M. Murthy, "Wave transmission characteristics for higher-order sandwich panel with flexible core using time-domain spectral element method," *Journal of Sandwich Structures & Materials*, vol. 19, no. 3, pp. 364–393, 2017.

[56] H. Schwarts-Givli, O. Rabinovitch, and Y. Frostig, "Free vibration of delaminated unidirectional sandwich panels with a transversely flexible core and general boundary conditions ł a high-order approach," *Journal of Sandwich Structures & Materials*, vol. 10, no. 2, pp. 99–131, 2008.

[57] D. Elmalich and O. Rabinovitch, "A high-order finite element for dynamic analysis of soft-core sandwich plates," *Journal of Sandwich Structures and Materials*, vol. 14, no. 5, pp. 525–555, 2012.

[58] C. N. Phan, G. A. Kardomateas, and Y. Frostig, "Blast response of a sandwich beam/wide plate based on the extended high-order sandwich panel theory and comparison with elasticity," *Journal of Applied Mechanics*, vol. 80, no. 6, pp. 061 005–061 005, 2013.

[59] Y. Frostig, N. Rodcheuy, and G. A. Kardomateas, "Blast response of sandwich plates with a compressible core: Extended high-order approach," *AIAA Journal*, vol. 53, no. 5, pp. 1211–1225, 2015.

[60] V. L. Tagarielli, V. S. Deshpande, and N. A. Fleck, "The dynamic response of composite sandwich beams to transverse impact," *International Journal of Solids and Structures*, vol. 44, no. 7, pp. 2442–2457, 2007.

[61] M. Jackson and A. Shukla, "Performance of sandwich composites subjected to sequential impact and air blast loading," *Composites Part B: Engineering*, vol. 42, no. 2, pp. 155–166, 2011.

[62] E. Wang and A. Shukla, "Blast performance of sandwich composites with in-plane compressive loading," *Experimental Mechanics*, vol. 52, no. 1, pp. 49–58, 2012.

[63] N. Gardner, E. Wang, P. Kumar, and A. Shukla, "Blast mitigation in a sandwich composite using graded core and polyurea interlayer," *Experimental Mechanics*, vol. 52, no. 2, pp. 119–133, 2012.

[64] S. Avachat and M. Zhou, "Compressive response of sandwich plates to water-based impulsive loading," *International Journal of Impact Engineering*, vol. 93, pp. 196–210, 2016.

[65] T. Qu, S. Avachat, and M. Zhou, "Response of cylindrical composite structures subjected to underwater impulsive loading: Experimentations and computations," *Journal of Engineering Materials and Technology*, vol. 139, no. 2, pp. 021 020–021020–11, 2017.

[66] R. Li, G. A. Kardomateas, and G. J. Simitses, "Point-wise impulse (blast) response of a composite sandwich plate including core compressibility effects," *International Journal of Solids and Structures*, vol. 46, no. 10, pp. 2216–2223, 2009.

[67] V. Y. Perel and A. N. Palazotto, "Dynamic geometrically nonlinear analysis of transversely compressible sandwich plates," *International Journal of Non-Linear Mechanics*, vol. 38, no. 3, pp. 337–356, 2003.

[68] N. J. Hoff and S. F. Mautner, "The buckling of sandwich-type panels," *Journal of the Aeronautical Sciences*, vol. 12, no. 3, pp. 285–297, 1945.

[69] G. W. Hunt, "Hidden (a)symmetries of elastic and plastic bifurcation," *Applied Mechanics Reviews*, vol. 39, no. 8, pp. 1165–1186, 1986.

[70] G. W. Hunt, L. S. D. Silva, and G. M. E. Manzocchi, "Interactive buckling in sandwich structures," *Proceedings of the Royal Society of London. A. Mathematical and Physical Sciences*, vol. 417, no. 1852, pp. 155–177, 1988.

[71] G. W. Hunt and M. A. Wadee, "Localization and mode interaction in sandwich structures," *Proceedings of the Royal Society of London. Series A: Mathematical, Physical and Engineering Sciences*, vol. 454, no. 1972, pp. 1197–1216, 1998.

[72] M. A. Wadee and G. W. Hunt, "Interactively induced localized buckling in sandwich structures with core orthotropy," *Journal of Applied Mechanics*, vol. 65, no. 2, pp. 523–528, 1998.

[73] M. A. Wadee, S. Yiatros, and M. Theofanous, "Comparative studies of localized buckling in sandwich struts with different core bending models," *International Journal of Non-Linear Mechanics*, vol. 45, no. 2, pp. 111–120, 2010.

[74] L. Lèotoing, S. Drapier, and A. Vautrin, "First applications of a novel unified model for global and local buckling of sandwich columns," *European Journal of Mechanics - A/Solids*, vol. 21, no. 4, pp. 683–701, 2002.

[75] M.-A. Douville and P. Le Grognec, "Exact analytical solutions for the local and global buckling of sandwich beam-columns under various loadings," *International Journal of Solids and Structures*, vol. 50, no. 16-17, pp. 2597–2609, 2013.

[76] G. A. Kardomateas, "Wrinkling of wide sandwich panelsmbeams with orthotropic phases by an elasticity approach," *Journal of Applied Mechanics*, vol. 72, no. 6, pp. 818–825, 2004.

[77] G. A. Kardomateas, "An elasticity solution for the global buckling of sandwich beams/wide panels with orthotropic phases," *Journal of Applied Mechanics*, vol. 77, no. 2, p. 021 015, 2010.

[78] M. K. Pandit, B. N. Singh, and A. H. Sheikh, "Buckling of laminated sandwich plates with soft core based on an improved higher order zigzag theory," *Thin-Walled Structures*, vol. 46, no. 11, pp. 1183–1191, 2008.

[79] V. Sokolinsky and Y Frostig, "Boundary condition effects in buckling of soft core sandwich panels," *Journal of Engineering Mechanics*, vol. 125, no. 8, pp. 865–874, 1999.

[80] V. Sokolinsky, "Nonlinear behavior of sandwich structures with transversely flexible core," PhD thesis, Technion - Israel Institute of Technology, 1999.

[81] C. N. Phan, G. A. Kardomateas, and Y. Frostig, "Global buckling of sandwich beams based on the extended high-order theory," *AIAA Journal*, vol. 50, no. 8, pp. 1707–1716, 2012.

[82] C. N. Phan, N. W. Bailey, G. A. Kardomateas, and M. A. Battley, "Wrinkling of sandwich wide panels/beams based on the extended high-order sandwich panel the-

ory: Formulation, comparison with elasticity and experiments," *Archive of Applied Mechanics*, vol. 82, no. 10-11, pp. 1585–1599, 2012.

[83] H. Huang and G. A. Kardomateas, "Buckling and initial postbuckling behavior of sandwich beams including transverse shear," *AIAA Journal*, vol. 40, no. 11, pp. 2331–2335, 2002.

[84] P. Le Grognec and A. Le van, "Some new analytical results for plastic buckling and initial post-buckling of plates and cylinders under uniform compression," *Thin-Walled Structures*, vol. 47, no. 8-9, pp. 879–889, 2009.

[85] P. Le Grognec and K. Sad Saoud, "Elastoplastic buckling and post-buckling analysis of sandwich columns," *International Journal of Non-Linear Mechanics*, vol. 72, pp. 67–79, 2015.

[86] S. Madhukar and M. K. Singha, "Geometrically nonlinear finite element analysis of sandwich plates using normal deformation theory," *Composite Structures*, vol. 97, no. 0, pp. 84–90, 2013.

[87] H. Hu, S. Belouettar, M. Potier-Ferry, and A. Makradi, "A novel finite element for global and local buckling analysis of sandwich beams," *Composite Structures*, vol. 90, no. 3, pp. 270–278, 2009.

[88] D. Elmalich and O. Rabinovitch, "Geometrically nonlinear behavior of sandwich plates," *AIAA Journal*, vol. 51, no. 8, pp. 1993–2008, 2013.

[89] S. Oskooei and J. S. Hansen, "Higher-order finite element for sandwich plates," *AIAA Journal*, vol. 38, no. 3, pp. 525–533, 2000.

[90] E. Riks, "The application of Newton's method to the problem of elastic stability," *Journal of Applied Mechanics*, vol. 39, no. 4, pp. 1060–1065, 1972.

[91] E. Riks, "An incremental approach to the solution of snapping and buckling problems," *International Journal of Solids and Structures*, vol. 15, no. 7, pp. 529–551, 1979.

[92] M. A. Crisfield, "A fast incremental/iterative solution procedure that handles snap-through," *Computers & Structures*, vol. 13, no. 1-3, pp. 55–62, 1981.

[93] M. A. Crisfield, "An arc-length method including line searches and accelerations," *International Journal for Numerical Methods in Engineering*, vol. 19, no. 9, pp. 1269–1289, 1983.

[94] M. A. Crisfield, *Non-Linear Finite Element Analysis of Solids and Structures, Volume 2: Advanced Topics*. John Wiley & Sons, Inc., 1997.

[95] M. J. Clarke and G. J. Hancock, "A study of incremental-iterative strategies for non-linear analyses," *International Journal for Numerical Methods in Engineering*, vol. 29, no. 7, pp. 1365–1391, 1990.

[96] H. B. Keller, *Numerical Methods in Bifurcation Problems*. Tata Institute Of Fundamental Research, Bombay, 1987.

[97] R. Seydel, *Practical Bifurcation and Stability Analysis*. New York: Springer, 2010.

[98] L. Librescu, W. Lin, M. DiSciuva, and U. Icardi, "Postbuckling of laminated composite and sandwich plates and shells: On the significance of the fulfillment of static interlayer continuity conditions," *Computer Methods in Applied Mechanics and Engineering*, vol. 148, no. 1, pp. 165–186, 1997.

[99] Z. Yuan, G. A. Kardomateas, and Y. Frostig, "Finite element formulation based on the extended high-order sandwich panel theory," *AIAA Journal*, vol. 53, no. 10, pp. 3006–3015, 2015.

[100] K.-J. Bathe, *Finite Element Procedures*. Prentice-Hall, 1996.

[101] J. N. Reddy, *Mechanics of Laminated Composite Plates and Shells: Theory and Analysis, Second Edition*. Boca Raton, FL: CRC Press, 2003.

[102] H. B. Keller, "Numerical solutions of bifurcation and nonlinear eigenvalue problem," in *Applications of Bifurcation Theory*, P. H. Rabinowitz, Ed. Academic Press, 1977, pp. 359–384.